AN ASSESSMENT OF STOCHASTIC CONTROL METHODS FOR HOME ENERGY MANAGEMENT USING A HIGH-FIDELITY RESIDENTIAL ENERGY MODEL AND REALISTIC LEVELS OF UNCERTAINTY

by

Michael Blonsky

A thesis submitted to the Faculty and the Board of Trustees of the Colorado School of Mines in partial fulfillment of the requirements for the degree of Doctor of Philosophy (Engineering Systems).

Golden, Colorado

Date _____

Signed: _____

Michael Blonsky

Signed: _____

Dr. Tyrone Vincent
Thesis Advisor

Signed: _____

Dr. Killian McKenna
Thesis Advisor

Golden, Colorado

Date _____

Signed: _____

Dr. Peter Aaen
Professor and Department Head
Department of Electrical Engineering

ABSTRACT

In the residential sector, there is considerable growth in smart, interactive devices including thermostats, water heaters, electric vehicle chargers, solar panels, and battery systems. These devices can all provide the electric grid with additional flexibility, which is a valuable resource for grid operators and helps reduce system costs and emissions. However, it is difficult to control these devices because there is considerable diversity in the residential housing stock and because the controls depend on stochastic variables such as weather and occupant behavior.

We present a stochastic control framework for home energy management systems that can control these devices while accounting for multiple sources of uncertainty. To do this, we first develop an integrated residential energy model that can simulate multiple controllable devices with high resolution and can interface with external controllers. We then design a control framework with a linear residential energy model, a forecast generator that provides realistic estimates of weather and occupancy variables, and a control objective that captures energy costs and occupant comfort. The control framework is used to evaluate the performance of heuristic, deterministic, and stochastic control methods, primarily model predictive control.

We show that the stochastic model predictive control performs best in scenarios with realistic levels of uncertainty. We also validate the residential energy models and show the benefits of high-fidelity modeling for building-to-grid co-simulation studies. The results shown in this dissertation provide a deeper understanding of residential load flexibility in uncertain conditions, and the frameworks developed enable future research for evaluating flexible loads in a broad set of applications.

TABLE OF CONTENTS

ABSTRACT iii

LIST OF FIGURES ix

LIST OF TABLES xii

LIST OF SYMBOLS xiii

LIST OF ABBREVIATIONS xviii

ACKNOWLEDGMENTS xx

CHAPTER 1 INTRODUCTION 1

1.1 Trends in Residential Energy Consumption 4

1.2 Load Flexibility 7

1.3 Residential Modeling and Model-Based Controls 8

1.4 Research Objectives 11

CHAPTER 2 LITERATURE REVIEW 14

2.1 Residential Energy Modeling 14

2.1.1 Building Envelope 14

2.1.2 HVAC Equipment 15

2.1.3 Water Heater Equipment 17

2.1.4 Electric Vehicles 18

2.1.5 Appliances, Lighting, and Other Loads 19

2.1.6 Distributed Generation and Storage 20

2.1.7 Integrated Residential Energy Modeling 21

2.1.8 State Space Model Techniques . . . 22
2.2 Home Energy Management Systems . . . 23
2.2.1 HEMS Control Methods . . . 23
2.2.2 Device Controllers . . . 25
2.2.3 Related Control Applications . . . 27
2.2.4 HEMS Limitations . . . 27
2.3 Uncertainty Considerations in HEMS . . . 28
2.3.1 Forecast Uncertainty . . . 28
2.3.2 Model Uncertainty . . . 30
2.3.3 Measurement Uncertainty . . . 31
2.3.4 Control Methods that Incorporate Uncertainty . . . 31
CHAPTER 3 INTEGRATED RESIDENTIAL ENERGY MODELING . . . 34
3.1 OCHRE Model Description . . . 34
3.1.1 Building Envelope . . . 34
3.1.2 HVAC Model . . . 39
3.1.3 Water Heater Model . . . 40
3.1.4 EV Model . . . 42
3.1.5 Other Loads . . . 47
3.1.6 Voltage-Dependent Load Model . . . 49
3.1.7 PV Model . . . 49
3.1.8 Battery Model . . . 50
3.2 New Construction Case Study . . . 51
3.3 Chapter Summary . . . 52

CHAPTER 4 A STOCHASTIC CONTROL FRAMEWORK FOR HOME ENERGY MANAGEMENT SYSTEMS 57

4.1 Control Model Description 58

4.1.1 Linear Controllable Load Model 58

4.1.2 HVAC and Envelope 59

4.1.3 Water Heater 61

4.1.4 Electric Vehicle 62

4.1.5 Battery 63

4.1.6 Combined House Model 63

4.1.7 Uncertainty Model 64

4.1.8 Model Implementation 65

4.2 Control Formulation 66

4.2.1 Heuristic Controls 67

4.2.2 Deterministic MPC 67

4.2.3 Stochastic MPC 70

4.2.4 Control Objective Extensions 72

4.3 Forecast Generators 73

4.3.1 Weather Forecast 73

4.3.2 Occupant Forecast 75

4.4 Chapter Summary 78

CHAPTER 5 MODEL VALIDATION 79

5.1 EnergyPlus Model Validation 79

5.2 EV Model Validation 82

5.3 Minimal Building Validation 84
5.4 Control Model Validation 88
5.5 Chapter Summary 90
CHAPTER 6 COMMUNITY CO-SIMULATION MODELING 92
6.1 Co-simulation Framework Description 92
6.1.1 House Models 92
6.1.2 Distribution Grid Model 93
6.1.3 House Controllers 94
6.2 New Construction Case Study 94
6.2.1 Simulation Inputs 95
6.2.2 Simulation Engine 96
6.2.3 Baseline Results 97
6.2.4 Load-Shedding and Load-Shifting Control 97
6.3 Case Study with foresee 102
6.3.1 Simulation Inputs 103
6.3.2 Baseline Results 103
6.3.3 HEMS Control 104
6.3.4 Demand Charge Control 106
6.4 Chapter Summary 107
CHAPTER 7 ASSESSMENT OF STOCHASTIC CONTROL METHODS FOR HOME ENERGY MANAGEMENT SYSTEMS 108
7.1 Battery Control with Demand Charge 108
7.1.1 Simulation Inputs 108

7.1.2 MPC Reference Scenarios 110
7.1.3 Baseline Scenario 111
7.1.4 Impacts of Varying Risk 114
7.1.5 Impacts of Varying Uncertainty 114
7.1.6 Case Study Summary 117
7.2 HEMS Control for a Typical Building 117
7.2.1 Simulation Inputs 118
7.2.2 Deterministic MPC 119
7.2.3 Stochastic MPC 123
7.2.4 Control Performance 125
7.2.5 Pareto Optimality Analysis 126
7.2.6 Case Study Summary 128
7.3 Chapter Summary 128
CHAPTER 8 CONCLUSIONS AND FUTURE WORK 129
8.1 Key Findings 129
8.1.1 Integrated Residential Energy Modeling 129
8.1.2 Model Validation 130
8.1.3 Distributed Control Strategies 131
8.1.4 Uncertainty in HEMS Controls 131
8.1.5 HEMS Control Performance 132
8.2 Future Work 133
REFERENCES 135
APPENDIX COPYRIGHT PERMISSIONS 155

LIST OF FIGURES

Figure 1.1 The "Duck Curve", past and present 3

Figure 1.2 Residential electricity consumption by end use 4

Figure 3.1 Schematic of the OCHRE envelope model 35

Figure 3.2 Schematic of the OCHRE envelope RC model 36

Figure 3.3 Schematic of a boundary in the envelope model 36

Figure 3.4 Heatmap of parking events for a large PHEV with Level 1 charging on weekdays 44

Figure 3.5 Heatmap of parking events for a small BEV with Level 1 charging on weekdays 45

Figure 3.6 Heatmap of parking events for a small BEV with Level 1 charging on weekends 46

Figure 3.7 Flow chart for EV model initialization and simulation 48

Figure 3.8 Single home simulation results at 1-minute resolution 53

Figure 3.9 Single home simulation results at 15-minute resolution 54

Figure 3.10 Simulation results with a load shifting controller 55

Figure 4.1 Schematic of an MPC algorithm with uncertainty 58

Figure 4.2 A linear envelope model 59

Figure 4.3 Flow diagram of the HEMS controller and OCHRE 65

Figure 4.4 An example temperature forecast 74

Figure 4.5 An example solar irradiance forecast 75

Figure 4.6 An example water draw forecast 77

Figure 4.7 An example EV driving forecast 77

Figure 5.1 Validation results for a summer day 80

Figure 5.2 Validation results for a winter day 81

Figure 5.3 Validation results for a shoulder season day 81

Figure 5.4 Daily load profile comparison for a 50-mile PHEV with a Level 1 charger . 83

Figure 5.5 Daily load profile comparison for a 100-mile BEV with a Level 2 charger . 83

Figure 5.6 Minimal building validation results in the summer 88

Figure 5.7 Minimal building validation results in the winter 89

Figure 5.8 Minimal building validation results in the shoulder season 89

Figure 5.9 Indoor temperature using the full and linearized models 91

Figure 5.10 HVAC energy consumption during peak hours using various models and controls. 91

Figure 6.1 Schematic for the OCHRE model in a co-simulation framework. 93

Figure 6.2 Total community power by end use for the baseline scenario at 1-minute time resolution. 98

Figure 6.3 Total community power by end use for the baseline scenario at 15-minute time resolution. 98

Figure 6.4 Community power and voltages for baseline scenarios 99

Figure 6.5 Total community power by end use for the load-shifting scenario at 1-minute time resolution. 101

Figure 6.6 Total community power for all scenarios. 101

Figure 6.7 Total community power by end use for the baseline scenario 104

Figure 6.8 Total community power for the EV delay scenario 105

Figure 6.9 Total community power for the HEMS control scenario 106

Figure 6.10 Total EV power in the community for all scenarios 107

Figure 7.1 Battery case study daily profiles 112

Figure 7.2 Results for SMPC Baseline Scenario on the Peak Load Day 113

Figure 7.3 Results for SMPC Scenario with ARX Model and High Risk Tolerance on the Peak Load Day 116

Figure 7.4 HEMS results for DMPC cases with exact forecasts and heuristic controls 121

Figure 7.5 Water heater results for DMPC cases with exact and ARIMAX forecasts 122

Figure 7.6 EV results for heuristic controls and DMPC cases with exact and ARIMAX forecasts 122

Figure 7.7 Water heater results for DMPC and SMPC cases with ARIMAX forecasts 123

Figure 7.8 HVAC simulation results for the DMPC and SMPC cases with ARIMAX forecasts. 124

Figure 7.9 Pareto front for water heater energy and discomfort costs for SMPC and DMPC optimizations. 127

LIST OF TABLES

Table 3.1 Overview of equipment used in OCHRE, including control options and main input parameters 51

Table 5.1 Annual validation results comparing energy consumption by end use. 82

Table 5.2 Validation of HVAC heating delivered for multiple locations and scenarios in the test suite. 86

Table 5.3 Validation of HVAC cooling delivered for multiple locations and scenarios in the test suite. 87

Table 7.1 Model and Control Parameters Used for Scenarios 110

Table 7.2 Performance Results for All Scenarios 117

Table 7.3 Key simulation parameter values 119

Table 7.4 Control performance results for each simulation 125

LIST OF SYMBOLS

General

$E[\cdot]$ . . . . . Expected value function

I . . . . . Identity matrix

$h \in \mathcal{H}$ . . . . . Index and set of discrete time steps in MPC horizon

$k \in \mathcal{K}$ . . . . . Index and set of discrete time steps

n_l . . . . . Length of set with index l, i.e., $n_l = |\mathcal{L}|$

n_x . . . . . Length of vector x, i.e., $n_x = |x|$

$\tilde{x} \sim \mathcal{N}(\hat{x}, \Sigma_x)$ . . . . . Gaussian random vector x with mean $\hat{x}$ and variance Σ_x

$\overline{x_i}$ . . . . . Maximum value of variable x_i

$\underline{x_i}$ . . . . . Minimum value of variable x_i

$\sigma^2_{x_i}$ . . . . . Variance of random variable x_i

$|x|_+$ . . . . . Positive orthant of variable x, i.e., $\max(x, 0)$

State Space Models

A_i . . . . . State matrix for discrete-time system i

B_i . . . . . Input matrix for discrete-time system i

C_i . . . . . Output matrix for discrete-time system i

G_i . . . . . Uncontrollable input matrix for discrete-time system i

t_s . . . . . Time resolution of simulation

u_i . . . . . Input vector for system i

x_i . . . . . State vector for system i

y_i . . . . . Output vector for system i

z_i . . . . . Uncontrollable input vector for system i

Equipment Models

ρ . . . . . Density of water

C_{batt} . . . . . Thermal capacitance of battery

E_l . . . . . Energy capacity of load l

$H_{l,i}$ . . . . . Heat injected into node i from load l

$M_{wh,i}$ . . . . . Water heater mode for water heater node i

P_{chg} . . . . . Battery charging power

P_{dis} . . . . . Battery discharging power

P_{drive} . . . . . Estimated EV power discharged due to driving

P_{inv} . . . . . PV inverter capacity

P_{irr} . . . . . Maximum AC power from PV

P_l . . . . . Power of load l

P_{lvl} . . . . . Maximum EV charging power

$R_{batt,a}$ . . . . . Thermal resistance between battery and ambient air

T_{avg} . . . . . Average daily ambient temperature

T_{batt} . . . . . Battery temperature

$T_{batt,high}$ . . . . . Soft maximum battery temperature

T_{cool} . . . . . HVAC cooling setpoint

T_{heat} . . . . . HVAC heating setpoint

V_{draw} . . . . . Hot water draw volume

$\eta_{batt,th}$ . . . . . Battery thermal efficiency

η_{chg} . . . . . Battery charging efficiency

c_p . . . . . Heat capacity of water

η_{dis} . . . . . Battery discharging efficiency

$e \in \mathcal{E}$ . . . . . Index and set of discrete events

g_l . . . . . Sensible heat gain fraction of load l

$\kappa_{hvac,0}$ . . . . . Nominal capacity of HVAC equipment

$\eta_{hvac,0}$ . . . . . Nominal efficiency of HVAC equipment

θ_i . . . . . Temperature of water tank node i

$k_{e,0}$ . . . . . Parking start time

$k_{e,end}$ . . . . . Parking end time

κ_l . . . . . Capacity of load l

η_l . . . . . Efficiency of load l

$l \in \mathcal{L}$ . . . . . Index and set of loads and other equipment

p_{drive} . . . . . Probability that the EV is driving

p_{leave} . . . . . Probability that the EV is leaving the parking space

$s_{ev,e,0}$ . . . . . Initial EV state of charge

s_l . . . . . State of charge of load l

w . . . . . Weekday/weekend indicator

$\kappa_{wh,i}$ . . . . . Nominal heating capacity for water heater node i

$\eta_{wh,i}$ . . . . . Nominal efficiency for water heater node i

θ_{wm} . . . . . Water mains temperature

Envelope Model

σ . . . . . Stefan-Boltzmann constant

C_i . . . . . Thermal capacitance of node i

$H_{az,inf}$ . . . . . Heat due to infiltration from ambient zone to zone z

H_i . . . . . Heat injected into node i

H_{int} . . . . . Internal heat gains injected into the main indoor zone

H_{sol} . . . . . Vector of heat gains from solar radiation on each external surface

$H_{zs,rad}$ . . . . . Heat due to radiation from zone z to surface s

$R_{az,inf}$ . . . . . Thermal resistance due to infiltration between zones a and z

R_{ij} . . . . . Thermal resistance between nodes i and j

$R_{zs,rad}$ . . . . . Thermal resistance due to radiation between zone z and surface s

T_a . . . . . Ambient temperature

T_g . . . . . Ground temperature

T_i . . . . . Temperature of envelope node i

T_m . . . . . Main indoor temperature

$T_{s,i}$ . . . . . Surface temperature of a boundary next to node i

a_s . . . . . Area of surface s

n_{ext} . . . . . Number of external nodes in envelope model

ϵ_s . . . . . Emissivity of surface s

Controls

Φ^{-1} . . . . . Inverse cumulative distribution function of the Gaussian distribution

J . . . . . Total cost function

J_i . . . . . Cost function term i

K . . . . . Kalman gain matrix

λ_i . . . . . Per-unit cost for term i

$\hat{\lambda}_{tou}$ . . . . . Average cost of power over the forecast horizon

β_{x_i} . . . . . Z-score associated with a constraint on random variable x_i

LIST OF ABBREVIATIONS

API . . . . . Application Programming Interface

ARIMAX . . . . . Auto-regressive Integrated Moving Average Exogenous

ARMAX . . . . . Auto-regressive Moving Average Exogenous

ARX . . . . . Auto-regressive Exogenous

ASHP . . . . . Air Source Heat Pump

BESS . . . . . Battery Energy Storage System

BEV . . . . . Battery Electric Vehicle

CAISO . . . . . California Independent System Operator

COP . . . . . Coefficient of Performance

DER . . . . . Distributed Energy Resource

DERMS . . . . . Distributed Energy Resource Management System

DG . . . . . Distributed Generation

DMPC . . . . . Deterministic Model Predictive Control

DSM . . . . . Demand-Side Management

EIA . . . . . Energy Information Agency

EIR . . . . . Energy Intensity Ratio

EV . . . . . Electric Vehicle

GEB . . . . . Grid-interactive Efficient Building

GHI . . . . . Global Horizontal Irradiance

HEMS . . . . . Home Energy Management System

HPWH . . . . . Heat Pump Water Heater

HPXML . . . . . Home Performance eXtensible Markup Language

HVAC . . . . . Heaving, Ventilation, and Air Conditioning

LP . . . . . Linear Program

LWR . . . . . Long-wave Radiation

MILP . . . . . Mixed-integer Linear Program

MPC . . . . . Model Predictive Control

NREL . . . . . National Renewable Energy Laboratory

OCHRE . . . . . Object-oriented Controllable High-resolution Residential Energy Model

PHEV . . . . . Plug-in Hybrid Electric Vehicle

PV . . . . . Photovoltaics

QP . . . . . Quadratic Program

RC . . . . . Resistor Capacitor

SHR . . . . . Sensible Heat Ratio

SMPC . . . . . Stochastic Model Predictive Control

SOC . . . . . State of Charge

TCL . . . . . Thermostatically Controlled Load

TMY3 . . . . . Typical Meteorological Year, version 3

TOU . . . . . Time-of-Use

VAR . . . . . Volt-Ampere Reactive

WH . . . . . Water Heater

ACKNOWLEDGMENTS

I would like to acknowledge everyone at the Colorado School of Mines and the National Renewable Energy Laboratory who has contributed their time and expertise to this dissertation. Thank you to my project team members and co-authors Sugirdhalakshmi Ramaraj, Sivasathya Pradha Balamurugan, Prateek Munankarmi, Utkarsh Kumar, Jeremy Keen, Shibani Ghosh, Santosh Veda, and Ben Kroposki.

Additional thanks go to multiple project team leaders that helped fund this work: Xin Jin, Fei Ding, Adarsh Nagarajan, Dylan Cutler, and Emma Elqvist. Funding was provided primarily by the U.S. Department of Energy Office of Energy Efficiency and Renewable Energy's Solar Energy Technologies Office and Building Technology Office. I appreciate their support for this research.

Many thanks to my committee members, Dr. Paulo Cesar Tabares-Velasco, Dr. Salman Mohagheghi, and Dr. Kathryn Johnson, for their active participation and suggestions to improve my work. A special thank you to committee member and colleague Jeff Maguire, who has helped drive the modeling work forward by advocating for my research and providing invaluable insights.

I am especially thankful to my co-advisors Dr. Tyrone Vincent and Dr. Killian McKenna for their mentorship, thoughtfulness, and commitment to my work. Thank you for all you have taught me, for pushing me to do my best work, and for giving me the autonomy to choose my own research path.

Finally, I want to thank my wife, Kira, our son, Levi for their love and support. I could not have done this without you.

CHAPTER 1

INTRODUCTION

The electric grid provides continuous, reliable energy to our homes that is essential to our safety and well-being. This energy costs money and resources to produce, and contributes to environmental issues including pollution and climate change. Reducing residential energy consumption through energy efficiency lowers energy costs for homeowners, alleviates the need for grid upgrades, and reduces carbon emissions and pollution.

While the importance of energy efficiency has been well understood for a long time, there has been a recent focus on shifting the timing of electricity usage. At times when electricity demand is high, more expensive—and often more polluting—power generators must be turned on. During these "peak" times, electricity becomes more expensive, and reductions in energy consumption becomes more valuable. For example, many areas of the U.S. with warm climates experience a peak in demand during hot summer afternoons when buildings require more energy for air conditioning. In these areas, energy savings from air conditioning is more valuable than an equivalent amount of savings from, for example, efficient lighting, because the air conditioning consumption is more coincident with the peak period when electricity is expensive.

Electricity prices are also becoming more variable due to the emergence of variable renewable energy resources including solar photovoltaics (PV) and wind turbines. These resources can only operate at certain times—when the sun is shining or the wind is blowing—and cannot store energy for other times. This can lead to an oversupply of energy at certain times, which may not be coincident with the peak demand. The "Duck Curve" in Figure 1.1, originally created in 2013 by the California grid operator CAISO, shows that solar PV reduces net demand (i.e., demand minus variable renewable generation) during the day and leads to a sharp increase in net demand in the evening [1].

Figure 1.1 shows CAISO data from March 2021, validating the net demand estimates from 2013 and showing that the variability is even larger than expected for some days. As solar and wind resources grow over time, this variation in net demand increases, which leads to larger variations in the temporal value of electricity.

As the variability in net load increases, electricity market prices and rate structures have become more variable as well. At the transmission level, electricity prices are set using day-ahead and real-time wholesale energy markets that often lead to price fluctuations and sometimes create negative energy prices [3]. Other components, including capacity markets and demand response programs, also help manage electricity prices and balance supply and demand. At the retail level, residential electricity rates have started becoming more complex, adding time-based features such as time-of-use (TOU) pricing, real-time prices, and demand charges. Rates for customers with rooftop solar may include net-energy metering, feed-in tariffs, or non-export agreements, which impact energy costs and encourage customers to self-consume on-site generation.

The traditional paradigm of grid operations uses flexible generation sources to match inflexible demand. The changes in electricity demand, generation resources, and electricity rate structures make it clear that this paradigm is being challenged. There is a growing need for demand flexibility, and residential energy sector is capable of providing some of that flexibility. However, in order to fully utilize flexible resources, we must understand their capabilities, limitations, and impacts on residential occupants' comfort and energy costs.

This dissertation aims to use residential energy modeling and controls to better understand how load flexibility impacts occupant comfort, energy costs, and grid operations, with a focus on the effects of uncertainty and limited information. The remainder of this introduction provides a background on recent residential energy trends, load flexibility, and residential energy modeling and controls. It concludes with a list of research questions and the potential impacts of the research.

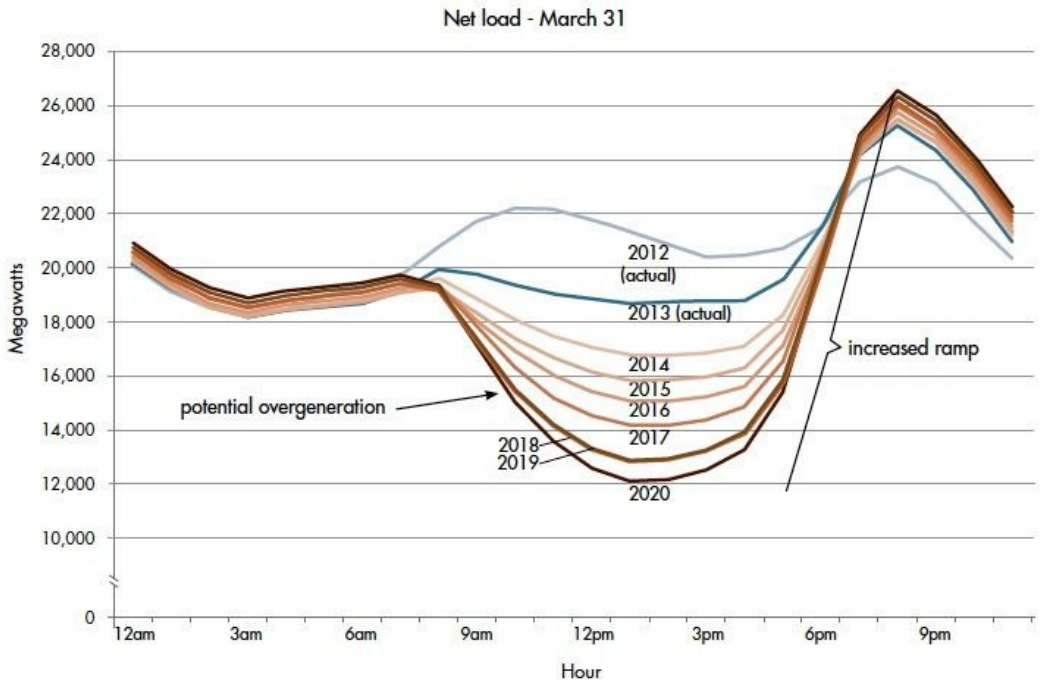

(a) Original "Duck Curve"

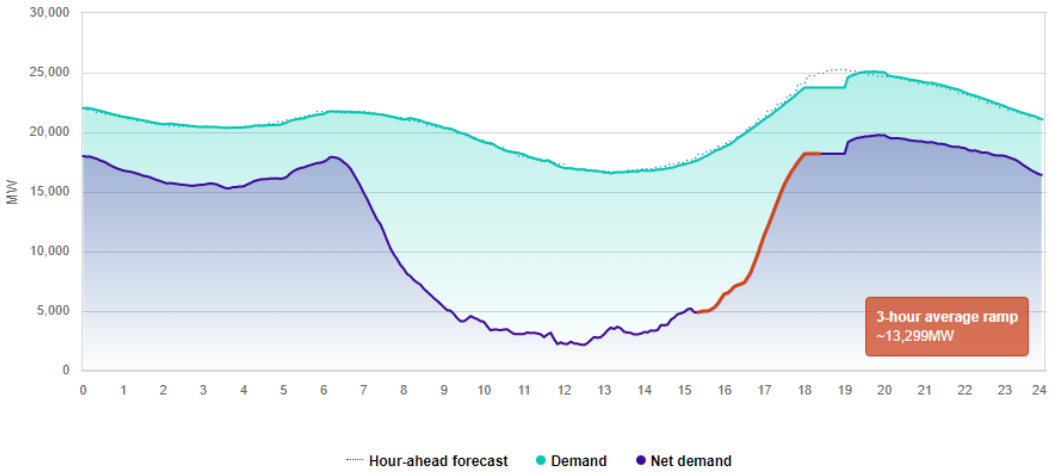

(b) CAISO Demand and Net Demand from a day in March 2021

Figure 1.1 The "Duck Curve", past and present. Variations in net electricity demand increase as renewable sources grow and the afternoon peak increases [1, 2].

1.1 Trends in Residential Energy Consumption

The latest data from the U.S. Energy Information Agency (EIA) states that residential buildings account for about 21% of all energy consumption and 36% of all electricity consumption in the U.S. [4]. Figure 1.2 shows the breakdown of residential electricity consumption by end use [5].

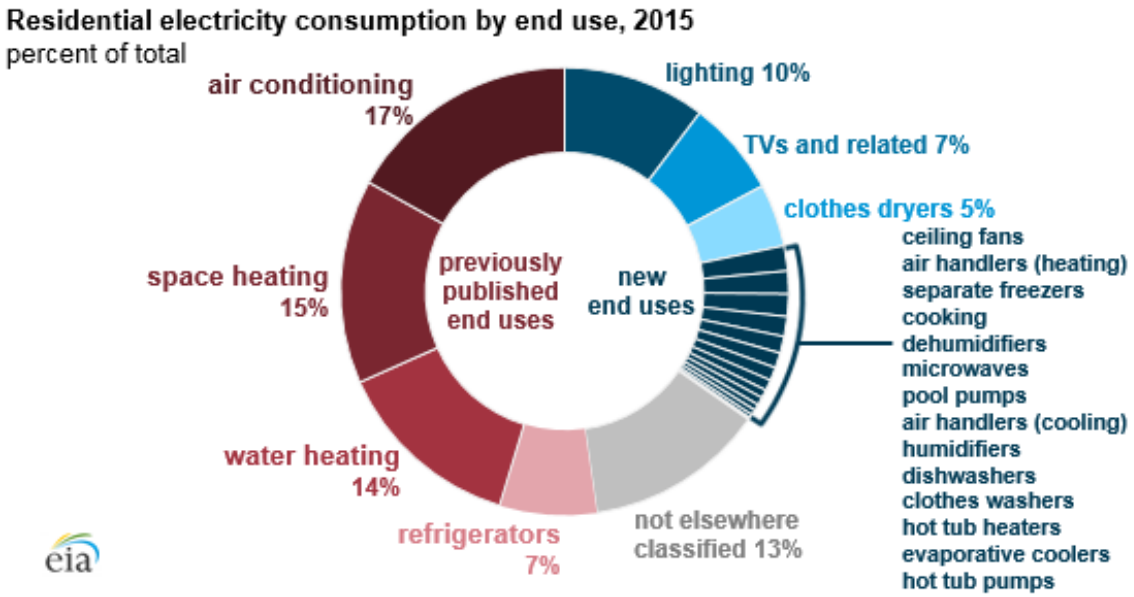

Figure 1.2 Residential electricity consumption by end use from the 2015 EIA Residential Energy Consumption Survey [5].

There is an opportunity to shift the way residential buildings use energy. More efficient equipment, improved controls, and tighter building envelopes can all reduce overall energy usage in residential buildings. Controls can further reduce costs by shifting when energy is consumed. Transitioning from fossil fuel-based to electricity-based equipment will lower the carbon footprint of residential buildings. These opportunities are already leading to multiple observable trends in building energy usage and in market adoption.

One major trend is electrification, or the shift toward electric equipment in residential buildings. Multiple papers have shown significant changes in the current and expected future adoption of electric equipment. Air source heat pumps (ASHP) are currently used

for space heating in about 10% of homes; reference estimates have heating electrification market share from 5-10% by 2030 and 18-35% by 2050, although many studies also run scenarios with much high electrification rates in which ASHP exceed 50% of the market [6, 7]. Electric vehicles accounted for about 1 million cars (about 0.5% of all cars) on the road in the U.S. in 2018. Projections for EV sales vary considerably, but reasonable estimates show 7-12% adoption by 2030 and 11-48% adoption by 2050. Scenarios with high penetration show adoption at 66-88% in 2050 [6–9]. Other equipment, including heat pump water heaters, ground source heat pumps, and electric cooking appliances and also expected to contribute to residential electrification [7, 9].

Another trend is the adoption of distributed energy resources (DERs) in residential buildings. We use the definition of DERs from [10]:

> "A DER is a resource sited close to customers that can provide all or some of their immediate electric and power needs and can also be used by the system to either reduce demand (such as energy efficiency) or provide supply to satisfy the energy, capacity, or ancillary service needs of the distribution grid. The resources, if providing electricity or thermal energy, are small in scale, connected to the distribution system, and close to load."

With this definition, DERs include rooftop solar PV and other on-site generation equipment, electrical storage systems (i.e., batteries), thermostatically controlled loads (TCLs), and other flexible loads. Thermostatically controlled loads refer to heating, ventilation, and air conditioning (HVAC) and water heating end uses. Other flexible loads include appliances and electric vehicles that have the capability to change when they consume energy.

Most DER markets are growing considerably. Rooftop PV in the U.S. has grown significantly from 6 GW cumulative installed capacity in 2015 to 16 GW in 2019, and it is expected to increase by 3-4 GW per year from 2020 to 2025 [11]. Some areas of the country, including California, have instituted policies that all new residential construction

include PV [12]. The U.S. residential battery market more than doubled in 2019 [13]. About 200 MW of residential batteries were installed in both 2019 and 2020, and total deployments are estimated at about 1 GW by 2025 [14]. Globally from 2020 to 2030, the EV market share of new car sales is projected to increase from 2.7% to 28%, and total EVs on the road are projected to increase from 8.5 to 116 million vehicles [15].

Equipment controls are generally a niche topic, but controls are at the core of smart technologies and the Internet of Things (IoT). Advances in information and communication technologies have created opportunities for many smart devices, including for energy applications. We define a "smart" energy device as a device that can communicate with any external controller and can change its energy demand based on a control signal. Smart thermostats accounted for 28 GW of flexible demand in 2019 and are expected to reach about 43 GW (43 million devices) by 2025 [16]. Smart water heaters are expected to grow from 300 MW to about 3 GW of flexible demand by 2025 [16]. Level 2 chargers, which can be a proxy for smart EV charging, are expected to increase from 50% of U.S. residential chargers in 2019 to 77% in 2030 [17]. Many commercially available devices and appliances are now wifi-enabled and can be controlled by an external system. Individually, each of these controllers can improve device efficiency, lower customer costs, and/or lower carbon emissions by changing how and when the device operates.

A home energy management system (HEMS) aggregates these individual device controllers into a single system, allowing for additional control benefits and easier integration and operation for the user. HEMS typically integrate with other smart home devices, including smart speakers and entertainment systems. Voice assistant devices have grown dramatically from 6 million households in 2015, to 39 million in 2018, and an expected 65 million in 2023 [18]. However, the HEMS component is still in development and is not widely used. Wood Mackenzie estimates smart home platform penetration at 14 million households in 2018 and an expected 48 million in 2023 [18]. The main benefits of HEMS are in the integration of information from sensor measurements, occupant

preferences, and external signals like electricity costs and weather. The HEMS can determine each device's usage with all this information, leading to more optimal outcomes for the occupant than if the controls had been executed separately within each device.

1.2 Load Flexibility

Electricity generation is becoming less flexible, mainly due to variable renewable sources, at the same time that residential energy consumption is becoming more flexible. Many of the devices described above—including batteries, smart devices, and HEMS—enable load flexibility for residential customers. We define load flexibility as the ability to change energy consumption for a given time period while maintaining a reasonable level of customer comfort and convenience. In many cases, a flexible load will shift energy consumption from one time to another while maintaining a similar level of overall energy consumption. Short-term load reductions, known as load shedding or demand response (DR), as well as energy storage, are included in the definition of load flexibility.

A wide range of residential energy-consuming devices can be considered flexible loads. HVAC loads are the most commonly considered flexible loads given their relatively large energy consumption and ease of control. Batteries, water heaters, appliances, EV chargers, and PV all have the ability to shift their energy usage as well. In order to shift load, a device must be able to respond to a control signal. Typically, a device also needs a communication method such as Wi-Fi to relay sensor information and to receive the control signal [19]. While some devices include manual controls—for example a dimming switch or a delay button on a dishwasher—it is much more convenient to control devices automatically via a HEMS or a cloud-based control hub.

As discussed in Section 1.1, many of these end uses are growing and incorporating more advanced control and communication technologies. These trends lead to an increase in the potential for the residential sector to serve as a source of load flexibility. The Brattle Group estimates approximately 200 GW of cost-effective demand flexibility potential in the

United States by 2030, with much of the increase coming from residential loads, including smart thermostats, smart water heaters, electric vehicle (EV) chargers, and behind-the-meter batteries [20]. The economic viability of these devices is driven by technology improvements, cost reductions, and an increase in the value of load flexibility.

To concentrate research and industry efforts in this area, the U.S. Department of Energy Building Technologies Office created the Grid-Interactive Efficient Buildings (GEB) Initiative [21]. Their work highlights ongoing research, best practices, and research gaps in load flexibility and other related areas. Current research needs include determining the potential value of load flexibility by end use, understanding the interactions between flexibility strategies, and assessing the impacts of flexibility on occupant preferences. Notably, they emphasize that GEB controls should have no negative impact on occupant comfort and in some cases can improve occupant comfort [22].

In addition to building and occupant impacts, load flexibility is expected to have considerable impacts on electric grid operations and planning. Grid resource planning at the transmission and distribution levels requires accurate forecasting of peak demand so that the grid has enough capacity to always meet demand. Most existing load flexibility services are used during grid contingency events (e.g., a large generator outage) to improve grid reliability. Many proposed load flexibility strategies are primarily used to reduce peak demand, thereby reducing the need for capacity expansion [23]. Flexible loads can also give grid operators a new tool to adjust demand, which can improve grid operations during normal conditions. However, depending on their implementation, they can also make load forecasting less predictable, making grid operations more difficult [24].

1.3 Residential Modeling and Model-Based Controls

Load flexibility presents a large opportunity to reduce energy consumption, costs, and pollution. Researchers use models to better understand the impacts of load flexibility on the energy system and on occupant well-being. Many models have been developed for residential energy systems; these models incorporate parameters for energy-consuming

devices, building insulation, weather, and occupant preferences and activities. More details are provided in Section 2.1.

An ideal residential energy model would be accurate and useful in a broad context of applications. Given the broad range of devices and inputs required, it is difficult and expensive to design an accurate residential energy model for an individual building. Instead, most models are designed to resemble a typical building or a typical set of buildings in a community or region. For models with this goal in mind, we suggest that ideal models should be:

- Occupancy-based: Connect energy usage to a range of occupant activities and capture occupant stochasticity
- Physics-based: Include white-box thermal models that incorporate weather data and building envelope properties
- Interdependent: Capture the co-dependencies between thermal systems, electrical systems, and occupant behavior and their effects on energy usage
- Controllable: Modify energy usage based on external control signals and provide state information to external controllers
- Diversified: Handle a diverse set of input parameters (e.g., building envelope, occupant schedules, equipment types) in order to produce diversified outputs (e.g., diverse load profiles)
- Integrated: Leverage state-of-the-art resources and tools, including weather data, and building stock data, and device models
- Modular: Integrate into co-simulation frameworks for applications that involve multiple modeling frameworks, for example buildings, distribution grids, energy markets, and urban energy systems

- Accurate: Produce results that have low systemic error with respect to field data and survey data
- High-fidelity: Capture high-resolution patterns and features (e.g., equipment cycling)
- Computationally efficient: For running large-scale analyses with many buildings
- Transparent and reproducible: For industry adoption and acceptance in the scientific community

We denote a model with these features as an "integrated residential energy model". These features are necessary for understanding the impacts of load flexibility because of its interactions with occupant preferences, device controllers, and the electric grid. Flexible loads depend on thermal systems (e.g., HVAC loads) and on occupant activities (e.g., EV charging), both of which should be incorporated in the model to fully capture the impact of load controls.

Models that are controllable and computationally efficient can also be used for model-based controls. Model-based controls use an underlying model to determine an optimal control strategy. While these control methods can be very useful, they rely on accurate models and state information to work well. An integrated residential energy model can be used within a model-based control framework for residential applications, for example a HEMS.

As discussed in Section 2.3, one of the difficulties with model-based controls is that model inputs and parameters are difficult to estimate and can vary significantly based on occupancy and geographic location. Uncertainty can lead to suboptimal control decisions, which can limit the value of load flexibility and potentially cause occupant discomfort or inconveniences. Uncertainty in residential energy applications primarily arises from weather and occupant activity forecasts, which are needed to quantify the amount of flexibility that can be provided.

1.4 Research Objectives

The goal of this dissertation is to use residential energy modeling and controls techniques to better understand how load flexibility can be utilized in real-world scenarios. We focus on techniques that are robust when used with limited or uncertain information. This is especially critical for residential applications, as energy usage depends on stochastic variables including occupant activities and weather. The research questions for this dissertation are:

1. How can integrated residential energy models accurately capture the impacts of load flexibility on house power usage and occupant comfort?

2. How do integrated residential energy models compare against existing state-of-the-art models?

3. How can integrated residential energy models capture the impacts of distributed control strategies on grid services?

4. How can uncertainty from weather and occupancy behavior be incorporated in model-based controls for residential energy systems?

5. Do model-based controls perform better than rule-based controls for residential energy systems with flexible loads when weather and occupancy forecasts are uncertain?

Answering these questions will provide a holistic understanding of load flexibility under uncertain conditions. An integrated residential energy model and robust control techniques are necessary components of an effective model-based controller operating in real-world conditions. This research can serve as a guide for developing tools for home energy management systems and as a foundation for future studies in residential load flexibility.

Some of the work presented in this dissertation has been presented in recent publications, including one publication under review. The author's publications that contributed to this dissertation are listed here:

1. Michael Blonsky, Adarsh Nagarajan, Shibani Ghosh, Killian McKenna, Santosh Veda, and Benjamin Kroposki. Potential Impacts of Transportation and Building Electrification on the Grid: A Review of Electrification Projections and Their Effects on Grid Infrastructure, Operation, and Planning. *Current Sustainable/Renewable Energy Reports*, Dec 2019. doi:10.1007/s40518-019-00140-5.

2. Michael Blonsky, Jeff Maguire, Killian McKenna, Dylan Cutler, Sivasathya Pradha Balamurugan, and Xin Jin. OCHRE: The Object-oriented, Controllable, High-resolution Residential Energy Model for Dynamic Integration Studies. *Applied Energy*, May 2021. doi:10.1016/j.apenergy.2021.116732.

3. Michael Blonsky, Prateek Munankarmi, and Sivasathya Pradha Balamurugan. Incorporating Residential Smart Electric Vehicle Charging in Home Energy Management Systems. *IEEE Green Technologies Conference*, Apr 2021. doi:10.1109/GREENTECH48523.2021.00039.

4. Michael Blonsky, Killian McKenna, Tyrone Vincent, and Adarsh Nagarajan. Time-of-use and Demand Charge Battery Controller using Stochastic Model Predictive Control. *IEEE SmartGridComm*, Nov 2020. doi:10.1109/SmartGridComm47815.2020.9302943.

5. Michael Blonsky, Killian McKenna, Jeff Maguire, and Tyrone Vincent. Home Energy Management under Realistic and Uncertain Conditions: A Comparison of Heuristic, Deterministic, and Stochastic Control Methods. *Applied Energy* (under review).

The dissertation is organized as follows. Chapter 2 provides a background and literature review on residential modeling and controls. Chapter 3 develops a residential

energy model that can simulate flexible loads and can serve as an underlying model in a control framework. Chapter 4 develops a stochastic model predictive control framework for HEMS that includes model linearization techniques and forecasting methods. Chapter 5 validates the model against existing state-of-the-art models. Chapter 6 applies the model to building-to-grid co-simulation applications. Chapter 7 presents case studies that assess the performance of heuristic, deterministic, and stochastic control methods using this HEMS control framework. Finally, Chapter 8 summarizes the key findings of the dissertation and provides recommendations for future work.

CHAPTER 2
LITERATURE REVIEW

This chapter provides a review of literature related to the research topics of this dissertation. The literature review is divided into sections on residential energy modeling, home energy management systems, and uncertainty considerations in HEMS applications.

2.1 Residential Energy Modeling

This section reviews the existing literature related to residential energy modeling. A comprehensive residential energy model accounts for all on-site energy usage, including from HVAC, water heating, appliances, lighting, miscellaneous loads, distributed generation, and storage. Significant attention is paid to the building envelope and HVAC device models, as HVAC accounts for 46% of residential energy consumption [25] and 32% of residential electricity consumption (see Figure 1.2).

2.1.1 Building Envelope

Building envelope models describe the thermal interactions between a building and its environment. Reviews of building envelope models show that they vary considerably in their complexity and their design [26, 27]. Specifically, many envelope models are white box models, which are designed using a bottom-up, physics-based approach that uses thermodynamic equations and material properties to determine the model parameters. Black box models are designed by fitting data to a model, and grey box models are hybrid models that combine physics-based and data-driven techniques [28].

White box models commonly use an equivalent circuit model (i.e., a Resistor Capacitor or RC model) to model thermal convection and conduction, in which the resistors and capacitors correspond to heat transfer coefficients and thermal masses, respectively. Many papers that do not focus in detail on the envelope model use an RC model with few nodes, where each node is defined by a capacitor [29–33]. More complex models include more RC

parameters and other methods of heat transfer. Henze et al. describe models that vary in size from 5 to 21 nodes and include solar radiation [34]. Models calculate resistances using material properties and air film coefficients [35, 36]. Fateh et al. uses a multi-node state space model that includes long wave radiation (LWR); they also model each individual boundary of the building (e.g. walls, roof) with multiple nodes and with an internal and external film resistance [37]. Other models include infiltration and ventilation of ambient air [38], and the ability to include an arbitrary number of nodes based on the type and shape of the building [39].

EnergyPlus, the U.S. Department of Energy's flagship building model, contains the most popular and thoroughly validated building envelope model in the literature [40]. EnergyPlus uses a comprehensive set of "fundamental heat balance principles" to model a building's thermal dynamics [41]; it includes modules for multi-zone heat balance, surface temperature heat balance, air flow between zones, sky temperature, shading, daylighting, window transmittance, and humidity. Multiple papers rely on EnergyPlus to develop their own building envelope models [27, 42, 43]. It has been validated against industry standard tests and field data in multiple studies [44–46]

Black box and grey box approaches to building modeling often result in more simplified models. Jimenez et al. use the Auto-regressive Moving Average Exogenous (ARMAX) method for system identification to develop a 2-node state space building model [47]. A similar model is used with a linear least squares approach in [48]. Grey box approaches are effective at evaluating the performance of varying model complexity [49]. They can also be used with a Kalman Filter or other estimation techniques to improve model accuracy over time [50, 51]. More complex models have been fitted to data using a genetic algorithm approach [35, 52].

2.1.2 HVAC Equipment

HVAC equipment models use information from the building envelope model to calculate heat flows and energy consumption for space heating and space cooling. HVAC equipment

control the indoor air temperature, which is an output of envelope models [29, 31, 34]. Some multi-zone models include multiple areas with separate temperatures that are controllable with HVAC equipment, although this is much more common for commercial buildings than for residential buildings [37, 39]. Many HVAC models also use signals for outdoor temperature and indoor and outdoor humidity to determine heating and cooling requirements and equipment efficiency [41, 53].

HVAC equipment models can be characterized by the type of equipment modeled and by the algorithm for determining the equipment capacity, which we define as the instantaneous amount of heating or cooling delivered by the HVAC equipment. Models can be generalized and used for many types of HVAC equipment [54, 55]. Some models use a constant (i.e. static) capacity for the HVAC equipment and allow the equipment to turn on and off using a thermostat control with a deadband. This method is often used for simplified models and for equipment with limited controllability like electric baseboard heaters, and electric and gas furnaces and boilers. Some models for heat pumps, air conditioners, and other equipment with a compressor cycle use a dynamic algorithm in which the equipment capacity depends on indoor and outdoor temperatures, humidity, and air flow rates [41, 53]. These models use a biquadratic equation to update the capacity and efficiency of the HVAC equipment at each time step to capture the impacts of indoor and ambient conditions.

Some HVAC models use an "ideal" capacity algorithm to perfectly achieve a given setpoint temperature. These models do not account for equipment cycling and are more commonly used for simulations with a low time resolution [41]. When using a state space building envelope model, the ideal HVAC capacity can be computed with a linear function using the state equation to solve for the HVAC capacity input [55].

Air source heat pumps are particularly important to model given their high efficiency and importance in electrification trends. While ASHPs in cooling mode are the same as air conditioners, modeling ASHP heating is challenging. ASHPs usually include a heat pump

to extract heat from ambient air as well as an electric resistance heating element that is less efficient and used when outdoor conditions are very cold. The heat pump and electric resistance elements can be on separately or simultaneously. Defrost requirements are also critical to modeling an ASHP's capacity and efficiency during cold outdoor conditions [41].

Many commercial HVAC systems use variable air volume systems that can vary the flow rate and temperature of conditioned air to multiple zones within the building. While commercial HVAC models often include variables for controlling flow rates [34, 56–58], residential models rarely do and instead model the HVAC capacity without calculating the flow rate or supply temperature. However, detailed residential models include parameters for air flow rates and fan power, which can vary with capacity and influence the efficiency and energy consumption of the equipment [41].

HVAC models rely on a variety of inputs and parameters, including the building envelope parameters, equipment capacity and efficiency, and weather conditions. In particular, HVAC models depend on the heating and cooling setpoint temperatures, which may depend on occupancy, occupant comfort preferences, time of day, or time of year [59, 60].

2.1.3 Water Heater Equipment

Compared the HVAC equipment, there is significantly less literature on models for water heating and other energy end uses, and these models tend to be simpler. Water heating models often follow the same logic as HVAC models, where a water tank model is the equivalent of the building envelope, and the water heater capacity and controls depend on the water tank temperature. Hao et al. suggest that any TCL, including HVAC, water heating, and refrigeration, can be modeled like a battery, with the temperature state modeled equivalently to a battery state of charge (SOC) [55].

The water tank model accounts for heat injected by the water heater, convection losses, and heat transfer due to hot water draws. Most water tank models use a single node [32, 61] or two nodes [29]. Multi-node models have been shown to improve accuracy [62].

Simpler models do not use a thermal model and instead use data or a water draw profile to determine energy usage [63].

Electric resistance water heaters and gas water heaters are the most common equipment types and are typically modeled as static capacity equipment. Thermostat control logic based on the water tank temperature (and sometimes the rate of change of these temperature) determines when the equipment turns on and off [61]. When modeling a water tank with two or more nodes, electric resistance water heater models usually include an upper and a lower heating element to accurately represent real products. These models require additional logic to control both elements, as most systems do not allow both elements to be on at the same time [64].

Heat pump water heaters (HPWH) share many features with air source heat pumps, including higher efficiency levels and additional control logic due to multiple methods of heating. HPWH products typically have a heat pump element as well as an upper and lower electric resistance heating element. Manufacturer control logic is typically very complex and only turns one element on at a time to reduce the maximum power output. HPWH models include up to 12 thermal nodes for improved accuracy and to model the heat gains of the heat pump element [65]. Lab testing has shown complex control logic is required to accurately model HPWH modes for some products [64].

The frequency, timing, and quantity of hot water draws are key inputs in a water heater model. Models tend to use real or simulated water draw profiles that represent a combination of hot water uses in a residential building. Simulated data are typically taken from a Markov chain-based occupancy model [66] or from the Domestic How Water Event Schedule Generator [67].

2.1.4 Electric Vehicles

While most residential building models focus on HVAC and other traditional loads, many studies have started considering electric vehicles (EVs) as a key component of residential energy consumption. The simplest models treat electric vehicles like most other

miscellaneous loads, using a static load profile that is not controllable. Other models treat the EV as a battery and track the EV SOC and the energy consumption used to charge the EV.

More advanced EV models account for variability in occupant schedules, driving needs, and weather conditions. One such model, EVI-Pro [68], uses survey data to build a database of residential EV charging events that include the parking start time, parking duration, and initial SOC of the EV. These parameters vary based on the type of EV (battery vs. plug-in hybrid), the EV range, and the charging level (Level 1 or Level 2). They also vary by day of the week, which impacts driving patterns, and the ambient temperature, which impacts the efficiency of driving.

2.1.5 Appliances, Lighting, and Other Loads

Appliances, lighting, and miscellaneous laods typically consume less energy than HVAC and water heating in residential buildings as shown in Figure 1.2. Most building models treat these loads as uncontrollable and prescribe an energy consumption schedule [30, 69], or do not consider them at all. Some papers include freezers and refrigerators as thermostatically controlled loads [55, 63]. McKenna and Keane use a 1-node model for these loads to model their controllability [29].

More detailed appliance and lighting models rely heavily on occupancy-based methods. Richardson et al. describe appliance and lighting models that use a stochastic assignment method to map activities to appliance use and house location [66, 70]. They use a Markov chain occupancy model for determining occupant activity, including the impacts of multiple occupants and correlations between activities. Switch-on probabilities are used for both lighting and appliances, and the lighting model accounts for natural light, efficiency levels, and the sharing of lit indoor spaces. These and other papers rely on time-use survey data to develop their occupancy models [29, 71].

2.1.6 Distributed Generation and Storage

Distributed Generation: As with EVs, holistic residential energy models have started incorporating distributed generation (DG) models to better understand their impact on net residential energy usage. Rooftop PV is the most common DG technology to include. As with appliances and lighting, many PV models are simple and rely on a prescribed schedule [30] or are proportional to solar irradiance [33]. Li and Wen include a PV model from Sandia National Laboratory that accounts for irradiance and temperature [26, 72]. Other papers use specific tools for generating PV generation profiles, including PVwatts [43, 73, 74] and SAM [75]. Other modeled distributed generation technologies include wind [30] and backup generators [33].

Batteries: Despite small adoption rates in residential buildings, electrical and thermal storage systems are included in many residential energy models. Battery models typically account for the battery SOC and efficiency [33]. More complex models may incorporate the battery terminal voltage [26, 76] or degradation [77]. Batteries may have a prescribed charge and discharge schedule [30], a controller to lower customer energy costs [77, 78], or more complicated controllers as discussed in the next section.

Battery models may include the impacts of battery cycling, temperature, and other conditions on battery performance and degradation. Detailed models for specific battery chemistries and configurations include many chemical, electrical, and thermal parameters [76, 79]. Many papers use lumped models for packaged battery products and general applications. Some models include a one- or two-node thermal model to track internal battery temperatures [78, 80, 81]. Battery temperatures and cycling behavior lead to capacity degradation, which may be more significant when batteries are installed outside or in unconditioned spaces [82].

Thermal Storage: Thermal storage may be considered a separate element of a building model or a feature of the building envelope or water tank model [69]. Fateh et al. study the effects of phase-change materials by incorporating their additional thermal mass into

their RC thermal model [37].

2.1.7 Integrated Residential Energy Modeling

As discussed in Section 1.3, building models are often split between models that focus on a specific building and models that resemble a typical set of buildings within a region. Few residential models are designed for a specific building due to the difficulty in collecting building parameters. For typical building models, McKenna and Thomson provide a comprehensive list of model requirements [31]:

- High temporal resolution
- Demand diversity (across multiple buildings)
- Dependency within and between buildings (e.g. occupancy and weather)
- Stochastic modeling
- Activity-based models
- Accuracy and computational efficiency
- Low-order thermal models
- Transparency and reproducibility
- Urban energy system modeling (e.g. water, transportation)

Other papers include additional requirements and features for residential energy models. Good et al. add key features of separating energy services and inputs (e.g. electricity and fuel) and estimating thermal storage capabilities [69]. McKenna and Keane add the need for controllable device models and a time-variant electrical load model for demand response applications [29].

There are a few tools used in the literature for integrating residential energy models with other simulators and controllers. The Building Control Virtual Test Bed is used to

integrate EnergyPlus building models with various types of controllers [83–85]. Spawn-of-EnergyPlus is another control framework under development by the Department of Energy Building Technologies Office [86]. GridLab-D [87] is a distribution system simulator that includes a simple building model and can co-simulate building and distribution grid systems. HELICS [88] is a new co-simulation platform that has been used to integrate OpenDSS [89] grid models, DER models, and controllers [90].

2.1.8 State Space Model Techniques

Many of the device models described above use linear, time-invariant state space models of the form:

$$\begin{aligned} \dot{x}(t) &= Ax(t) + Bu(t) \\ y(t) &= Cx(t) \end{aligned} \tag{2.1}$$

where x is the state vector, u is the input vector, y is the output vector, and A, B, and C are the state space matrices.

Building envelope and water heater tank models have temperatures as states, while battery and EV models have battery SOC as a state. Other state variables include the current status of appliances or occupant activities, although models with these states are often nonlinear, for example Markov chain-based models.

Linear state space models offer useful techniques for simplification and estimation. Model reduction is a common technique that reduces the number of states in a model while minimizing the difference in the norm of the Hankel operator between the reduced and original model [91]. Balanced model reduction is a common method used in reducing building models for model predictive control [39, 84].

Another common technique for model simplification involves linearization. Models often include bilinear terms due to HVAC heat flows [34, 56–58, 69] and solar irradiance through window blinds [92]. Equipment with discrete operating states (e.g., on and off) or with requirements for minimum on-time or off-time are sometimes modeled without these features [32, 93]. Other nonlinearities arise from long wave radiation [39], infiltration [38],

battery degradation [33], and device efficiency [43].

Building modeling research leverages the large field of research using state space models for state estimation and parameter estimation (i.e., system identification) [26]. State estimation usually involves a version of Kalman filtering [94], including linear Kalman filtering [83, 92, 95] for linear systems, and Extended Kalman filtering [26, 50] or unscented Kalman filtering [51, 96] for nonlinear systems. Maasoumy et al. show that unscented Kalman filtering outperforms extended Kalman filtering for some building modeling applications [97]. Parameter estimation methods tend to be grey box methods [98], including using a genetic algorithm [35, 52], and Kalman filters [49, 51, 96].

2.2 Home Energy Management Systems

One of the primary reasons for modeling energy usage in residential buildings is to use these models in residential building controls to enable load flexibility. Beaudin and Zareipour provide a comprehensive review of Home Energy Management Systems (HEMS), which they describe as a "demand response tool that shifts and curtails demand to improve the energy consumption and production profile of a house according to electricity price and consumer comfort" [99]. This section broadly describes the main methods for HEMS, individual device controls, and related control applications, and reviews the current limitations for HEMS.

2.2.1 HEMS Control Methods

According to [99], model predictive control (MPC) is by far the most common methodology for HEMS. MPC determines an optimal control strategy given a model, constraints on model states and inputs, and a forecast of future inputs for a finite horizon. MPC is typically solved in a "receding-horizon manner" in which only the current control strategy is implemented, and the optimization is re-solved at the next time step with an equally long forecast horizon [100]. While there are many techniques within MPC, the most common usage within HEMS applications include [99]:

- Pricing scheme: Time-of-use (TOU), Real-time dynamic pricing
- Objectives: Energy cost, energy consumption, emissions, occupant comfort or well-being
- Uncertainty: None, robust optimization, stochastic optimization (see Section 2.3.4 for details)
- Optimization type: Mixed-integer linear programming (MILP), linear programming (LP), quadratic programming (QP), heuristic methods
- Time resolution: 24-hour horizon with 1-hour, 15-minute, or 6-minute time steps

Objective functions used in HEMS optimization vary considerably in the literature and have a significant impact on the control strategy and outcomes. Energy cost and occupant comfort are the most common objectives to consider. Energy costs include electricity costs, gas costs, peak demand charges, and carbon emissions [59, 101]. Comfort objectives include air temperature and hot water temperature [32, 102]. Other objectives involve equipment degradation [103], load flexibility [104], PV curtailment [105], and self-consumption of DG or the amount of grid imports or exports [32, 106]. Most papers use a multi-objective approach, either using a weighted sum of objectives or by bounding objectives by converting them into optimization constraints [99]. Studies on survey methods have shown that relative weighting of objectives can effectively align the optimization with customer preferences [59, 107].

The complexity of the objective function and underlying building and device models greatly impact the optimization type and the computational needs for solving the control problem. Linear models are a necessary condition for most optimization types including LP, MILP, and QP. Objectives with linear terms for energy costs and thermal comfort enable LP optimization, which is the fastest optimization type. Some papers use QP to enable a quadratic relationship with thermal comfort for air temperature and water

temperature [32, 59, 104]. LP and QP are convex optimization types, which guarantee that an optimal solution is globally optimal [108]. MILP is necessary for equipment models with Boolean constraints due to on/off characteristics, fixed cycle durations, or minimum and maximum on-times; these features are often used for appliances and sometimes used for HVAC, water heating, or EV charging [102, 103, 106]. Computational requirements depend heavily on the optimization type, as well as the horizon time and time resolution, which can be a factor in determining the MPC objective in some applications [99].

Non-MPC control methods for HEMS include heuristic methods and optimization methods that do not involve a forecast horizon. Some optimization methods are very similar to MPC but do not use a receding time horizon [102].

2.2.2 Device Controllers

As more residential energy devices develop capabilities for control, there is a larger need to integrate a diverse set of models and controllers in a HEMS framework. We discuss here the literature on individual control strategies for HVAC, water heaters, PV, batteries, EVs, and smart appliances.

HVAC and Thermostats: Most HEMS controllers involve space heating and/or cooling control, and many papers only consider HVAC and no other equipment [28]. Most controllers assume a continuous HVAC capacity [84, 96], although some assume on/off behavior that leads to a mixed-integer optimization [109]. It is rare for residential HVAC controllers to consider non-linearities in HVAC capacity or efficiency based on temperature or flow rate. Most papers include energy costs and air temperature comfort in the objective [59]. Temperature comfort is sometimes considered a soft constraint to prevent optimization failures in extreme conditions [51, 96].

HVAC control signals depend on the type of HVAC models used. Most HEMS papers do not specify the exact control signal sent to the HVAC model. Some controls send a temperature setpoint signal, which "ideal" capacity HVAC models will follow exactly, if feasible [56, 110]. Others send a direct load control signal to turn the equipment off

[55, 109], or a duty cycle control to fix the energy consumption of the equipment rather than the temperature [104, 105]. Real HVAC products have been shown to follow direct load control signals and thermostat setpoints, but not duty cycles.

Smart Water Heaters: Water heater controls are often similar to HVAC controls. Water heaters are either modeled with a continuous capacity (for linear models) or a fixed capacity with on/off behavior (for mixed-integer optimization). Water temperature is sometimes included in the objective [59, 109] or in the constraints to account for occupant comfort. Water heater control signals can be temperature setpoints, duty cycles, or a direct load control signal, although the exact control signal is often not specified.

PV and Batteries: There has been extensive literature on PV and battery controls (both separate and combined), mostly focused on commercial-, industrial-, or utility-scale systems. On-site commercial and industrial systems are often used to save money for the asset owner by arbitraging energy prices and reducing peak demand. Others incorporate value streams for grid services including demand response, resource adequacy, and voltage regulation [111–113].

Residential PV and battery systems within HEMS are often controlled to reduce energy costs and to maximize PV self-consumption [59]. They have also been used to provide load flexibility services to a DER aggregator [104, 106]. PVs with smart inverters can also provide reactive power for voltage regulation services [114, 115]. Control signals tend to be real and reactive power setpoints for the PV and battery models to follow.

Electric Vehicles: Many studies have shown the benefits of residential EV charging control coupled with other controllable devices. Some papers use a coordinated approach for an aggregation of EVs within a region to reduce peak demand or provide ancillary services to the grid [116, 117]. Others include similar control strategies for commercial charging stations with multiple EV chargers [118–120]. Studies that focus on a single household tend to use MILP optimization to dispatch flexible devices and a hard constraint for the EV SOC at the departure time [73, 121–123]. Mirakhorli and Dong [124] use MILP

for a HEMS that considers energy costs as well as soft constraints for EV SOC. Mixed-integer optimization techniques are also used to enforce discrete charging levels for EVs [125].

Smart Appliances: Similar to EVs, smart appliances are less common in MPC frameworks and are often optimized using mixed-integer techniques. Most papers use mixed-integer constraints to ensure that appliances are on for a certain duration and do not cycle [122, 126]. Others allow for cycling [127] or require a minimum on-time and minimum down-time [101].

2.2.3 Related Control Applications

Compared to other energy-related controls applications, there is relatively little literature on HEMS. There is more literature in the related areas of commercial building energy management systems [56, 128, 129] and demand side management (DSM) strategies for the electric grid [121, 130–133]. There is also some overlap with distributed energy resource management systems (DERMS) and utility-scale PV and battery controls. Although HEMS focuses on the objectives of the homeowner rather than commercial building owners and operators, utilities, DER aggregators, or power producers, there are many similarities across these control areas and insights from these areas can be leveraged to expand understanding in HEMS controls.

2.2.4 HEMS Limitations

While many studies have shown that MPC is an effective control strategy for HEMS, limitations exist that few studies have addressed. Beaudin and Zareipour identify difficulties in controlling a diverse set of devices, in handling multiple objectives, in handling forecast uncertainty, and in implementation in hardware [99]. We discuss device diversity and uncertainty in the sections 2.2.2 and 2.3, respectively.

The U.S. Department of Energy's Building Technologies Office presents additional limitations around underlying building models for MPC. They write that models "are

unable to represent and simulate the performance of actual control sequences because they model buildings under idealized conditions instead of actual operations, and with deterministic rather than stochastic outputs." MPC requires models that are "simple enough" to enable optimization with limited computational resources and that are sufficiently accurate. White box models tend to be overly complicated, while grey- and black-box models depend on the quality and quantity of training data and may not be able to handle extreme conditions. Model generation is a time- and resource-intensive process that is difficult to scale. Finally, MPC has only been "demonstrated in buildings for limited conditions," primarily for HVAC [86].

2.3 Uncertainty Considerations in HEMS

Residential energy modeling requires a variety of inputs and parameters, including weather inputs, building envelope parameters, equipment parameters, and occupant behavior and preferences. These parameters can vary significantly for different homes and can be difficult or expensive to estimate. Weather and occupant behavior are especially important in estimating energy consumption, and both are stochastic and difficult to forecast. Given these challenges, it is inevitable that uncertainty exists when modeling and controlling residential systems. Incorporating uncertainty often leads to more conservative control strategies that reduces the risk of high energy costs or occupant discomfort, but that also reduces the amount of available flexibility. In this section, we describe the sources of uncertainty in HEMS applications.

2.3.1 Forecast Uncertainty

Forecasts for weather and occupant behavior likely have the largest amount of uncertainty in residential applications due to their stochastic nature. Residential energy consumption is highly dependent on both occupant activity and weather, making these forecasts critical pieces of information when optimizing for future control decisions. For example, preconditioning air to shift HVAC consumption away from a peak demand period

requires knowledge of weather variables that are used to calculate required HVAC loads [56, 105]. Other examples include preheating a water heater before a large water draw event [134] or charging an EV such that it is fully charged before the occupant leaves [120].

Weather Modeling: HEMS algorithms without uncertainty use a deterministic weather forecast, meaning the optimization assumes that the weather forecast is exact. Most papers use the same weather data in the forecast and in the building model. Some papers adjust the forecast data with random noise to account for forecasting errors [51].

Some HEMS papers use more advanced weather models. Zhang et al. use forecast data and an auto-regressive model to create a more realistic weather forecast [58]. Another paper uses a similar method for commercial building controls [92]. Pedersen and Petersen use detailed weather data including multiple weather forecast ensembles to forecast and determine the uncertainty of weather variables [83]. Other models are discussed in [26].

State-of-the-art weather forecasting techniques tend to have either high reliability and low resolution or low reliability and high resolution [135]. Numerical weather prediction ensembles offer high resolution and low reliability and are typically used for weather forecasts. The National Weather Service and the European Centre for Medium-Range Weather Forecasts include datasets that may be useful for evaluating algorithms that use weather forecasts [136, 137].

Occupant Modeling: Similar to weather forecasting, most HEMS algorithms assume a deterministic occupant forecast, or they do not consider the effects of occupancy at all. Some papers use a low-resolution profile or a time-average profile for loads and internal heat gains to estimate an occupancy forecast [58]. Others use an exact profile that is unreasonable to use in real systems given the uncertainty in occupant behavior.

Many papers use Markov chain techniques to estimate occupant behavior, although the complexity of these models varies considerably. Most papers use a first-order [29, 71, 138] or higher order [83] time-inhomogenous Markov chain that varies by time of day and day of week. Others use related methods for modeling specific activities [73, 139]. The Markov

process can incorporate occupant presence (i.e. present or absent) [71], specific occupant activities [29, 70], or an aggregation of "other" energy consumption [32]. It is also effective in modeling discrete and discontinuous occupancy patterns, for example, hot water draws or discrete activity changes such as plugging in an EV or turning on an oven [140]. Most papers cite time-use surveys for underlying data of the occupancy model [138].

Other methods for occupancy modeling use occupancy measurement data. Multiple studies use occupancy sensor data to develop models and estimators for commercial buildings [28]. A review on occupancy and comfort describes many dimensions of occupant comfort that are not typically considered in HEMS controls [60].

In many papers, forecast uncertainty is quantified using heuristics [123] or is not defined at all. Auto-regressive moving average models have been used to estimate uncertainty for weather variables [132, 141, 142] as well as for occupancy variables [60]. Other forecasting methods usually do not quantify uncertainty, for example, sophisticated weather forecasts [73, 92] and Markov chain-based stochastic occupancy models [71, 141].

2.3.2 Model Uncertainty

An MPC framework requires an underlying model that represents the system, but it is often an imperfect approximation of the system. Many MPC frameworks use a linear model, which is required to use fast and convex optimization methods, including linear programming, quadratic programming, and mixed-integer linear programming methods [99, 143, 144]. Linear models must either simplify or ignore nonlinearities such as device efficiency parameters, device degradation, and radiative thermal processes. Models for specific homes often lack detailed data, including envelope and equipment parameters as well as training data for black box models, which can lead to inaccurate model parameters [71, 96]. Because every house is different, it can be very time consuming and costly to create an accurate model representation [145].

Another key source of uncertainty is the time resolution of the model and the MPC controller. Time resolutions may be constrained by the time resolution or update frequency

of the forecast, by measurement or actuator update rates, or by the computational complexity of the MPC algorithm. Time resolution may also be purposefully reduced to eliminate the need to consider fast system dynamics, for example, equipment cycling behavior or high-resolution occupant activities [31]. Although low-resolution controllers might work well for some objectives—for example, reducing energy costs with an hourly electricity price—they are likely to reduce the performance of any objective with real-time impacts on the occupant, for example, thermal comfort or convenience associated with EV charging.

2.3.3 Measurement Uncertainty

Uncertainty can also arise from sensor measurements [97, 146]. Sensor noise is not typically an issue, but sensors can have low time resolution or low precision, which leads to reduced control performance. Sensors can also be biased, especially if the sensor is not directly capturing the variable of interest. For example, a thermostat located near a vent or a sunny window might report a temperature that is not accurately representing the house temperature [60]. Some sensors might also have limited communication abilities, for example, an EV charger that can only measure the EV SOC when the vehicle is parked and plugged in.

2.3.4 Control Methods that Incorporate Uncertainty

As mentioned in Section 2.2.1, many HEMS frameworks do not incorporate uncertainty in their optimization function. Uncertainty is most commonly included for HVAC controllers. Robust optimization is the most common method for incorporating uncertainty in HEMS, likely due to its relative simplicity. Robust optimization minimizes the cost of the "worst-case scenario" by using the worst-case value of uncertain parameters. While beneficial for risk-averse problems, this method may not be the most cost-effective solution [99].

Maasoumy et al. use robust control to handle model uncertainties, and use an Unscented Kalman Filter to estimate model parameters and states at a slower rate than the MPC [96]. A related paper shows that robust MPC outperforms deterministic MPC and rule-based controls for moderate levels of uncertainty [57]. Robust control has also been shown to handle uncertainty in weather [147].

In contrast, stochastic optimization considers the probability distribution of uncertain variables to reduce the risk of exceeding certain limits. Stochastic model predictive control (SMPC) (also referred to as chance-constrained optimization [99] and conditional value at risk [122, 127]) optimizes to minimize costs at a chosen risk tolerance level. SMPC also includes "chance constraints" that ensure hard constraints are met with a certain probability.

SMPC is often used with scenario-based methods to determine the probability distribution of uncertain variables [148]. Pederson and Peterson use stochastic control and scenario-based (i.e. ensemble) Kalman Filtering to control HVAC with uncertainty in the outdoor air temperature, solar irradiance, and energy use due to occupancy [83]. Stochastic dynamic optimization and other multistage optimization methods optimize over a set of discrete state transitions, which can greatly increase the computational complexity of the controller [73, 99].

Some papers assume a probability distribution rather than using scenario-based methods. Multiple papers assume a Gaussian distribution in uncertain inputs including irradiance and dry and wet bulb temperature [92, 123]. Other distributions are used for PV irradiance [122]. Zhang et al. show that scenario-based MPC outperforms deterministic MPC as well as SMPC with Gaussian assumptions [58].

Papers on HEMS often focus on novel control architectures and their performance benefits over existing strategies, but they pay little attention to quantifying uncertainty in their simulations or to assessing its impact on their findings. A study on commercial building heating, ventilating, and air-conditioning (HVAC) controls found that DMPC

performed best at low levels of uncertainty, robust MPC performed best at intermediate levels, and heuristic controls performed best at high levels [57]. The authors are not aware of any similar studies on residential buildings or on non-HVAC devices.

CHAPTER 3
INTEGRATED RESIDENTIAL ENERGY MODELING

This chapter presents the Object-oriented, Controllable, High-resolution Residential Energy (OCHRE) model, a Python-based framework for simulating residential energy systems. OCHRE includes a building envelope model, models for individual energy-consuming devices, and a voltage-dependency model. The author's contributions to the OCHRE model include conceptualization, software development, testing, and validation.

Section 3.1 outlines the components of the OCHRE model. In Section 3.2, we show case study results for a sample building. Finally, we summarize the benefits of the model for grid studies, and additional use cases for the model. Note that additional case studies are shown in Chapter 6.

3.1 OCHRE Model Description

In this section, we describe the components of the OCHRE model, including the building envelope, HVAC system, water heater, EV, other loads, PV, and battery. Figure 3.1 and Figure 3.2 show a schematic of the building envelope, and Table 3.1 provides an overview of the equipment models and their key parameters.

3.1.1 Building Envelope

OCHRE represents the residential building envelope using an equivalent circuit model (i.e., an RC model) as shown in Figure 3.2. Capacitors represent the thermal mass of a node, which is either an air zone (e.g., garage) or a physical boundary between zones (e.g., walls, floor). Resistances correspond to thermal resistances between different masses and include the effects of conduction and convection. All parameters are calculated from the dimensions and thermal properties of building materials, making the envelope a fully white-box model.

To improve the accuracy of the thermal model, most boundaries have multiple nodes similar to the model in [37]. We use up to six resistors and four capacitors for some boundaries, including for the external walls, the foundation, and the roof. These parameters allow the model to account for temperature gradients and different heat transfer coefficients from different materials within a boundary. Two resistances at the edge of the boundary account for the film resistance and are critical in accurately modeling the solar and long-wave radiation gains injected into the building's surfaces. Figure 3.3 shows a schematic of the reduced-order external wall boundary with four materials and separate film coefficients on the interior and exterior of the wall.

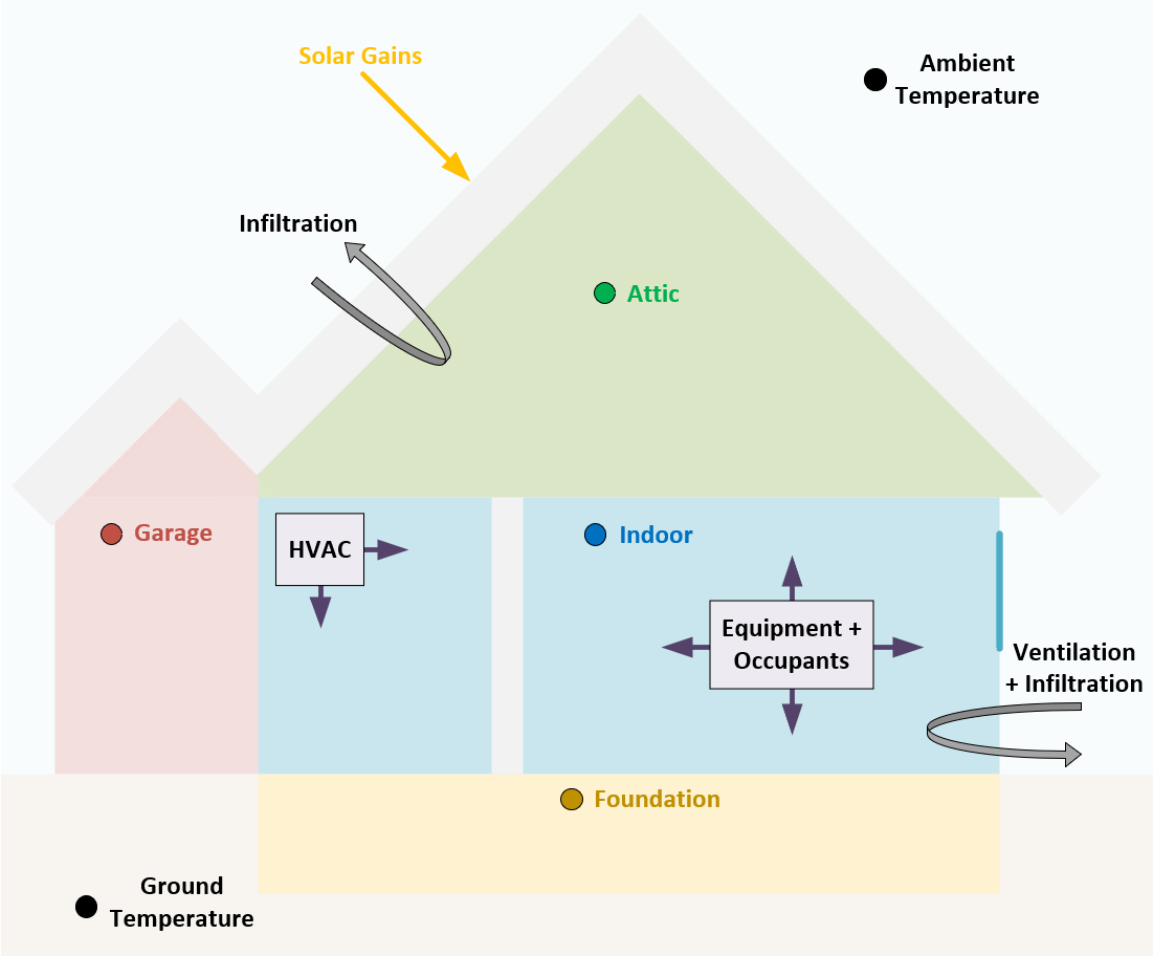

Figure 3.1 Schematic of the OCHRE envelope model showing the main thermal zones and main heat transfer mechanisms.

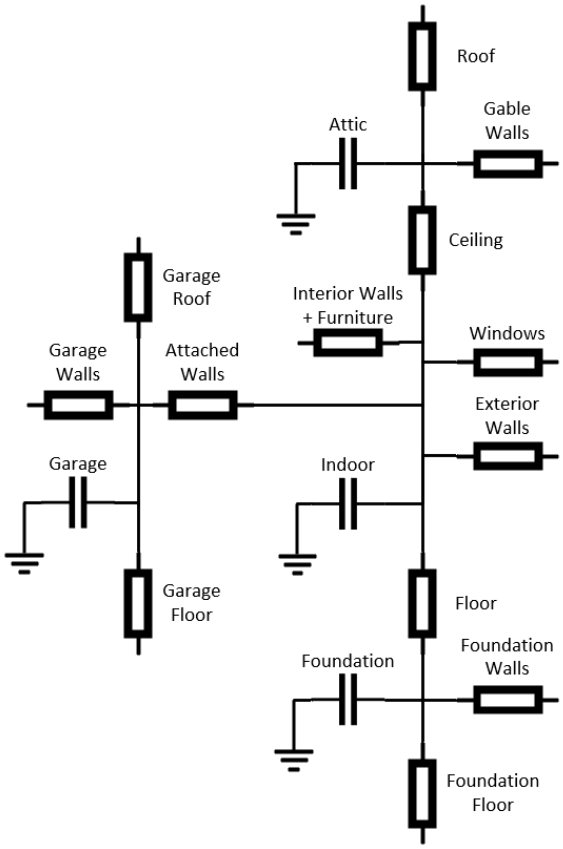

Figure 3.2 Schematic of the OCHRE envelope RC model showing all conduction/convention pathways. See Figure 3.3 for more details on an individual boundary.

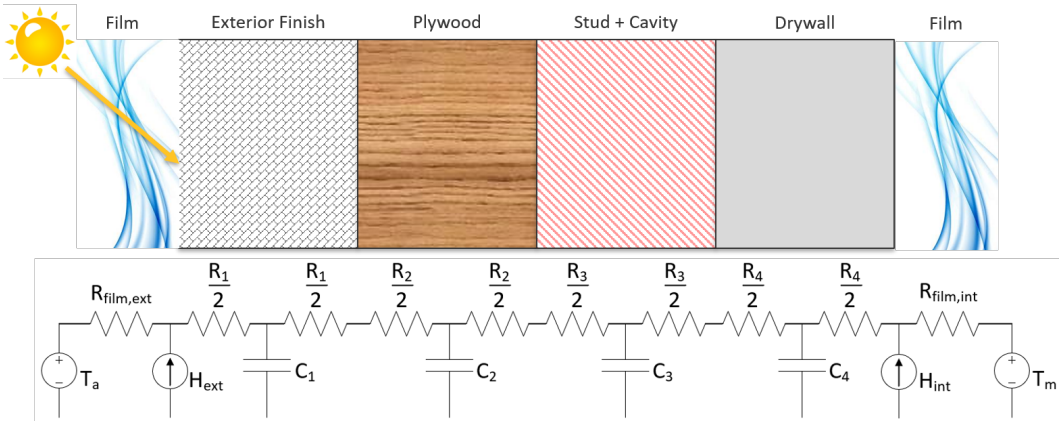

Figure 3.3 Schematic of a boundary in the envelope model. T_a is the ambient temperature, and T_m is the main indoor temperature.

We define a thermal model with n_x interior nodes and n_{ext} exterior nodes. Interior nodes are within the building envelope and have a corresponding thermal mass; exterior nodes do not have a thermal mass and are prescribed by a time-series schedule (e.g., outdoor temperature). The heat equation for the interior node i is:

$$C_i \frac{dT_i}{dt} = \sum_{j=1}^{n_x+n_{ext}} \frac{T_j - T_i}{R_{ij}} + H_i \tag{3.1}$$

where T_i is the temperature at node i, T_j is the temperature at node j, C_i is the thermal mass of node i, R_{ij} is the thermal resistance between nodes i and j, and H_i is the sensible heat injection into node i. If necessary, resistances are combined in series to determine R_{ij} (see Figure 3.3). Note that the thermal resistance between disconnected nodes is considered to be infinite, and $R_{ii} \equiv 1$.

We reconfigure the thermal model into a linear, discrete-time state space system with state equation:

$$x(k+1) = Ax(k) + Bu(k) \tag{3.2}$$

where the states x and inputs u are defined as:

$$x = \begin{bmatrix} T_1 \\ \vdots \\ T_{n_x} \end{bmatrix} \qquad u = \begin{bmatrix} T_{n_x+1} \\ \vdots \\ T_{n_x+n_{ext}} \\ H_1 \\ \vdots \\ H_{n_x} \end{bmatrix} \tag{3.3}$$

where the index $i \in [1, n_x]$ corresponds to an interior node, and $i \in [n_x + 1, n_x + n_{ext}]$ corresponds to an exterior node. The continuous time matrices $A^{(c)} \in \mathbb{R}^{n_x \times n_x}$ and $B^{(c)} \in \mathbb{R}^{n_x \times (n_x+n_u)}$ are derived from Equation (3.1) and then used to discretize the system at a given time step:

$$\begin{aligned} A &= e^{A^{(c)} T_s} \\ B &= {A^{(c)}}^{-1}(A - I)B^{(c)} \end{aligned} \tag{3.4}$$

As shown in Figure 3.1, sensible heat injections arise from solar radiation, heating or cooling delivered from HVAC, air infiltration and ventilation, long-wave radiation, and heat gains from occupants and energy-consuming equipment. Solar radiation heat gains depend on absorptivity parameters (or transmittance for windows) and are assumed to be injected into the outermost node of the external boundaries. Solar radiation through windows is injected into the interior walls and the floor nodes.

Long wave radiation is considered at each exterior and interior boundary surface. The radiation equation for the surface of boundary material i is:

$$H_{iz,rad} = \epsilon_i \sigma a_i (T_{z,rad}^4 - T_{s,i}^4) \tag{3.5}$$

where $H_{iz,rad}$ is the heat transfer away from boundary i, ϵ_i is the emissivity of material i, a_i is the area of the material i, $T_{z,rad}$ is the effective zone temperature, $T_{s,i}$ is the surface temperature, and σ is the Stefan-Boltzmann constant. For exterior surfaces, the effective zone temperature accounts for the ambient and sky temperature [41]. For interior surfaces, the effective zone temperature is a weighted average of all surface temperatures within the zone, weighted by their respective area. OCHRE uses an iterative nonlinear equation solver to calculate the surface temperatures and the radiation heat transfer.

We use the Sherman-Grimsrud model [38] to determine the heat gains from infiltration and ventilation in the living space, garage, and attic. We use a constant flow rate infiltration model for crawl spaces and basements.

Moisture is also tracked using a mass balance to determine indoor humidity and wet-bulb temperature, which is an important variable for simulating heat pump-based HVAC equipment. Occupant and equipment heat injections use constant sensible and latent heat gain fractions and hourly schedules taken from the Building America House Simulation Protocols [149].

OCHRE can simulate multiple zones, including an unfinished attic, a basement or crawl space, and an attached garage. When an attached zone is included, the RC network is expanded to include any additional boundaries. These zones have their own space

temperature, thermal mass, and heat injections. Modeling unconditioned zones captures interactions between the zone and any equipment within it, such as a water heater in a basement. In the most complete case where all of these unconditioned zones are included, the full network will include 50 resistors and 41 capacitors.

3.1.2 HVAC Model

OCHRE can model many HVAC equipment types, including electric and gas furnaces, boilers, electric baseboard heaters, and air source heat pumps (ASHPs). We describe the single-speed ASHP model in detail. We note that the other models follow a similar logic. The model used here is based on the model used in EnergyPlus [41].

The capacity and efficiency of ASHPs vary with the indoor temperature, outdoor dry-bulb temperature, and the HVAC air flow rate. We use a biquadratic model from [53] to calculate the instantaneous HVAC capacity κ_{hvac} and energy intensity ratio (EIR) $\frac{1}{\eta_{hvac}}$:

$$\begin{aligned} \kappa_{hvac} &= \kappa_{hvac,0}(a_0 + a_1 T_m + a_2 T_m^2 + \\ &\qquad a_3 T_a + a_4 T_a^2 + a_5 T_m T_a) \\ \frac{1}{\eta_{hvac}} &= \frac{1}{\eta_{hvac,0}}(b_0 + b_1 T_m + b_2 T_m^2 + \\ &\qquad b_3 T_a + b_4 T_a^2 + b_5 T_m T_a) \end{aligned} \tag{3.6}$$

where $\kappa_{hvac,0}$ is the rated HVAC capacity, $\eta_{hvac,0}$ is the rated coefficient of performance (COP), T_m is the indoor temperature (wet-bulb for cooling, dry-bulb for heating), T_a is the ambient dry-bulb temperature, and a_i and b_i are coefficients taken from [53]. Different parameters are used in Equation (3.6) for heating and cooling modes, including the rated capacity and rated EIR. Note that EIR is the ratio of electrical energy input to heating or cooling delivered, or the inverse of the COP.

When the HVAC system is on, the heating or cooling delivered to the living space $H_{hvac,m}$ is equal in magnitude to κ_{hvac} and is positive when heating and negative when cooling. When operating in cooling mode, the sensible heat ratio (SHR) splits κ_{hvac} into sensible and latent components, and it is dynamically calculated using the apparatus dew point/bypass factor methodology [53].

The heating model captures the performance impacts of low outdoor air temperatures. It includes a reverse cycle defrost and a supplemental electric resistance element that turns on if the ASHP does not have enough capacity to maintain the indoor air temperature. We refer readers to [41] for details.

We use a thermostat control with a deadband to determine when the HVAC equipment turns on and off. The thermostat control uses the main indoor dry-bulb temperature T_m from the building envelope system state. We also enforce a minimum on and off time to reduce equipment cycling.

The thermostat control breaks down at low time resolutions when the time step discretization results in large temperature changes. We define an alternative model for HVAC consumption that solves Equation (3.2) for $H_{hvac,m}$ (a component of u) and enforces a house temperature within the thermostat deadband [41]:

$$\begin{aligned} H_{hvac,m} &= \max(H_{heat,m}, 0) + \min(H_{cool,m}, 0) \\ H_{heat,m} &= \frac{1}{B_{mm}}(T_{heat} - A_m x - B_m u) \\ H_{cool,m} &= \frac{1}{B_{mm}}(T_{cool} - A_m x - B_m u) \end{aligned} \tag{3.7}$$

where T_{heat} and T_{cool} are the heating and cooling setpoints, A_m and B_m are the rows of A and B corresponding to T_m, and B_{mm} is the element of B that relates T_m and H_m. Note that the u does not include $H_{hvac,m}$ in this equation. The heating and cooling systems will not be on simultaneously as long as $T_{heat} \leq T_{cool}$, which is strictly enforced in OCHRE.

In both models, the power output is:

$$P_{hvac}(k) = \frac{1}{\eta_{hvac}(k)} |H_{hvac,m}(k)| \tag{3.8}$$

The HVAC model can be externally controlled either by directly setting the delivered heat $H_{hvac,m}$ through a duty cycle or by setting the thermostat setpoints T_{heat} and T_{cool}.

3.1.3 Water Heater Model

The water heater is modeled similarly to the HVAC and building envelope. A two-node RC thermal model is used to track the water tank temperature, representing the upper and

lower volumes of the tank. This model is converted to a linear state space system using equations similar to (3.1–3.3). The external temperature is set to the temperature T_z where z is the envelope node corresponding to the zone where the water heater is located. Heat losses from the tank are included in the building envelope model as injections into zone z (H_z).

Heat injections into the water tank model come from the water heating element and from water displacement caused by hot water draws [62]. OCHRE can model gas and electric tank and tankless water heaters as well as heat pump water heaters. The electric resistance water heater model has upper and lower heating elements and a constant heating capacity. The heat injection into node i in the water heater model is:

$$H_{wh,i} = M_{wh,i}\kappa_{wh,i} + V_{draw}c_p\rho(\theta_{i+1} - \theta_i),\ i \in \{1, 2\} \tag{3.9}$$

where $\kappa_{wh,i}$ is the water heater rated capacity, $M_{wh,i}$ is the water heating mode, V_{draw} is the water draw volume, c_p is the heat capacity of water, ρ is the density of water, and θ_i is the temperature of water node i. The water heater mode $M_{wh,i}$ is 1 when the heating element in node i is on and 0 otherwise. Note that in the two-node model, $i = 1$ corresponds to the top of the tank, and $\theta_3 = \theta_{wm}$ is the incoming mains water temperature. For heat pump water heaters, $\eta_{wh,1}$ corresponds to the electric resistance backup element and $\eta_{wh,2}$ corresponds to the heat pump element. Additionally, an inversion mixing rule captures buoyancy effects and ensures that $\theta_1 \geq \theta_2$ by transferring heat to the top node when necessary.

Water draw schedules were generated using the Building America Domestic Hot Water Event Schedule Generator [67] at a 1-minute time resolution. The incoming cold water temperature is calculated using a correlation based on climate [150].

The water heater operates using a thermostat control with a single-sided deadband for both the upper and lower elements [61]. The two elements cannot be on at the same time; if both node temperatures are less than the deadband, the upper element is prioritized and will stay on until the top node reaches the setpoint, then the bottom element will turn on.

Similar to the HVAC model, we use an alternative water heater model for simulations with a large time step. This model uses a single-node water tank model, and it uses a method similar to Equation (3.7), although without a cooling mode.

The power output of the water heater (for a two node tank model) is:

$$P_{wh}(k) = \sum_{i=1}^{2} M_{wh,i}\kappa_{wh,i}\eta_{wh,i} \tag{3.10}$$

where $\eta_{wh,i}$ is the efficiency of the water heating element at node i.

The water heater can be externally controlled by directly setting the mode with $M_{wh,i}$ through a duty cycle or by setting the water heater thermostat deadband limits.

3.1.4 EV Model

The EV model combines a standard battery model with a random parking event generator using residential parking survey data. The data set is taken from EVI-Pro [68] based on a vehicle travel study in California [151]. A parking event e is characterized by three parameters: the arrival time $k_{e,0}$, departure time $k_{e,end}$, and arrival state of charge $s_{ev,e,0}$. Events are sampled by day, with at least one event occurring on each day. EVI-Pro assumes that the EV is fully charged at the beginning of each day (i.e., the first departure time of the day). The set of events used for the random sampling varies by day according to the following parameters [68]:

- EV Type: Plug-in hybrid (PHEV) or Battery (BEV) options. PHEVs tend to deplete a larger percentage of their battery than BEVs, leading to lower values for $s_{ev,e,0}$.
- EV Battery Capacity: EVs with larger batteries can drive further, but tend to use less energy relative to the battery capacity, leading to higher values for $s_{ev,e,0}$. PHEVs are split into small and large sizes based on a threshold of 35 mile range (or 11.4 kWh capacity). BEVs are split based on a threshold of 175 mile range (or 56.9 kWh).
- Charging Level: Level 1 (1.4 kW) or Level 2 (3.6 kW for PHEV, 9.0 kW for BEV) options. EVs with Level 1 chargers tend to charge more often, leading to more

parking events per day compared to the same EV with a Level 2 charger.

- Average Daily Temperature: EVs tend to use more energy on days with very high temperatures (due to air conditioning use) and days with very low temperatures (due to lower battery efficiency), leading to lower values for $s_{ev,e,0}$. The data are split into 5°C increments from -20°C to 40°C.

- Day of Week: Weekday and weekend options. EV parking times follow different patterns for weekdays and weekends. Weekdays tend to have fewer parking events.

Figure 3.4, Figure 3.5, and Figure 3.6 show the distribution of parking events in the EVI-Pro data set for a large PHEV on weekdays, and a small BEV on weekdays, and a small BEV on weekends, respectively. All vehicles have about 34,000 days of parking events in the data set. The majority of events are overnight events that start in the evening and end in the morning of the next day. The arrival SOC is typically greater than 70% for BEVs; for PHEVs, the arrival SOC is significantly more variable, and 9% of events have an arrival SOC of 0%. Weekend events tend to be more distributed than weekday events.

The EV model tracks the EV battery SOC using:

$$\begin{aligned} s(k+1) &= s(k) + \frac{t_s \eta_{ev}}{\kappa_{ev}} P_{ev}(k) \\ s(k_{e,0}) &= s_{ev,e,0} \forall e \in \mathcal{E} \end{aligned} \tag{3.11}$$

where t_s is the time resolution, η_{ev} is the efficiency of charging, κ_{ev} is the battery energy capacity, and P_{ev} is the AC power input to the EV charger. When charging without any external control, the EV begins charging at $k_{e,0}$ at its maximum power, accounting for the power limits and SOC limits. The EV input power is calculated as:

$$P_{ev}(k) = \begin{cases} \min(\frac{\kappa_{ev}}{t_s \eta_{ev}}(1 - s(k)), \overline{P_{ev}}) & k_{e,0} \leq k < k_{e,end} \\ 0 & \text{otherwise} \end{cases} \tag{3.12}$$

where $\overline{P_{ev}}$ is the maximum EV charging power. Note that the maximum SOC is assumed to be 100%.

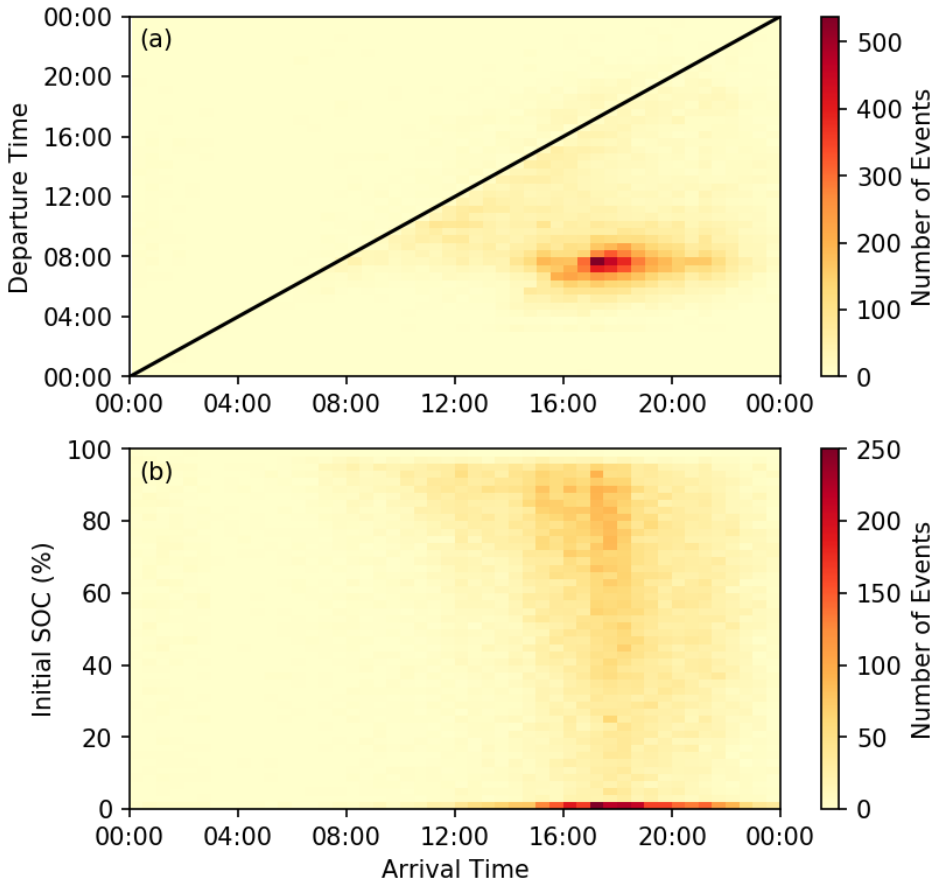

Figure 3.4 Heatmap of parking events for a large PHEV with Level 1 charging on weekdays. Shows the distribution of arrival time with (a) departure time (events in the bottom right half correspond to overnight events), and (b) arrival SOC. ©2021 IEEE

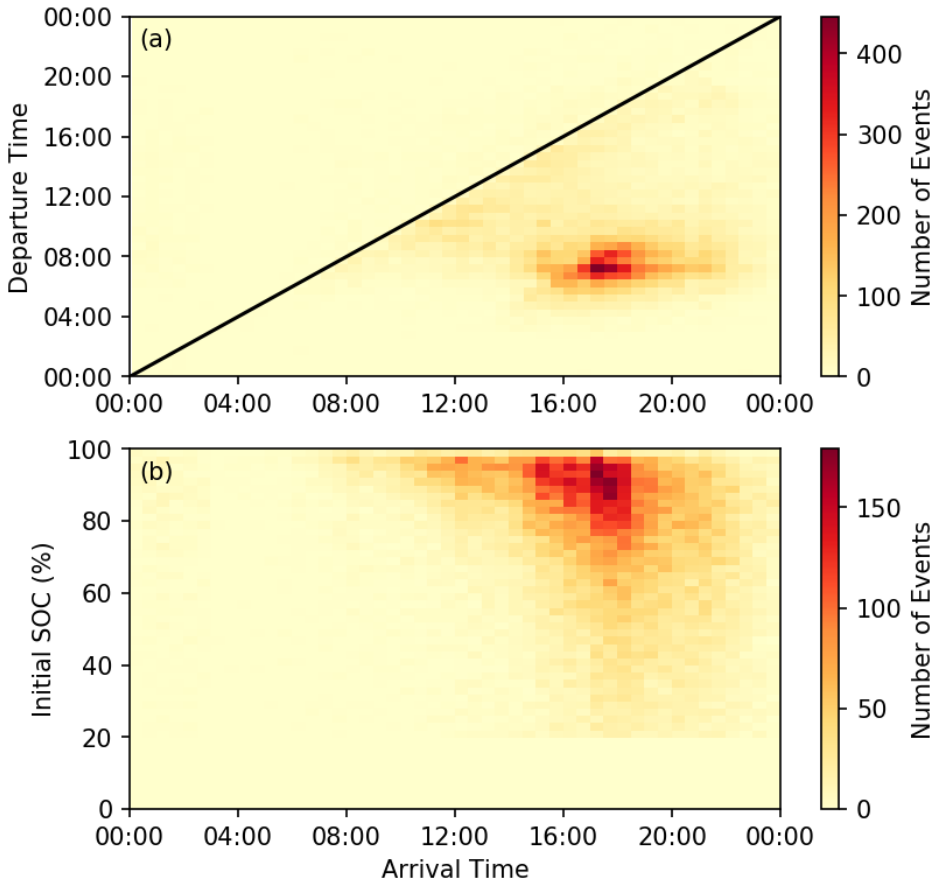

Figure 3.5 Heatmap of parking events for a small BEV with Level 1 charging on weekdays. Shows the distribution of arrival time with (a) departure time (events in the bottom right half correspond to overnight events), and (b) arrival SOC. ©2021 IEEE

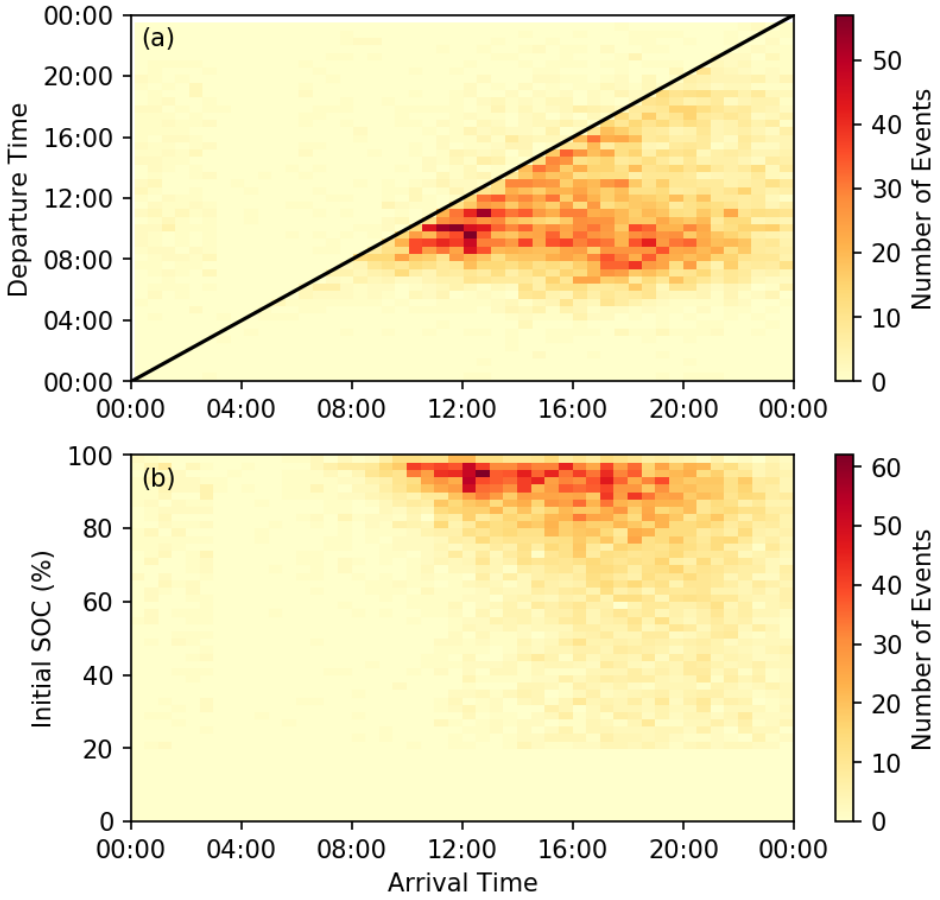

Figure 3.6 Heatmap of parking events for a small BEV with Level 1 charging on weekends. Shows the distribution of arrival time with (a) departure time (event in the bottom right half correspond to overnight events), and (b) arrival SOC.

The EV model can be controlled by directly setting P_{ev} or by updating $k_{e,0}$ in Equation (3.12), which leads to a delay in the EV charging start time. Level 1 charge controllers can update $k_{e,0}$, and Level 2 chargers can update $k_{e,0}$ or directly set P_{ev}.

Each day of parking events is considered to be independent of the events before and after it. However, in some instances the departure time of one parking event is very close to, and may overlap with, the arrival time of the next event. The model checks for these overlaps and, when necessary, will move the departure time of a parking event earlier to ensure at least a 1-hour gap between each parking event.

The arrival SOC of the EV is also impacted by the previous charging event if a control signal impacts the SOC on departure. When the departure SOC is less that the maximum departure SOC, the arrival SOC is reduced by the same amount, if possible:

$$\begin{aligned} \overline{s_{ev,e,end}} &= \min(s_{ev,e,0} + \frac{t_s \eta_{ev}}{\kappa_{ev}}(k_{e,end} - k_{e,0})\overline{P_{ev}}, 1) \\ {s'}_{ev,e+1,0} &= \max(s_{ev,e+1,0} - (\overline{s_{ev,e,end}} - s_{ev,e,end}), 0) \end{aligned} \tag{3.13}$$

where $\overline{s_{ev,e,end}}$ is the maximum possible departure SOC from event e, $s_{ev,e,end}$ is the actual departure SOC from event e, and ${s'}_{ev,e+1,0}$ is the updated arrival SOC for the next event.

The full procedure for the EV model is outlined in Figure 3.7.

3.1.5 Other Loads

Other energy-consuming equipment are modeled using an hourly schedule. Schedules can be generated from the Building America House Simulation Protocols [67] or from ResStock's stochastic occupancy model [152]. This equipment includes appliances (e.g., refrigerator, cooking range, clothes washer, clothes dryer, and dishwasher), lighting, and miscellaneous electric loads. Each piece of equipment has a corresponding heat gain that is injected into the zone containing the equipment:

$$H_{l,z}(k) = P_l(k) g_l \tag{3.14}$$

where $H_{l,z}$ is the heat injection into zone z, P_l is the equipment power, and g_l is the sensible heat gain fraction for equipment l.

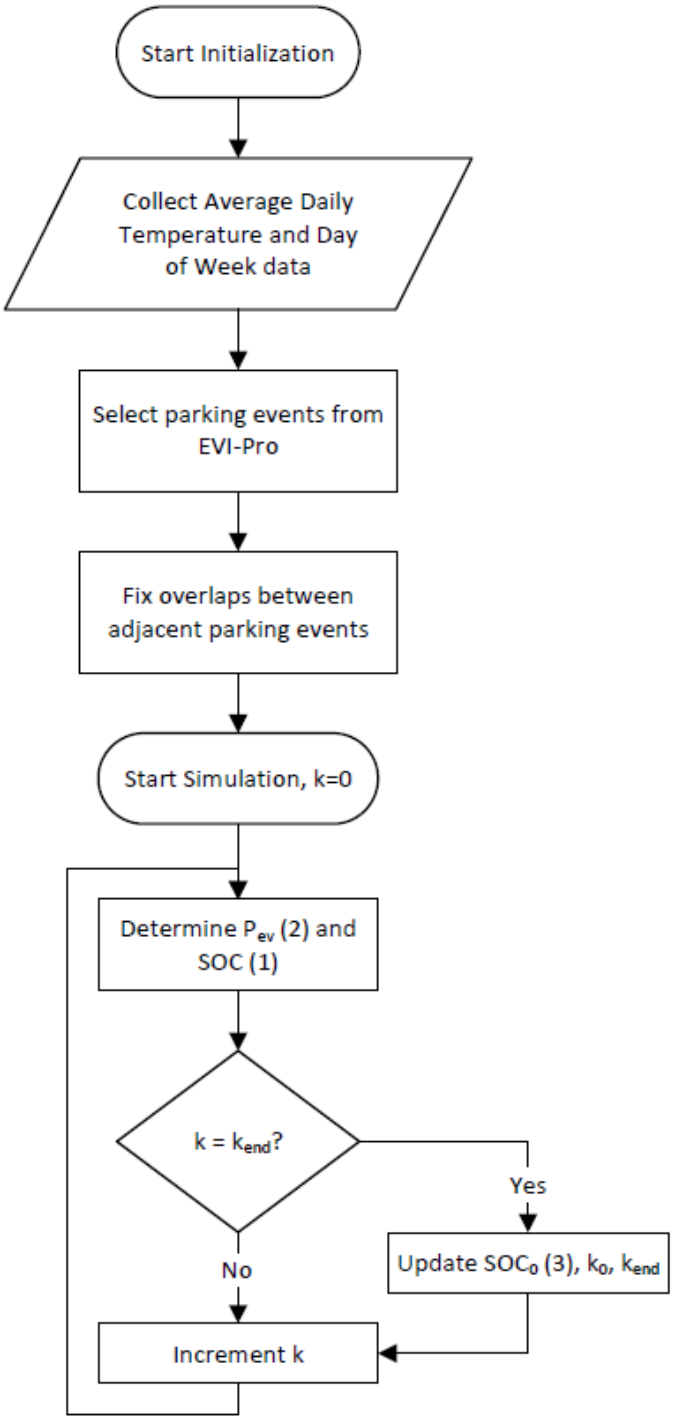

Figure 3.7 Flow chart for EV model initialization and simulation. ©2021 IEEE

Most equipment are located in the main indoor zone m, but lighting is modeled in multiple zones, including the garage and basement. Most equipment also include a latent heat gain fraction that is incorporated in the humidity model.

3.1.6 Voltage-Dependent Load Model

The HVAC, water heater, and other load models use a "ZIP" model to account for the load's power dependence on voltage [29]. Each load has prescribed parameters for constant impedance (Z), constant current (I), and constant power (P), as well as a prescribed power factor to calculate the load's reactive power. The real and reactive power of each load is:

$$\begin{aligned} P'_l(k) &= P_l(k)(Z_{p,l}v(k)^2 + I_{p,l}v(k) + \Pi_{p,l}) \\ Q'_l(k) &= P_l(k)\tan(\phi)(Z_{q,l}v(k)^2 + I_{q,l}v(k) + \Pi_{q,l}) \end{aligned} \tag{3.15}$$

where v is the per-unit house voltage; $\cos(\phi)$ is the power factor; $Z_{p,l}$, $I_{p,l}$, and $\Pi_{p,l}$ are the ZIP parameters for real power; and $Z_{q,l}$, $I_{q,l}$, and $\Pi_{q,l}$ are the ZIP parameters for reactive power for load l. For EVs and other loads without defined ZIP parameters, $P'_l = P_l$ and $Q'_l = 0$. ZIP parameter values are taken from [153–156].

The total house load power is:

$$\begin{aligned} P_{load} &= \sum P'_l \\ Q_{load} &= \sum Q'_l \end{aligned} \tag{3.16}$$

3.1.7 PV Model

The rooftop PV model uses the System Advisor Model (SAM) [75] and a controllable inverter model to determine PV generation. We run SAM within OCHRE to generate an AC power profile, which incorporates weather data, the PV capacity, the inverter efficiency, a tilt angle equal to the roof pitch, and an orientation aligned with the building orientation. Typical or default values are used for other required parameters in the SAM model.

Without control, the PV power is defined as:

$$P_{pv}(k) = -\min(P_{irr}(k), P_{inv}) \tag{3.17}$$

where P_{irr} is the AC electric power from the PV profile generated by SAM, and P_{inv} is the inverter capacity. Note that P_{pv} is negative, indicating power generation. There are no heat injections from the PV model.

Real power P_{pv} and reactive power Q_{pv} can be controlled through direct setpoint control, with options for watt and volt ampere reactive (VAR) priority. This enables many other control strategies including constant power factor and volt-VAR control.

Automated reactive power control from smart PV inverters is not considered in OCHRE. Although voltage-dependent reactive power controls, such as Volt-VAR control, may be incorporated into this model, these controls might not perform well when the simulation time step is much larger than the control loop period of the smart inverter. Studies have shown that additional convergence loops are critical when large numbers of smart inverters are added to a distribution system [114, 115].

3.1.8 Battery Model

A stationary battery energy storage system (BESS) is modeled in OCHRE. The model tracks the SOC of the BESS as:

$$s(k+1) = s(k) + \frac{t_s}{\kappa_{batt}}(\eta_{chg} P_{chg} - \frac{1}{\eta_{dis}} P_{dis}) \tag{3.18}$$

where $P_{batt} = P_{chg} - P_{dis}$ is the AC BESS power, κ_{batt} is the battery energy capacity, η_{chg} is the charging efficiency, and η_{dis} is the discharging efficiency. Efficiencies account for battery losses as well as power electronic losses. The model includes minimum and maximum limits for s and P_{batt} and ensures that the battery cannot be charging and discharging simultaneously.

OCHRE can optionally track the battery temperature as well. The thermal model is a lumped model based on [78] that tracks the battery internal temperature as:

$$\frac{dT_{batt}}{dt} = \frac{1}{C_{batt}} \left(\frac{T_z - T_{batt}}{R_{batt,z}} + (1 - \eta_{batt,th}) P_{chg} + \frac{1 - \eta_{batt,th}}{\eta_{batt,th}} P_{dis} \right) \tag{3.19}$$

where T_{batt} is the battery temperature, T_z is the temperature of the envelope zone where the battery is located, $R_{batt,z}$ is the thermal resistance, C_{batt} is the thermal mass, and $\eta_{batt,th}$ is the efficiency associated with the heat losses to the battery. Heat gains from the battery are not included in OCHRE. The BESS model is discretized in a similar way to the building envelope model.

The BESS model can follow a daily schedule, operate in self-consumption mode, or follow an external control signal. All control modes directly set P_{batt}. We note that the BESS and PV equipment are modeled as an AC-coupled system. Reactive power from smart battery inverters is not presently considered.

Table 3.1 Overview of equipment used in OCHRE, including control options and main input parameters

Equipment	**Control Options**	**Time-Varying Inputs**	**Static Inputs**
HVAC	Temperature setpoint, duty cycle	Indoor and outdoor temperature, humidity	Capacity, COP, SHR
Water heater	Temperature setpoint, duty cycle	Water draw profile, indoor temperature	Capacity, efficiency
EV	Power setpoint, delayed charge	Outdoor temperature, day of week	Range, charging level
PV	Power setpoint	Weather data	Capacity, inverter size
Battery	Power setpoint, self-consumption mode	Total load power, PV power	Capacity, SOC limits thermal parameters
Other loads	None	Occupancy profile	Rated power

3.2 New Construction Case Study

In this section, we run OCHRE for individual houses to demonstrate the features and benefits of OCHRE. We show the differences in simulation results when using 1-minute and 15-minute time resolutions and when sending control signals to multiple controllable device models. Results show the impacts on the house demand profile and on occupant comfort.

We develop a model for a new single family home in Fort Collins, CO. The home contains all electric, efficient equipment and is designed to be eligible for the U.S.

Department of Energy's Zero Energy Ready program [157]. For more details on simulation inputs, see Section 6.2.1.

Figure 3.8 shows the results for a single-family home with an EV and a battery at 1 minute time resolution. The HVAC and water heating loads lead to considerable variability in the net power. EV begins charging in the evening when the occupants arrive home. The battery charges in the morning when PV power exceeds load power, until the battery achieves 100% SOC. During the critical peak period, the battery discharges to reduce the net load.

The house power profile looks much smoother at 15 minute time resolution as shown in Figure 3.9. The HVAC and water heater models use the alternative methods to exactly match setpoint temperatures. This smooths the power profile and reduces the variability in the air temperature and hot water temperature.

We apply a basic load shifting control to the home before and during the critical peak period (see Section 6.2 for details). Figure 3.10 shows that control shifted the HVAC, water heater, EV, and battery profiles to reduce net demand during the critical peak period. The temperature and SOC states also adjust to provide more load flexibility during that time.

3.3 Chapter Summary

In this chapter, we presented the OCHRE model, an object-oriented, controllable, high-resolution, residential energy model for use in dynamic integration studies. The model combines valuable features of existing building models and grid load models, including a validated building envelope model that can include multiple zones, controllable device models for multiple DERs, and a voltage-dependency ZIP model. The model outputs high-resolution outputs for power usage, air temperature, water temperature, battery and EV SOC, and many other time-series data. These detailed results are critical in controls applications and in evaluating system performance in terms of energy consumption, costs, and occupant comfort.

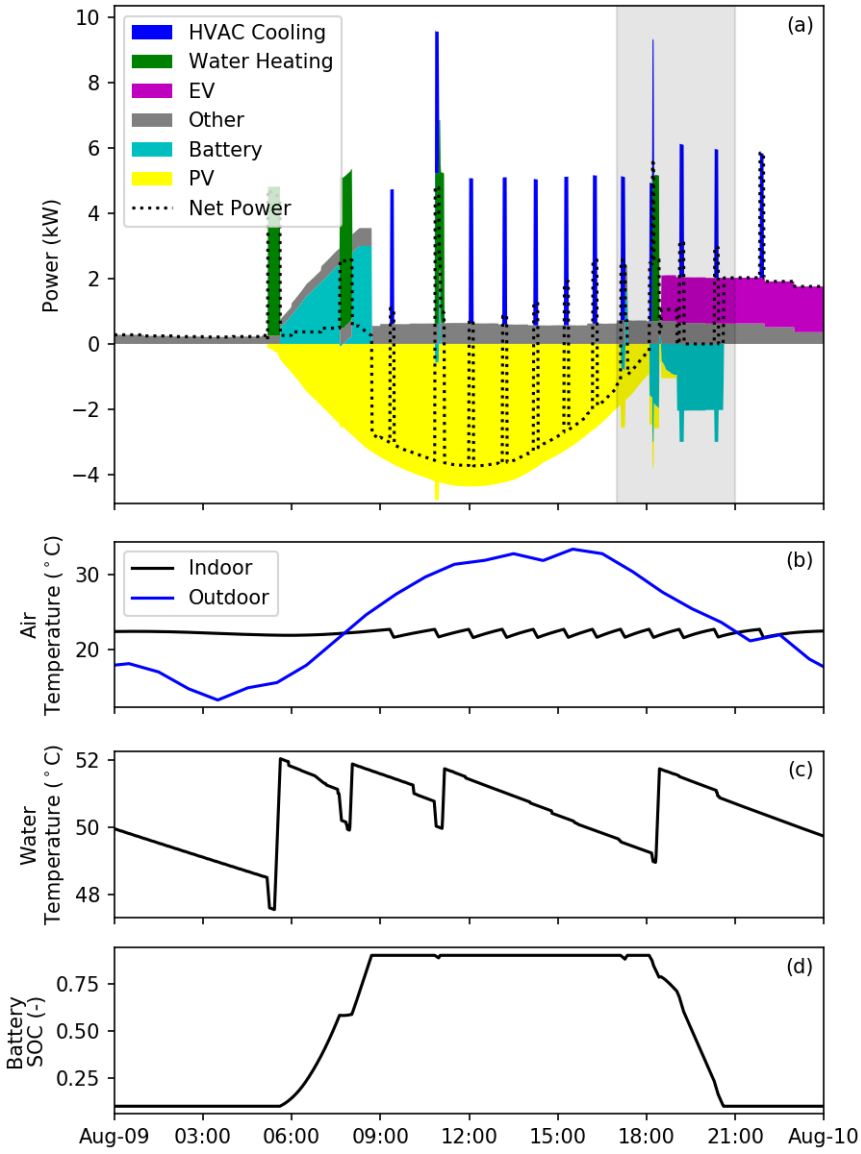

Figure 3.8 Single home simulation results at 1-minute resolution, including power by end use (a), air temperature (b), hot water temperature (c), and battery SOC (d). The critical peak period is shaded.

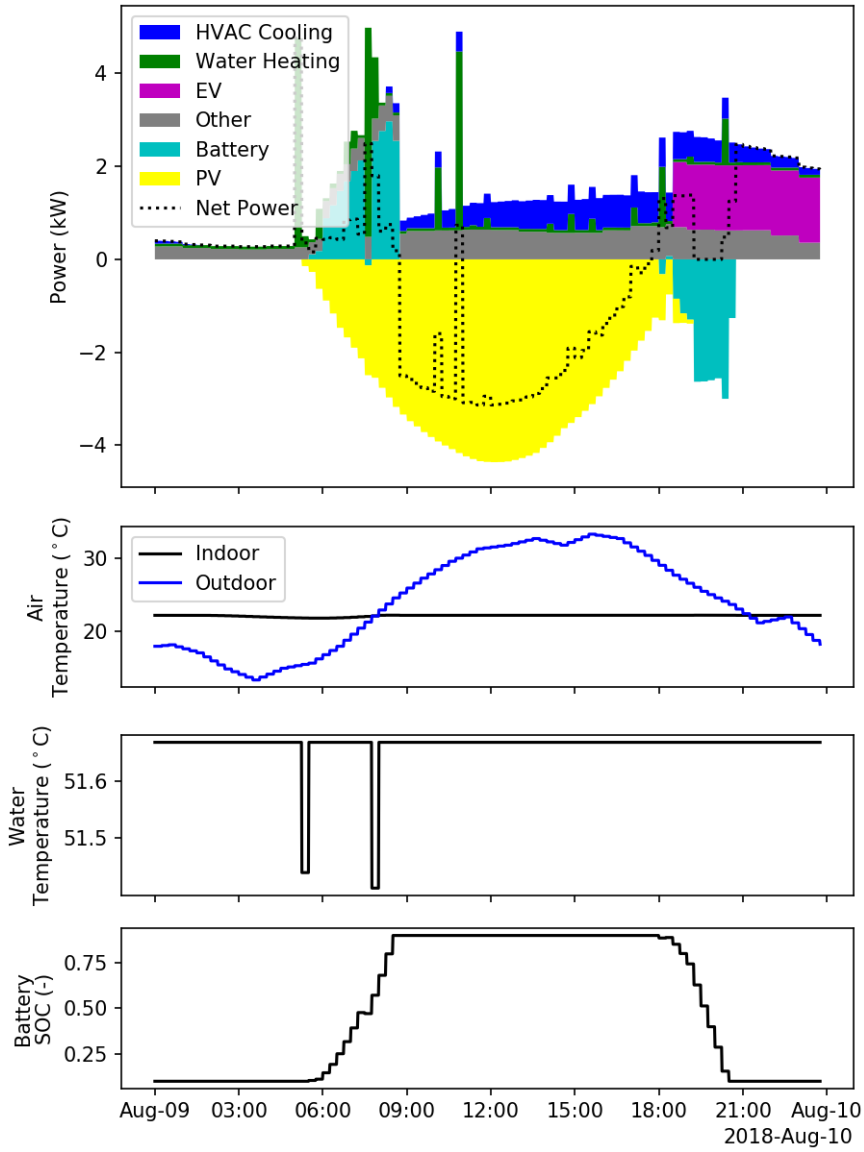

Figure 3.9 Single home simulation results at 15-minute resolution, including power by end use (a), air temperature (b), hot water temperature (c), and battery SOC (d). The critical peak period is shaded.

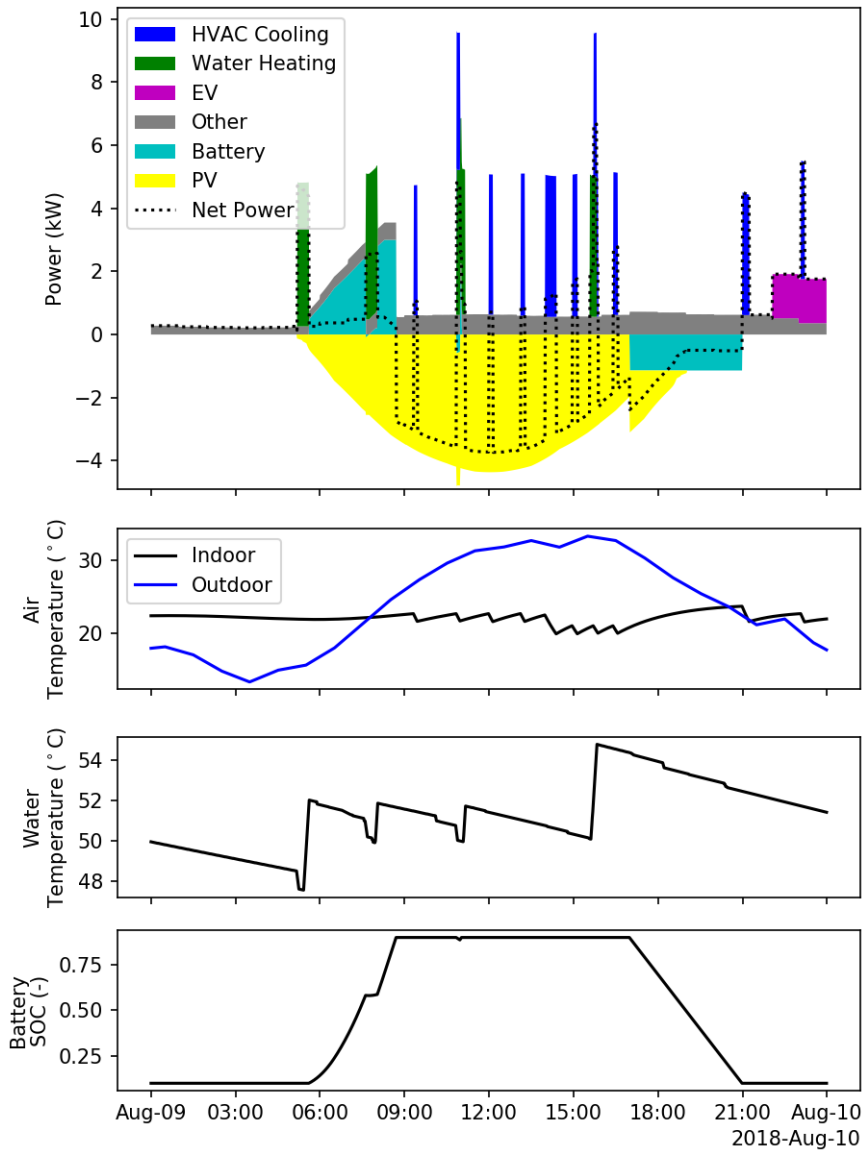

Figure 3.10 Simulation results with a load shifting controller at 1-minute time resolution, including power by end use (a), air temperature (b), hot water temperature (c), and battery SOC (d). The critical peak period is shaded.

The OCHRE model meets the requirements for an integrated residential energy model as described in Section 1.3. This chapter addresses Research Question 1 by showing that OCHRE can accurately capture the impacts of load flexibility on power usage and occupant comfort. This ability is especially useful in assessing control applications, for example in distributed control strategies as shown in Chapter 6.

CHAPTER 4

A STOCHASTIC CONTROL FRAMEWORK FOR HOME ENERGY MANAGEMENT SYSTEMS

This chapter presents a control framework for HEMS that incorporates uncertainties related to the prediction forecast, control model, and sensor measurements. The framework integrates the OCHRE model from Section 3 and multiple control components, including a reduced-order linear model, an MPC optimization, and a forecast generator. The framework can incorporate a wide variety of objective functions, and is designed to evaluate heuristic, deterministic, and stochastic control methods in conditions with significant amounts of uncertainty.

As described in Section 2.3, most studies on HEMS do not consider the impact of uncertainty on control performance. When MPC methods are tested in a hypothetical scenario with exact forecasts, simplified models, and little or no noise in communication signals, they are nearly always shown to be optimal strategies that perform better than heuristic or other methods; however, real systems are not so simple, and we argue that HEMS control strategies should be evaluated in conditions with realistic uncertainty to truly understand their value.

Figure 4.1 shows a schematic of an MPC algorithm and highlights the data that are likely to be stochastic due to uncertainty or noise. MPC requires forecasts for model inputs in the horizon window that often cannot be estimated with high accuracy at the controller run time. The MPC control model is not a perfect representation of the system model because of simplifications required for computational speed, which causes the predicted states and outputs to deviate from the actual model states. Finally, sensor measurements from the system model can be noisy or biased, leading to uncertainty in the current state of the system.

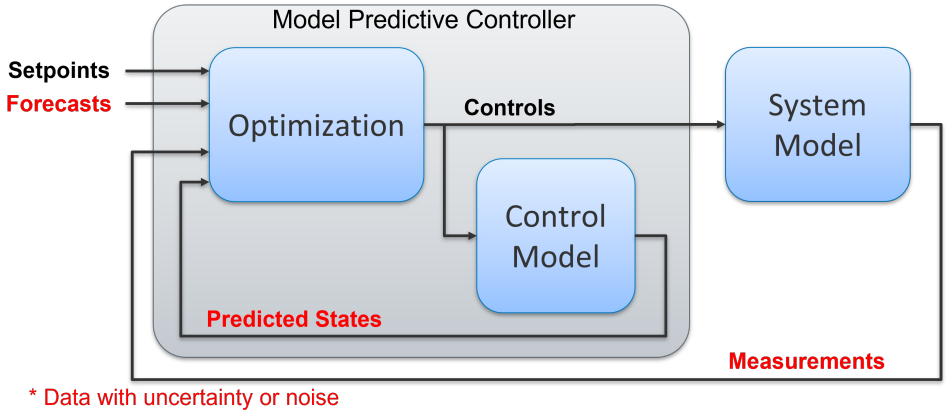

Figure 4.1 Schematic of an MPC algorithm with uncertainty, highlighting the data that are likely to be noisy or stochastic.

4.1 Control Model Description

To simulate model uncertainty in the control framework, we define two models for each end use: one is used for the building system, and the other is used as the underlying control model for the MPC as shown in Figure 4.3. The system models for each load are from OCHRE as described in Section 3.1. The MPC device models are derived from the OCHRE models. This section describes the linearization and other techniques used to derive the MPC models.

4.1.1 Linear Controllable Load Model

In general, a linear model is defined for each controllable load $l \in \mathcal{L}$ in state space form:

$$\begin{aligned} x_l(k+1) &= A_l x_l(k) + B_l u_l(k) + G_l z_l(k) \\ y_l(k) &= C_l x_l(k) \end{aligned} \tag{4.1}$$

where x_l is the state vector, u_l is the controllable input vector, z_l is the uncontrollable input vector, y_l is the output vector, and A_l, B_l, G_l, and C_l are state space system matrices.

The set of controllable loads $\mathcal{L} = [hvac, wh, ev, batt]$ corresponds to an air conditioner, water heater, electric vehicle, and battery, respectively. Each load model contains at least one state and at least one controllable input that corresponds to the load power. Most models include at least one uncontrollable input that corresponds to an uncertain variable

that must be forecasted. If the output vector y_l is not defined, it is assumed that $y_l = x_l$, and C_l is the identity matrix. The following sections describe the individual control models in detail.

4.1.2 HVAC and Envelope

To develop a linear envelope model for the MPC, we linearize OCHRE's envelope model, which includes nonlinear components for infiltration, interior long-wave radiation, and exterior long-wave radiation. We linearize each heat transfer pathway separately. For each pathway, we add resistors to OCHRE's equivalent circuit model (see Figure 3.2 and Figure 3.3), as shown in Figure 4.2. In the figure, T_a is the ambient temperature, T_z is the temperature of an interior zone, $T_{s,i}$ is the surface temperature of boundary i, and subscripts 1, 2, and 3 correspond to boundary materials connected to either the ambient or an interior zone.

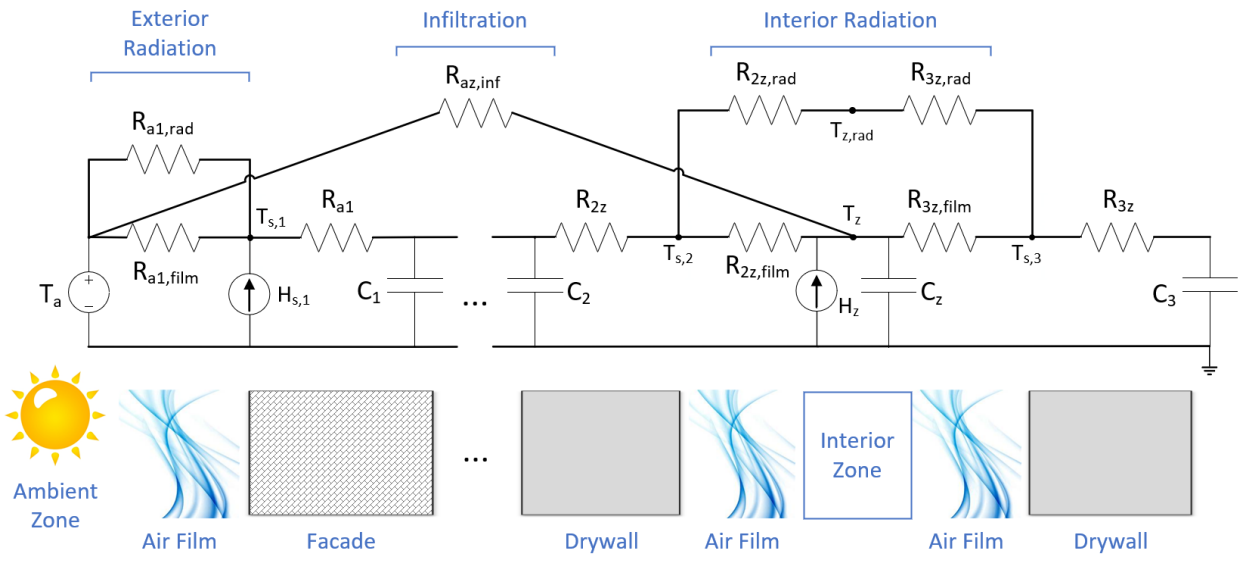

Figure 4.2 A linear envelope model with infiltration and interior and exterior radiation elements.

For infiltration (and mechanical ventilation), we add a resistance $R_{az,inf}$ between an interior air zone and the ambient air zone. We calculate the resistance value by linearizing

the heat gain at an operating point:

$$R_{az,inf} = \frac{\Delta T_{op}}{H_{az,inf}} \tag{4.2}$$

where ΔT_{op} is the temperature difference between zone z and ambient at the operating point, and $H_{az,inf}$ is the infiltration and ventilation heat gains to zone i at the operating point. $H_{az,inf}$ also depends on wind speed, which must also be defined in the operating point. This resistance value gets incorporated into the linear envelope model before calculating the state space matrices.

We use a similar approach to linearize the interior and exterior radiation. The radiation equation for the surface of boundary material i is:

$$H_{iz,rad} = \epsilon_i \sigma a_i (T_{z,rad}^4 - T_{s,i}^4) \tag{4.3}$$

where ϵ_i is the emissivity of material i, a_i is the area of the material i, and σ is the Stefan-Boltzmann constant. For the ambient zone, we assume $T_{z,rad} = T_a$, ignoring effects of the sky radiation temperature. For interior zones, $T_{z,rad}$ depends on the surface temperatures of all boundaries facing the zone. Linearizing with the operating point $T_{z,rad} = T_{s,i} = T_{op,rad}$ gives:

$$\frac{1}{R_{iz,rad}} = \frac{dH_{iz,rad}}{d(T_{z,rad} - T_{s,i})} = 4\epsilon_i \sigma a_i T_{op,rad}^3 \tag{4.4}$$

where $R_{iz,rad}$ is a resistance value that accounts for radiation effects. For exterior radiation, the resistor is applied in parallel with an exterior film resistance that models the effects of convection (see Figure 4.2, $R_{a1,film}$).

For interior radiation, the resistor is applied between the boundary surface and a fictional node $T_{z,rad}$ representing all of the radiation within an interior zone. Using Kirchoff's Current Law, this network topology ensures that all radiative heat within a zone sums to zero. The fictional node and all boundary surface nodes are eliminated by using the star-mesh transform to generate resistance values between each boundary surface within an interior zone [158].

The envelope model is converted into a linear, discrete-time state space model using equations (3.2–3.3). OCHRE's envelope model includes many interior nodes (30–45 for a typical home), which can lead to slow computational speed when used within an MPC framework. We use balanced truncated model reduction to reduce the number of states of the envelope model [159, 160]. In the use cases in Chapter 7, the reduced order model has seven states.

Before the model reduction, we eliminate inputs and outputs from Equation 3.3 that are not relevant to the control model and normalize inputs based on typical variability. The main indoor temperature is the only output, and the HVAC power is the only controllable input, i.e., $y_{hvac} = T_m$ and $u_{hvac} = P_{hvac}$. The uncontrollable inputs are $z_{hvac} = [T_a, T_g, H_{int}, H_s^T]^T$, where T_g is the ground temperature, H_{int} is the internal heat gains in the main zone, and H_s is a vector of the heat gains from solar radiation on each exterior surface (e.g., walls, roof, attic walls). The state vector x_{hvac} is an output of the model reduction algorithm and has no physical meaning.

Internal heat gains include heat from occupants, other equipment, and solar radiation from windows. The total heat gain to the main zone H_m is a combination of the internal heat gains and the heat from the HVAC equipment. When an air conditioner is used:

$$H_m(k) = -\eta_{hvac} P_{hvac}(k) + H_{int}(k) \tag{4.5}$$

where η_{hvac} is the HVAC COP and is assumed to be constant.

4.1.3 Water Heater

We use OCHRE's heat pump water heater and 2-node water tank models for the system model. The 2-node tank model includes nonlinearities due to heat transfer from water draws. Similar to the HVAC model, OCHRE's water heater model uses a thermostat with deadband control that converts a temperature setpoint into an on/off power signal. The temperature setpoint can be controlled externally, but the thermostat ensures that the deadband remains within the thermal comfort region.

We define a 1-node linear model for the control model that accounts for convection and conduction similarly to the envelope model described in Section 4.1.2. Heat injections into the tank come from water heater power and water draws:

$$H_{wh}(k) = \eta_{wh} P_{wh}(k) + V_{draw} c_p \rho (\theta_{wm} - \theta_1(k)) \tag{4.6}$$

where η_{wh} is the nominal coefficient of performance of the heat pump water heater, θ_1 is the tank temperature, θ_{wm} is the water mains temperature, V_{draw} is the water draw volumetric flow rate, c_p is the heat capacity of water, and ρ is the density of water. To linearize the biquadratic term for water draws, we assume constant temperature differences. We note that this formulation does not include a backup heating element for the heat pump water heater, which is included in OCHRE's model.

The linear state space equation for the water heater has one state for the water tank temperature, $x_{wh} = \theta_1$, and one controllable input, $u_{wh} = P_{wh}$. The uncontrollable inputs are $z_{wh} = [V_{draw}, \theta_a]^T$, and we assume that the water mains temperature is known and constant.

4.1.4 Electric Vehicle

OCHRE's EV model tracks EV charging but does not model battery discharging during driving. To account for discharging, we add a term that decreases the EV SOC when the EV is driving:

$$s_{ev}(k+1) = s_{ev}(k) + \frac{\eta_{ev}}{E_{ev}} (P_{ev}(k) - P_{drive} p_{drive}(k)) \tag{4.7}$$

where s_{ev} is the EV SOC, E_{ev} is the EV energy capacity, η_{ev} is the charge efficiency, P_{ev} is the EV charging power, P_{drive} is the power lost while driving, and p_{drive} is the percentage of time that the EV is driving.

The linear state space equation for the EV has one state for the EV SOC, $x_{ev} = s_{ev}$. The only uncontrollable input is $z_{wh} = p_{drive}$.

4.1.5 Battery

We use OCHRE's linear battery model to track the battery SOC (Equation 3.18) and, optionally, battery temperature (Equation 3.19). Due to separate charging and discharging efficiencies, the controllable input is split into two variables, i.e., $u_{batt} = [P_{chg}, P_{dis}]^T$, and we define $P_{batt} = P_{chg} - P_{dis}$. The battery model has two states for the battery SOC and temperature, $x_{batt} = [s_{batt}, T_{batt}]$. The only uncontrollable input for the battery model $z_{batt} = T_a$, which only impacts the battery temperature, not the SOC. We note that the battery SOC and temperature equations are fully separable.

4.1.6 Combined House Model

The four controllable equipment models are combined in parallel create a linear model for the house:

$$\begin{aligned} x(k+1) &= Ax(k) + Bu(k) + Gz(k) \\ y(k) &= Cx(k) \end{aligned} \tag{4.8}$$

where:

$$\begin{aligned} x &= [x_{hvac}^T, \theta_1, s_{ev}, s_{batt}, T_{batt}]^T \\ u &= [P_{hvac}, P_{wh}, P_{ev}, P_{chg}, P_{dis}]^T \\ z &= [T_a, T_g, H_{int}, H_s^T, V_{draw}, \theta_a, p_{drive}]^T \\ y &= [T_m, \theta_1, s_{ev}, s_{batt}]^T \\ A &= \text{diag}([A_{hvac}, A_{wh}, A_{ev}, A_{batt}]) \end{aligned}$$

and the other matrices are defined similarly to A. We define the whole house power as:

$$P_{house}(k) = \sum_{l \in \mathcal{L}} P_l(k) + P_{unc}(k) \tag{4.9}$$

where P_{unc} is the power from all uncontrollable house loads. The uncontrollable load power is considered as an uncertain input, similar to the inputs in z.

For scenarios with a demand charge, we track the peak house power:

$$P_{peak}(k) = \max(P_{house}(k), P_{peak}(k-1)) \tag{4.10}$$

4.1.7 Uncertainty Model

The control model in (4.8) can be used directly in a deterministic control framework. For SMPC, the uncontrollable inputs become random variables, and noise $\tilde{v}$ is added to the outputs. The stochastic model becomes:

$$\begin{aligned} \tilde{x}(k+1) &= A\tilde{x}(k) + Bu(k) + G\tilde{z}(k) \\ \tilde{y}(k) &= C\tilde{x}(k) + \tilde{v} \end{aligned} \tag{4.11}$$

where:

$$\begin{aligned} \tilde{x}(k) &\sim \mathcal{N}(\hat{x}(k), \Sigma_x(k)) \\ \tilde{z}(k) &\sim \mathcal{N}(\hat{z}(k), \Sigma_z(k)) \\ \tilde{y}(k) &\sim \mathcal{N}(\hat{y}(k), \Sigma_y(k)) \\ \tilde{v} &\sim \mathcal{N}(0, \Sigma_v) \end{aligned}$$

are all Gaussian random vectors, and $\mathcal{N}(\hat{x}, \Sigma_x)$ defines a Gaussian vector distribution with mean $\hat{x}$ and covariance matrix Σ_x. The mean and variance of all the uncontrollable inputs distributions $\tilde{z}(k)$ are based on forecast estimates (see Section 4.3), and we assume that there is no covariance between any of the inputs. The diagonals of the covariance matrices correspond to the variance of individual input or output variables, which we denote as $\sigma^2_{x_i}$, for example, $\text{diag}(\Sigma_y) = [\sigma^2_{T_m}, \sigma^2_{\theta_1}, \sigma^2_{s_{ev}}, \sigma^2_{s_{batt}}]$. The probability distributions of the state and output matrices are calculated using a Kalman filter [94]:

$$\begin{aligned} \hat{x}(k) &= \hat{x}^{(-)}(k) + K(y^{(-)}(k) - C\hat{x}^{(-)}(k)) \\ \Sigma_x(k) &= (I - KC)\Sigma_x^{(-)}(k) \\ \hat{y}(k) &= C\hat{x}(k) \\ \Sigma_y(k) &= C\Sigma_x(k)C^T \end{aligned} \tag{4.12}$$

where $y^{(-)}(k)$ is the house status received from OCHRE, and:

$$\begin{aligned} K &= \Sigma_x^{(-)}(k)C^T(C\Sigma_x^{(-)}(k)C^T + \Sigma_v)^{-1} \\ \hat{x}^{(-)}(k+1) &= A\hat{x}(k) + Bu(k) + G\hat{z}(k) \\ \Sigma_x^{(-)}(k+1) &= A\Sigma_x(k)A^T + G\Sigma_z(k)G^T \end{aligned} \tag{4.13}$$

The equations above can be used directly when k is the current time. When calculating the state and output distributions in the future, $y^{(-)}(k)$ is unknown and we set $\hat{x}(k) = \hat{x}^{(-)}(k)$. We also assume a closed-loop control strategy that accounts for past

disturbances and reduces the expected uncertainty in future states. This is achieved by ignoring the $\Sigma_x(k)$ term when calculating $\Sigma_x^{(-)}(k+1)$.

Assuming Gaussian distributions for all uncontrollable inputs enables the use of a basic Kalman Filter and simplifies the calculation of future probability distributions. However, Gaussian distributions are unlikely to be a good approximation to many variables including solar irradiance, categorical variables (e.g., driving state) and bimodal variables (e.g., hot water draws). In these cases, the Gaussian approximation is likely to overestimate the uncertainty of the variable, leading to a more conservative control strategy. This issue can be reduced by tuning risk tolerance parameters as described in Section 4.2.3. However, it is likely that more accurate probability distributions can lead to better uncertainty estimates and better control performance.

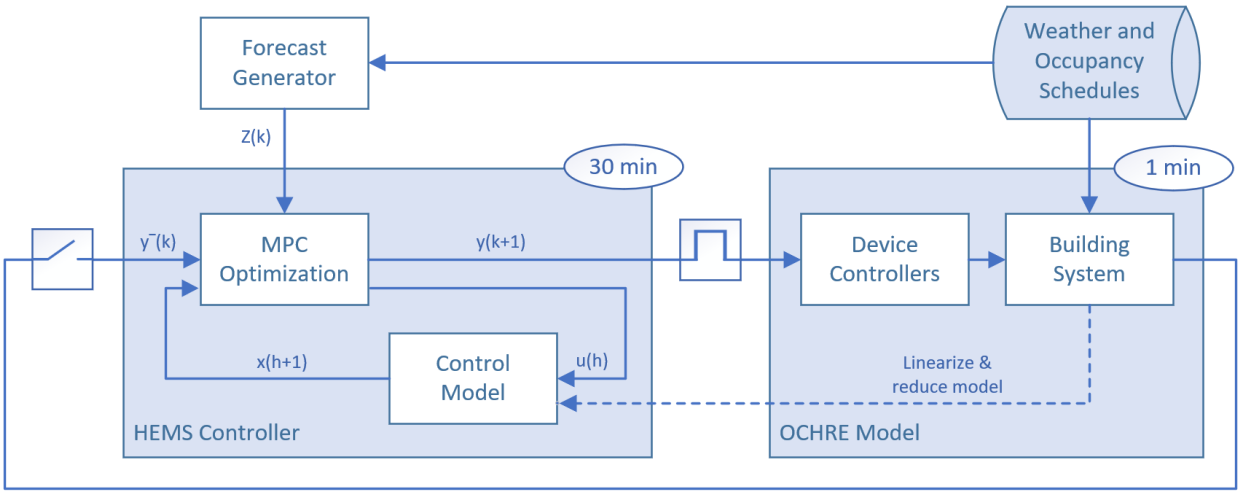

Figure 4.3 Flow diagram of the HEMS controller and OCHRE showing the inputs and outputs of each component.

4.1.8 Model Implementation

The implementation of the HEMS controller and OCHRE is described in Figure 4.3. At time k, the HEMS controller receives the most recent house status $y^{(-)}(k)$ from OCHRE. It receives forecasts from a forecast generator of the form

$Z(k) = \{z(k,h) : h \in [k, k+n_h-1]\}$, where $z(k,h)$ is the forecast at time h evaluated at

time k, and n_h is the number of steps in the MPC horizon. The HEMS controller uses an MPC optimization to solve for $u(h)$, and the control model predicts the future states $x(h+1)$ and outputs throughout the forecast horizon. The controller sends the optimal set points, which correspond to the future output $y(k+1)$, to OCHRE, which implements the controls at 1-minute resolution. This process repeats every 30 minutes throughout the simulation.

Note that the HEMS controller sends the temperature and SOC set points $y(k+1)$, not the power set points $u(k)$, to OCHRE. This allows OCHRE's device controllers to determine the device power at 1-minute resolution, which enables equipment cycling for the air conditioner and the water heater. Providing OCHRE with these set points reduces the effects of model and forecast uncertainty in achieving the desired set points, but it could cause the device power to deviate from the power expected by the MPC. This control signal works best for the MPC formulation in this paper; however, power set points might be more appropriate if a demand charge or a demand response event is involved and precise power controls are desired.

We also note that the HEMS controller receives all state variables $x(k)$ from OCHRE in the deterministic case. This gives the DMPC perfect knowledge of the initial system state. In the SMPC case, the house status only includes output variables and the Kalman filter is used to estimate the states.

4.2 Control Formulation

We include three types of HEMS controls in the control framework: heuristic controls, DMPC, and SMPC. In this section, we outline these three control strategies for each controllable device. All controllers operate at a 30 minute time resolution.

For multiple equipment types, a soft constraint is used to limit discomfort or inconvenience costs. Soft constraints were chosen to more easily compare the different control strategies and to define how to quantify the costs when constraints are exceeded [161].

4.2.1 Heuristic Controls

The heuristic controls for HVAC and water heating use a thermostat control with a deadband and a precooling strategy designed around a time-of-use rate. The top of the HVAC deadband defines the comfort temperature $\overline{T_m}$ that is used to evaluate all of the HVAC control strategies, with a comfort cost incurred when that threshold is exceeded. The water heater control uses a minimum comfort temperature, $\underline{\theta_1} = 46.1°\text{C}$, which is also used to evaluate all control strategies [67].

The heuristic controller charges the EV at its maximum power immediately upon arrival. This control strategy ensures that the EV SOC will be at its maximum possible value when the EV leaves, but it disregards the variable cost of charging at different times of day.

The heuristic battery controller performs energy arbitrage based on a time-of-use rate. The battery begins charging at 10 AM and begins discharging at the start of the peak period.

4.2.2 Deterministic MPC

The DMPC formulation uses the linear house model described in Section 4.1.6 to optimize energy costs and occupant comfort and convenience. All terms in the objective function include a "cost coefficient" λ that normalizes the term into units of dollars. The first term defines energy costs for a TOU rate:

$$J_{tou}(k) = \lambda_{tou}(k) t_s P_{house}(k) \tag{4.14}$$

where λ_{tou} is a time-varying price of electricity, and t_s is the control time resolution. We assume that electricity exports are allowed with net energy metering. For scenarios with a demand charge, we include a term for the demand charge cost:

$$J_{peak}(k) = \lambda_{peak} \max_{h \in [k, k+n_h-1]} |P_{house}(h) - P_{peak}(k)|_+ \tag{4.15}$$

where λ_{peak} is the demand charge rate, n_k is the number of steps in the MPC horizon, and $|\cdot|_+ = \max(\cdot, 0)$. We note that the cost term only accounts for the incremental increase in the demand charge across the horizon.

The objective includes occupant comfort and convenience costs for HVAC, water heating, and EV charging, which depend on air temperature, hot water temperature, and EV SOC, respectively. The EV control is designed to minimize any inconvenience associated with a low SOC at the time the EV leaves, similar to the control in Section 6.3.3. The costs are defined as:

$$\begin{aligned} J_{hvac}(k) &= \lambda_{hvac}|T_m(k) - \overline{T_m}|_+ \\ J_{wh}(k) &= \lambda_{wh} V_{draw} |\underline{\theta_1} - \theta_1(k)|_+ \\ J_{ev}(k) &= (\lambda_{ev}(1 - s_{ev}(k)) + \lambda_{ev,low}(s_{ev,low} - s_{ev}(k)))\, p_{leave}(k) \end{aligned} \tag{4.16}$$

where λ_l is a cost coefficient associated with each device, $s_{ev,low}$ is a low cutoff for EV SOC, and $p_{leave}(k) = p_{drive}(k) - p_{drive}(k-1)$ is the probability that the EV is leaving during time step k. The cost coefficients convert all cost terms to units of dollars so that all of the terms can be combined into a single objective function; for example, λ_{wh} has units of \$/°C-L. The values of these cost coefficients can be estimated by assessing an occupant's willingness to pay for a typical level of comfort, and they can be adjusted based on trial and error.

For simplicity and computational efficiency, we choose piece-wise linear equations for each of the comfort cost functions above. The HVAC comfort increases linearly as the indoor temperature exceeds $\overline{T_m}$. The hot water comfort increases linearly as the hot water temperature drops below $\underline{\theta_1}$ and is proportional to the water draw flow rate V_{draw}. The EV comfort cost includes two intervals; there is a linear cost of λ_{ev} when the EV SOC is between $s_{ev,low}$ and 100%, and a larger linear cost of $\lambda_{ev} + \lambda_{ev,low}$ when the SOC is below $s_{ev,low}$.

For the battery, we include cost terms to minimize degradation based on battery power and temperature:

$$\begin{aligned} J_{batt,P}(k) &= \lambda_{batt,P}(P_{chg}^2(k) + P_{dis}^2(k)) \\ J_{batt,T}(k) &= \lambda_{batt,T}|T_{batt}(k) - \overline{T_{batt}}|_+^2 \end{aligned} \tag{4.17}$$

where $\lambda_{batt,P}$ and $\lambda_{batt,T}$ are cost coefficients for battery power and temperature, respectively, and $\overline{T_{batt}}$ is a high battery temperature that would start to induce degradation.

In addition, we include a terminal cost term that is designed to make the battery control indifferent to discharging at the end of the horizon by valuing the remaining charge in the battery based on the electricity rate:

$$J_{batt}(k) = -\hat{\lambda}_{tou}(k) E_{batt} \eta_{dis} s_{batt}(k + n_h) \tag{4.18}$$

where $\hat{\lambda}_{tou}$ is the average cost of electricity over the forecast horizon, and E_{batt} is the battery energy capacity. Note that this objective only depends on the battery SOC at the end of the horizon, i.e., at time $k + n_h$.

We also include a term to smooth the power profile of each controllable device. This term can help reduce device degradation and reduce the set of optimal solutions, which improves the solver's consistency across multiple scenarios. The peak cost term is:

$$J_{smooth}(k) = \lambda_{smooth} \sum_{l \in \mathcal{L}} \max_{h \in [k, k+n_h-1]} |P_l(h)| \tag{4.19}$$

where λ_{smooth} is a small positive number.

When all cost terms are included, the DMPC objective function at current time k with n_h steps in the horizon is:

$$\begin{aligned} J(k) = \sum_{h=k}^{k+n_h-1} \big(& J_{tou}(h) + J_{peak}(h) + J_{hvac}(h+1) + J_{wh}(h+1) \\ & + J_{ev}(h+1) + J_{batt,P}(h) + J_{batt,T}(h+1) \big) \\ & + J_{batt}(k) + J_{smooth}(k) \end{aligned} \tag{4.20}$$

The deterministic optimization problem is defined as:

$$
\begin{aligned}
(\mathcal{P}_1) \min_{u(h)} : \quad & J(k) \\
\text{s.t.} \quad & x(h+1) = Ax(h) + Bu(h) + Gz(h) \\
& y(h) = Cx(h) \\
& 0 \leq u(h) \leq \overline{u} \\
& \underline{s_{batt}} \leq s_{batt}(h+1) \leq \overline{s_{batt}} \\
& s_{ev}(h+1) \leq 1 \\
& 0 \leq P_{ev}(k) \leq \overline{P_{ev}}(1 - p_{drive}(k)) \\
& \forall h \in [k, k+n_h-1]
\end{aligned}
\tag{4.21}
$$

where, in general, $\bar{\cdot}$ and $\underline{\cdot}$ are the minimum and maximum values of a given variable. Note that there is no minimum SOC constraint for the EV because of the uncertainty due to driving loss. Because p_{drive} is either 0 or 1, the maximum EV power is constrained to zero when the EV is driving and to the maximum charging power when the EV is parked.

All constraints are linear, and the objective function is strictly convex (when assuming reasonable values for some parameters, e.g., all $\lambda > 0$). This makes $\mathcal{P}_1$ a convex optimization problem that guarantees a globally optimum solution and can be solved efficiently. The formulation also ensures that P_{chg} and P_{dis} are never non-zero at the same time step when $\lambda_{tou} > 0$ and $0 < \eta_{chg}, \eta_{dis} < 1$ (see [162]).

4.2.3 Stochastic MPC

Under stochastic conditions, all uncontrollable inputs and all outputs are Gaussian random variables. The stochastic optimization incorporates uncertainty in these variables by using back-off magnitudes based on the standard deviation σ_{x_i} of each scalar variable x_i and a probability ϵ_{x_i} of exceeding a constraint [100]:

$$
\Pr(\tilde{x}_i \leq \overline{x_i}) \geq 1 - \epsilon_{x_i} \rightarrow \beta_{x_i} = \Phi^{-1}(1 - \epsilon_{x_i}) \tag{4.22}
$$

where Φ^{-1} is the inverse cumulative distribution function of the normal distribution and β_{x_i} is the number of standard deviations between the mean and the probability $1 - \epsilon_{x_i}$. As the tolerance for risk decreases, ϵ_{x_i} decreases and β_{x_i} increases.

The back-off magnitude is the product of β_{x_i} and σ_{x_i}. As risk tolerance decreases or as uncertainty increases, the back-off magnitude increases, leading to more conservative control behavior. In addition, the β_{x_i} parameter can be tuned to offset any bias in the estimated uncertainty. Back-off magnitudes are included in most cost terms from Equations (4.15), (4.16) and (4.17). The updated costs for the SMPC formulation are:

$$\begin{aligned}
J_{peak}(k) &= \lambda_{peak} \max_{h\in[k,k+n_h-1]} |\hat{P}_{house}(h) - P_{peak}(k) + \beta_{P_{unc}}\sigma_{P_{unc}}(k)|_+ \\
J_{hvac}(k) &= \lambda_{hvac}|\hat{T}_m(k) - \overline{T_m} + \beta_{T_m}\sigma_{T_m}(k)|_+ \\
J_{wh}(k) &= \lambda_{wh}\hat{V}_{draw}|\underline{\theta_1} - \hat{\theta}_1(k) - \beta_{\theta_1}\sigma_{\theta_1}(k)|_+ \\
J_{ev}(k) &= \lambda_{ev}(1-\hat{s}_{ev}(k))(p_{leave}(k) + \beta_{p_{leave}}\sigma_{p_{leave}}(k)) \\
J_{batt,T}(k) &= \lambda_{batt,T}|\hat{T}_{batt}(k) - \overline{T_{batt}} + \beta_{T_{batt}}\sigma_{T_{batt}}(k)|_+^2
\end{aligned} \tag{4.23}$$

where $\sigma_{P_{unc}}$ is the standard deviation of $\tilde{P}_{unc}$, and $\sigma_{p_{leave}}$ is the standard deviation of $\tilde{p}_{leave}$.

The SMPC optimization problem is very similar to Problem $\mathcal{P}_1$. The only changes are updating the cost terms in Equation (4.23) and using the mean values of each random variable throughout the formulation. The stochastic control formulation is:

$$\begin{aligned}
(\mathcal{P}_2)\min_{u(h)}: \quad & \sum_{h=k}^{k+n_h-1} J_{tou}(h) + J_{peak}(h) + J_{hvac}(h+1) + J_{wh}(h+1) + J_{ev}(h+1) \\
& + J_{batt}(k) + J_{smooth}(k) \\
\text{s.t.} \quad & \hat{x}(h+1) = A\hat{x}(h) + Bu(h) + G\hat{z}(h) \\
& \hat{y}(h) = C\hat{x}(h) \\
& 0 \le u(h) \le \overline{u} \\
& \underline{s_{batt}} \le \hat{s}_{batt}(h+1) \le \overline{s_{batt}} \\
& \hat{s}_{ev}(h+1) \le 1 \\
& 0 \le P_{ev}(k) \le \overline{P_{ev}}(1-\hat{p}_{drive}(k)) \\
& \forall h \in [k, k+n_h-1]
\end{aligned} \tag{4.24}$$

We note that p_{drive} is no longer a Boolean input. No back-off magnitude is used in the maximum battery or EV SOC constraints because battery SOC and EV charging are fully deterministic.

4.2.4 Control Objective Extensions

There are many extensions to the MPC objective functions described in equations (4.20) and (4.24). Objective cost terms can be removed if unnecessary, or new terms can be added. New cost terms to add include energy resilience in case of an outage as a function of battery SOC, an HVAC comfort cost due to cold temperatures in the winter, or a hot water comfort cost that only applies to showers.

Both the deterministic and stochastic objective functions are composed of linear functions, making both optimization problems linear programs. Modifying the objectives to include quadratic or other nonlinear convex functions maintain the convexity of the problems, which keeps the problems computationally efficient and ensures a global optimum solution as long as the problem is feasible. In particular, extending the comfort cost terms to include quadratics may more accurately model the true comfort cost of occupants.

Finally, many parameters in the formulation are assumed to be constant, including the comfort cost coefficients λ_l and the risk tolerance parameters β_{x_i}. While constant values are easier to define, there is no restriction to vary these and other parameters over time, depending on occupant preferences, current conditions, or past events. For example, occupants may have a stronger preference for comfort at certain times of day or when performing certain activities, which could indicate an increase in comfort cost coefficients. Risk tolerance parameters can increase if recent events have caused significant discomfort conditions to ensure that such events are unlikely to occur again. Parameters could also adjust based on real-time feedback from the occupant, for example if they know they will be away or if they need a fully charged EV. These considerations may be particularly important when deploying HEMS in the field to provide the user with many options and features that ensure the user feels in control of their energy decisions.

4.3 Forecast Generators

Realistic forecasts were developed for uncertain inputs z, including weather data and occupancy schedules. Multiple forecasts were derived from the same underlying data, but with varying levels of complexity and accuracy. Common forecast methods from practice and from research literature were chosen, although we note that more sophisticated forecast methods can lead to forecasts with lower uncertainty.

4.3.1 Weather Forecast

Weather data is required to calculate forecasts for uncertain inputs T_a and H_s. Historical weather and current weather forecasts are widely available, and we assume the forecast generator has access to these datasets.

Weather forecasts typically do not provide an estimate of the uncertainty in the forecast; we estimate the uncertainty using historical weather data and historical forecasts. The ambient temperature distribution is calculated using the difference between the actual historical temperature and the forecast, aggregated by the time difference between the current time k and the prediction time h, denoted $\Delta k = h - k$:

$$\begin{aligned} T_a^{(b)}(\Delta k) &= \frac{1}{n_k} \sum_{k=1}^{n_k} \left(T_a^{(f)}(k,h) - T_a(h) \right) \\ \sigma_{T_a}^2(\Delta k) &= \frac{1}{n_k - 1} \sum_{k=1}^{n_k} \left(T_a^{(f)}(k,h) - T_a(h) - T_a^{(b)}(\Delta k) \right)^2 \end{aligned} \tag{4.25}$$

where, $T_a^{(f)}(k,h)$ is the forecasted temperature at time h evaluated at time k, and n_k is the number of time steps with valid data. The ambient temperature distribution is:

$$\tilde{T}_a(k,h) \sim \mathcal{N}(T_a^{(f)}(k,h) - T_a^{(b)}(h-k), \sigma_{T_a}^2(h-k)) \tag{4.26}$$

Figure 4.4 shows a temperature forecast at noon for summer day in Denver, CO. The shaded region shows the 95% confidence interval. The standard deviation of the temperature forecast with a time difference of 1 hour was 0.6°C. The uncertainty increases for the first 3 hours of the forecast and then remains stable near 2°C. We note that this

analysis covers only temporal uncertainty; there could also be locational uncertainty because of weather differences between the weather station and the house.

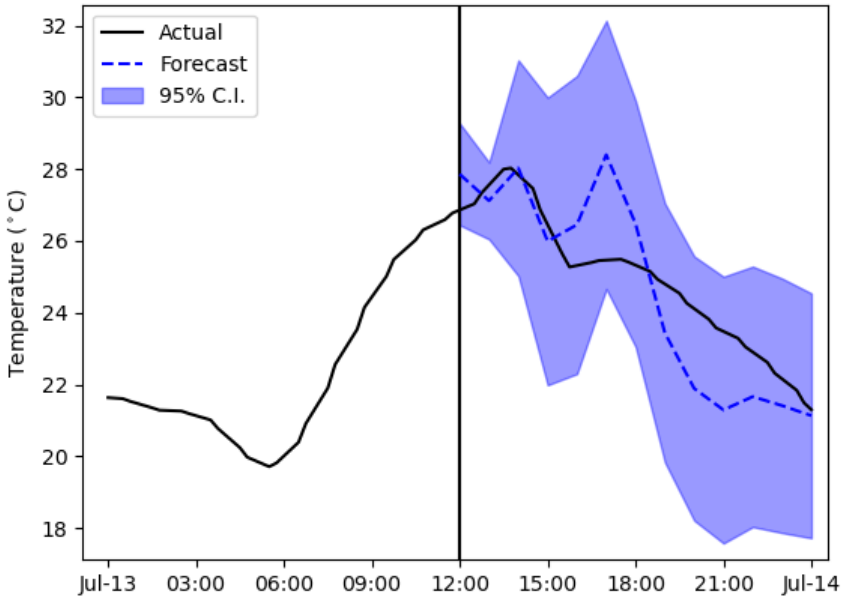

Figure 4.4 An example temperature forecast, created at noon on a summer day in Denver, CO.

The solar heat gain distribution is calculated using a slightly different method to keep uncertainty low when solar irradiance is low, for example, at night. The standard deviation of global horizontal irradiance (GHI) is calculated in the same way as (4.25) and was used to calculate the solar heat gain standard deviation:

$$\sigma_{H_s}(k,h) = H_s^{(f)}(k,h)\frac{\sigma_{GHI}(h-k)}{\mu_{GHI}(h-k)} \tag{4.27}$$

where $H_s^{(f)}(k,h)$ is the forecasted solar gain vector, and $\mu_{GHI}(\Delta k)$ is the average forecasted GHI.

Figure 4.5 shows the GHI forecast for the same time as Figure 4.4. The uncertainty follows a similar pattern to temperature; the standard deviation increases during the first few hours of the forecast and then remains stable. For a typical GHI of 500 W/m^2, the

standard deviation is about 100 W/m^2. When irradiance is very low, the standard deviation is also low.

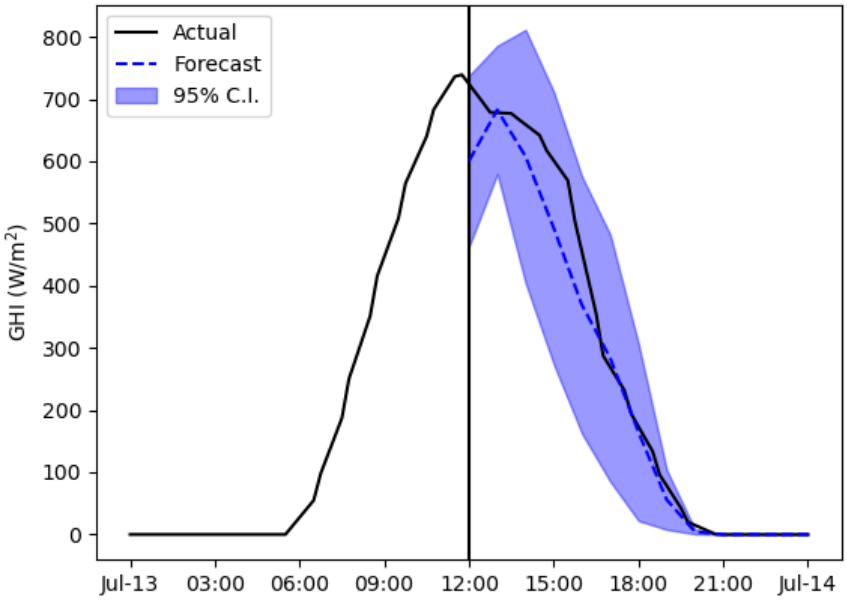

Figure 4.5 An example solar irradiance forecast, created at noon on a summer day in Denver, CO.

4.3.2 Occupant Forecast

Historical occupancy behavior is needed to calculate occupant forecasts. Forecasts are required for driving state (for p_{drive} and p_{leave}), total hot water draws, total uncontrollable load power, and internal heat gains. Uncontrollable power includes appliances, lighting, and other electrical equipment that are not modeled in the MPC framework. Internal heat gains incorporate heat gains from occupants, equipment, radiation from windows, and infiltration.

Three types of forecasts are generated from the historical data. All forecasts define the uncertainty of the random variable by assuming a Gaussian distribution at each time step. An exact forecast directly uses the results of the simulation as the mean and sets the

standard deviation of the variable to zero:

$$\tilde{z}_{i,exact}(k,h) \sim \mathcal{N}(z_i(h), 0) \tag{4.28}$$

where $z_i(h)$ is the exact value of z_i at the prediction time h.

A second forecast uses a backward-looking 30-day moving horizon to estimate random variables based on the time of day. For example, the water draw at noon on July 1 is estimated using the water draw values at noon from the month of June. The sample mean and sample variance are used to define the random variable distribution at that time.

A third forecast uses an autoregressive integrated moving average exogenous (ARIMAX) filter to estimate random variable distributions. The 30-day horizon forecast is used as the exogenous component. The ARIMAX filter is best run at 30-minute resolution using an order of (2, 1, 1) for autoregressive, difference, and moving average parameters [163].

It is very difficult to measure internal gains in a real environment, and it would be impossible to use an ARIMAX forecast without data measurements. For this reason, we do not calculate an ARIMAX forecast for internal gains; instead, we use the 30-day horizon forecast for internal gains.

Figure 4.6 and Figure 4.7 show the three forecast options at a single simulation time step for the water draw and EV driving variables, respectively. The forecasts were calculated using annual occupancy data at a time resolution of 30 minutes. The figures show the mean and the 95% confidence interval for the 30-day horizon and ARIMAX forecasts. Both variables have a considerable amount of uncertainty using these forecasts. In the near term, the ARIMAX forecast does a better job of estimating the EV driving state and reducing its uncertainty by using current and past data in its prediction; however, the two long-term estimates perform about the same, with the ARIMAX predicting larger uncertainty. The ARIMAX method also does not significantly impact the water draw forecast; this implies that the recent water draw data does not help improve the forecast, which is understandable given the highly stochastic nature of water draws.

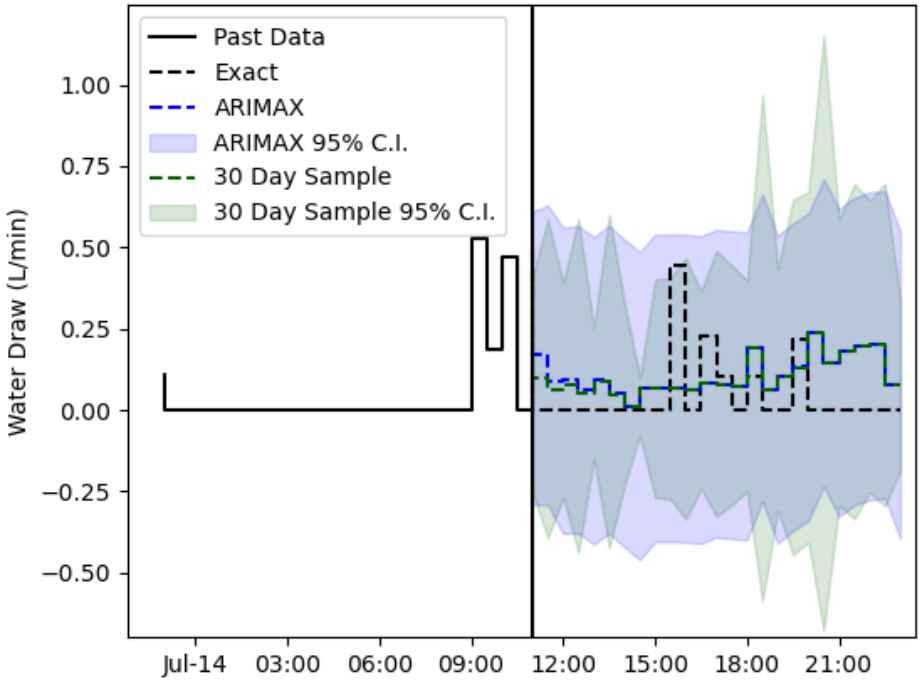

Figure 4.6 An example water draw forecast for a sample occupant profile at a single time step.

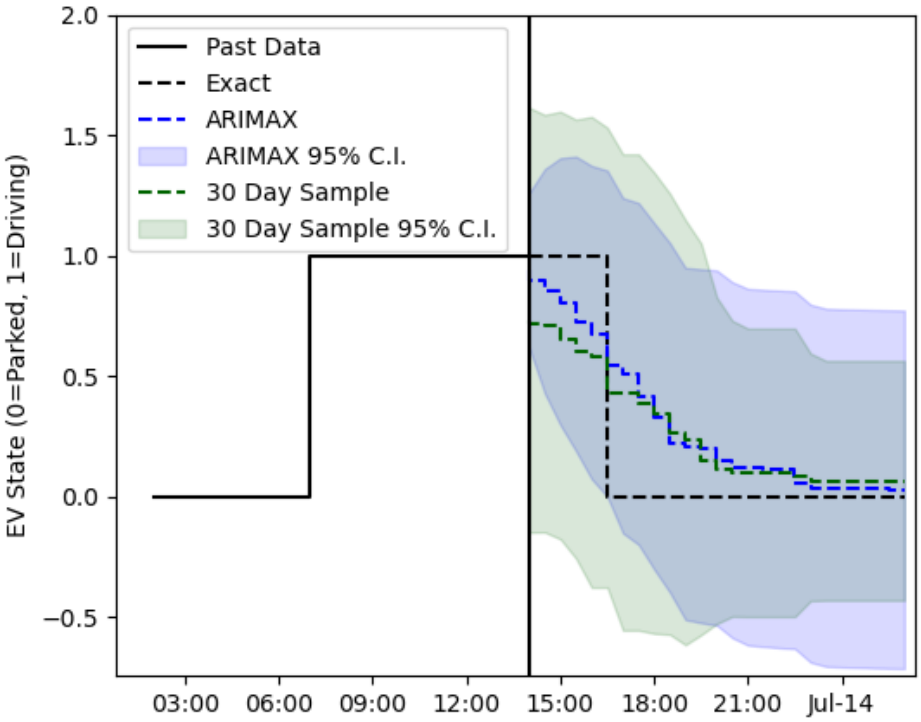

Figure 4.7 An example EV driving forecast for a sample occupant profile at a single time step.

As noted in Section 4.1.7, Gaussian distributions may not be accurate representations of some occupancy variables, including the EV driving state. However, the mean and standard deviation of the forecast distribution is required in the control formulation, so Gaussian forecasts are appropriate in this case. Future control improvements that incorporate other parameters for uncertainty could use different types of forecasts, for example classifiers or ensemble-based methods.

4.4 Chapter Summary

In this chapter, we develop a control framework for HEMS that can account for multiple sources of uncertainty. We linearize device models from Chapter 3 and create deterministic and stochastic house models for use in MPC. We define heuristic, deterministic, and stochastic control strategies that account for energy and demand charges, occupant comfort and convenience, and device degradation. We also define multiple forecasting methods to predict the expected value and distribution of weather and occupancy variables. The framework enables researchers to evaluate the control strategies against each other under various conditions.

This chapter addresses Research Question 4 by incorporating uncertainty from multiple sources in a model-based control framework for residential buildings. The forecasting methods quantify the uncertainty in weather and occupant behavior, and the stochastic MPC implementation accounts for this uncertainty in its objective function. The framework also incorporates uncertainty from the control model and from errors in sensor measurements.

CHAPTER 5
MODEL VALIDATION

This chapter contains preliminary model validation results for OCHRE, the residential energy model presented in Chapter 3, and for the linear model presented in Chapter 4. We first validate OCHRE's building envelope, HVAC, and water heater models against EnergyPlus and OCHRE's EV model against EVI-pro. We show preliminary results using a software-to-software validation method comparing OCHRE and EnergyPlus with multiple test cases. We then validate the linear model against OCHRE. Results show reasonable agreement between OCHRE and the other models.

5.1 EnergyPlus Model Validation

OCHRE and EnergyPlus are two energy models that have different modeling goals, different features, and different benefits for certain use cases. EnergyPlus is a very detailed model that is designed to model an individual building with very high accuracy. OCHRE focuses less on model accuracy and specificity in building parameters and more on other features of an integrated residential energy model including controllability, modularity, and computational efficiency. Many of OCHRE's components—including the building envelope, HVAC equipment, and water heating—use algorithms that are derived from EnergyPlus, making it a useful tool for validating OCHRE.

We validate the OCHRE model against EnergyPlus using one of the house models described in Section 6.2. The house model represents an energy efficient all-electric single family home in Fort Collins. It includes an ASHP and an electric resistance water heater. Weather data from Fort Collins was used from 2018.

Annual simulations were performed at a 1-minute resolution in OCHRE and a 10-minute resolution in EnergyPlus. The alternative methods for modeling HVAC and water heating at a lower time resolution (as discussed in sections 3.1.2 and 3.1.3) were also tested at a 10-minute resolution.

Figure 5.1, Figure 5.2, and Figure 5.3 show the hourly validation results for three days in the summer, winter, and shoulder seasons, respectively. HVAC power is shifted slightly earlier in the day compared to EnergyPlus; this may be caused by differences between the models with regard to the thermal mass of the interior space or the solar transmitted through the windows. Water heating energy is about equal, but the timing of consumption is different, likely because of small differences in the water tank temperatures.

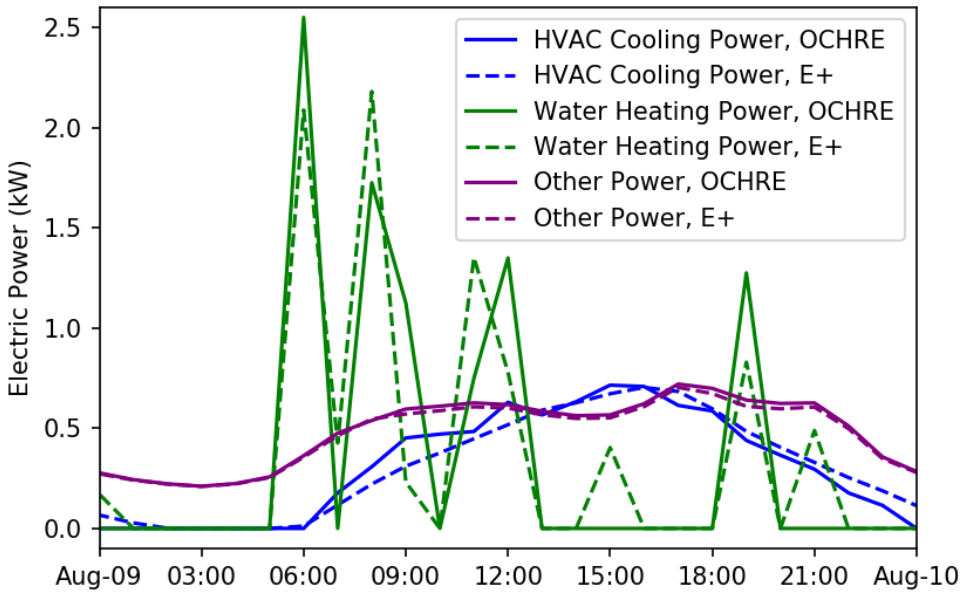

Figure 5.1 Validation results for a summer day comparing hourly energy consumption by end use from OCHRE (solid) and EnergyPlus (dashed).

Table 5.1 shows the validation results across a full year of simulation. Compared to EnergyPlus, OCHRE underestimates HVAC heating energy and slightly overestimates HVAC cooling energy. Differences in HVAC-delivered heating and cooling are small, indicating that the majority of the difference is caused by an overestimation in ASHP efficiency. Differences in solar radiation heat transfer through the windows might contribute to more heating and less cooling in OCHRE.

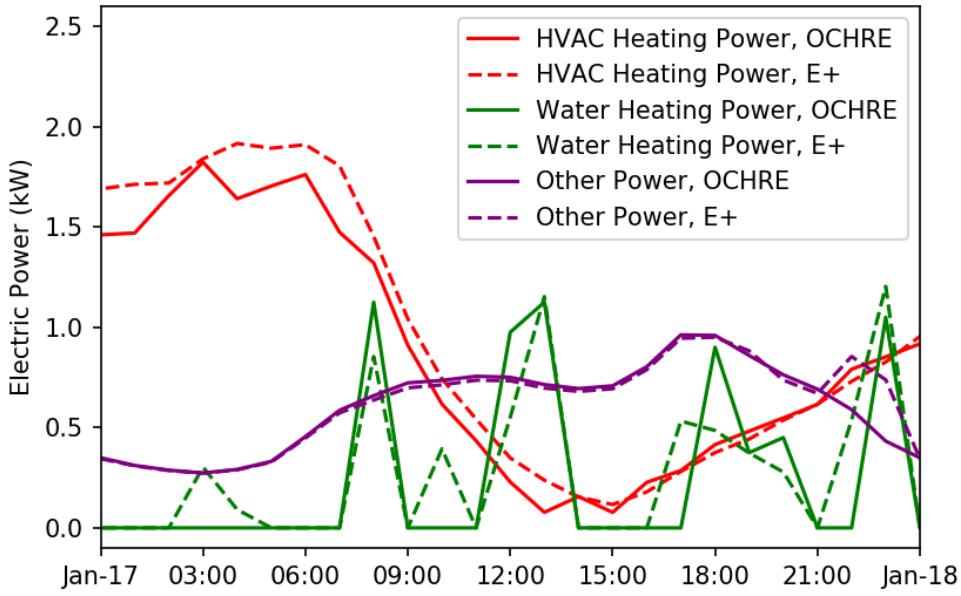

Figure 5.2 Validation results for a winter day comparing hourly energy consumption by end use from OCHRE (solid) and EnergyPlus (dashed).

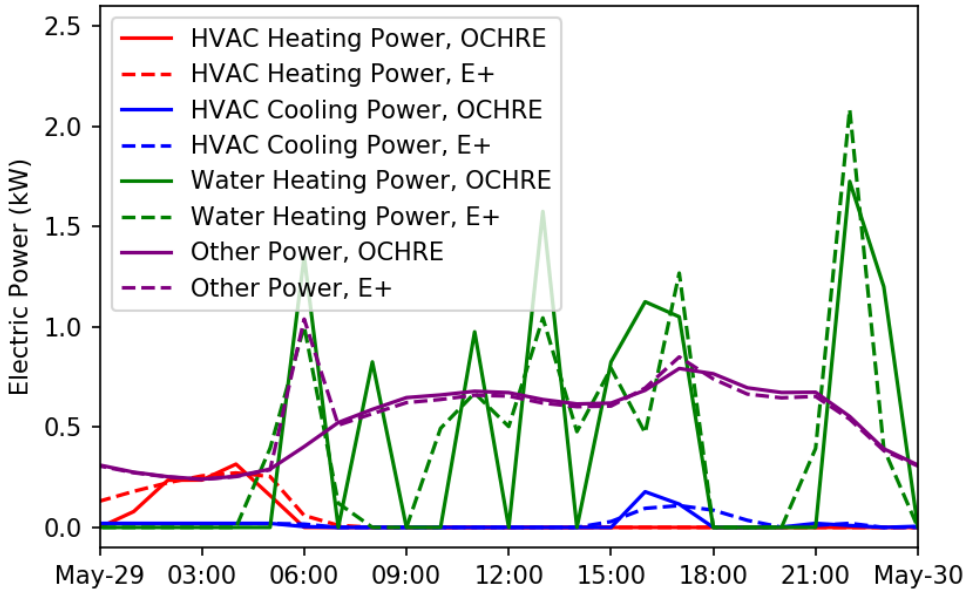

Figure 5.3 Validation results for a shoulder season day comparing hourly energy consumption by end use from OCHRE (solid) and EnergyPlus (dashed).

Table 5.1 Annual validation results comparing energy consumption by end use.

End Use	OCHRE (kWh)	EnergyPlus (kWh)	Percentage Error
HVAC heating	2,795	3,063	-8.7%
HVAC cooling	739	733	0.8%
Water heating	4,369	4,199	4.1%
Other loads	4,832	4,786	1.0%
Total	12,736	12,781	-0.4%

5.2 EV Model Validation

We validate the OCHRE EV model to ensure that the daily load profile is similar to the profile from EVI-Pro. The OCHRE and EVI-pro models are very similar because they both use the same underlying data for EV driving and charging parameters. However, EVI-pro does not create multi-day time-series profiles. The primary differences in the models are due to issues with overlapping parking events that occur overnight. OCHRE's assumption may lead to small differences in EV arrival and departure times, which can influence the EV load profile.

Profiles are generated for each vehicle type and size, charging level, ambient temperature bin, and day of week option (see Section 3.1.4 for details). OCHRE was run for 1000 days at 1-minute resolution. The weekday and ambient temperature were held constant for validation purposes.

Figure 5.4 and Figure 5.5 show the daily load profiles for a 50-mile PHEV with a Level 1 charger and a 100-mile BEV with a Level 2 charger during weekdays at 15°C, respectively. OCHRE estimates a slightly larger peak for both profiles, which is likely due to the effects of random sampling. The root-mean-square error is about 0.02 kW for the PHEV and 0.05 kW for the BEV.

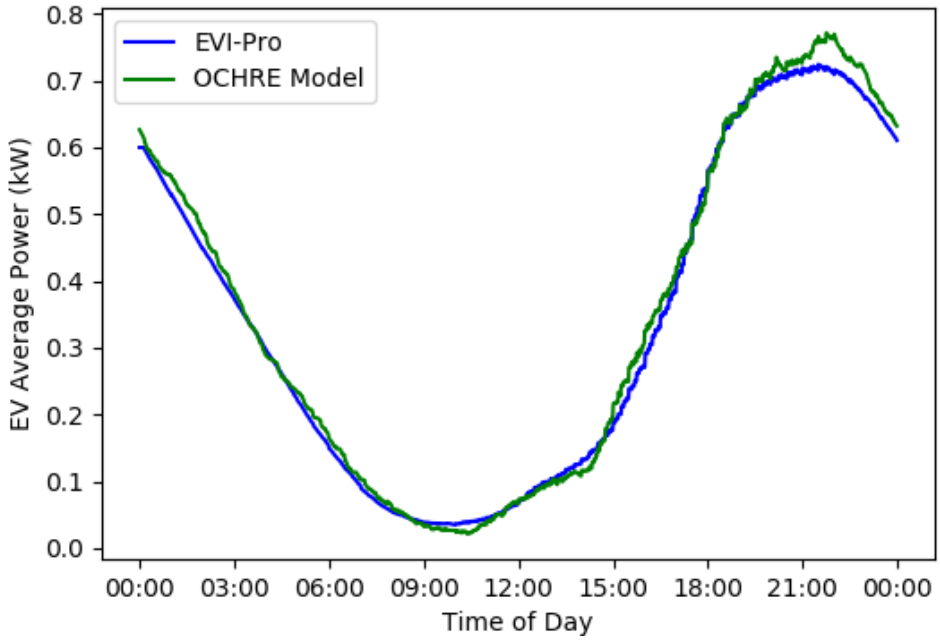

Figure 5.4 Daily load profile comparison for a 50-mile PHEV with a Level 1 charger. ©2021 IEEE

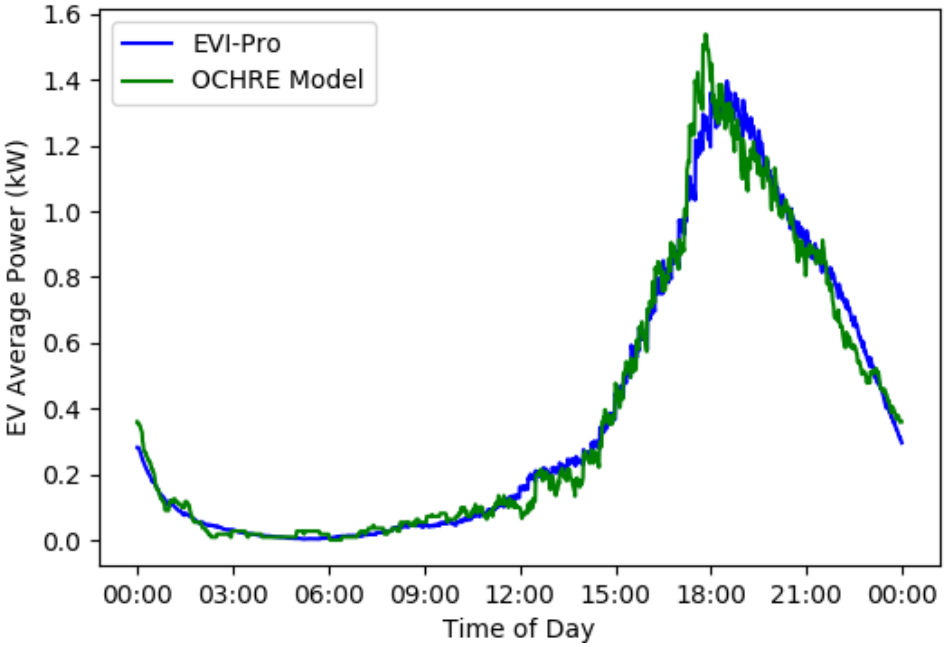

Figure 5.5 Daily load profile comparison for a 100-mile BEV with a Level 2 charger. ©2021 IEEE

5.3 Minimal Building Validation

We have begun a more extensive validation process that evaluates individual components of OCHRE's envelope model. We use software-to-software validation methods that have been used to evaluate many building modeling tools [36, 164]. Software-to-software methods allow model developers to quickly and easily compare building models with different insulation levels and different climates. Using modeling tools with detailed outputs enables faster and easier debugging and refining to align the model with existing models.

We validate OCHRE against EnergyPlus using a method that includes a test suite of "minimal" buildings with very high insulation and few heat transfer pathways [165]. The test cases are created using OpenStudio to generate Home Performance eXtensible Markup Language (HPXML) files that contain all of the building parameters [166]. One test case is used as a baseline with nearly zero heat transfer and minimal internal heat gains. Every other test case changes one envelope feature and evaluates the difference in HVAC consumption from that change. This method helps to isolate model features to identify differences in the modeling tools.

The baseline case models a single family home with a superinsulated building envelope with R-500 walls, ceiling, and floor. There are no windows and negligible infiltration or ventilation. The only internal heat gains are due to HVAC and a single occupant. The house includes an unvented attic with an uninsulated roof and attic walls. Interior wall and furniture mass is included. The house is 2700 square feet (251 m^2), with one floor and three bedrooms. The house includes an oversized electric resistance heater and a SEER 13 central air conditioner that is autosized using Manual J [167]. No other equipment is included, although there are internal gains from a single occupant.

Test suite cases are run for a full year at 10 minute resolution. We run each case in two locations: Denver, Colorado and Phoenix, Arizona. Both locations use Typical Meteorological Year (TMY3) weather data. Both locations use thermostat setpoints of

71°F (21.67°C) for heating and 76°F (24.44°C) for cooling. Occupant schedules are included, which only account for heat gains due to occupancy.

Table 5.2 and Table 5.3 show the results from infiltration and wall insulation test cases in two locations. We compare the total annual heat delivered and the root mean squared error (RMSE) of heat delivered for both heating and cooling loads at hourly resolution. The absolute error and percent errors are reported for annual energy consumption, with positive values indicating that OCHRE overestimates the metric when compared to EnergyPlus. The percent error for RMSE is the RMSE divided by the variance of the time series data from EnergyPlus.

Most cases have HVAC delivered errors less than 200 kWh/year or less than 10%. RMSE values are typically less than 0.1 kW or 20%. Cases with less insulation or more infiltration tend to have more heat delivered and lower percentage errors than cases that are closer to the baseline case. This indicates that OCHRE's envelope converges with EnergyPlus as insulation decreases and infiltration increases. For real homes, HVAC delivered is usually higher than in these test cases. For this reason, we expect that differences in HVAC delivered and in HVAC consumption to be smaller in more realistic cases.

Figure 5.6, Figure 5.7, and Figure 5.8 show the validation results for hourly HVAC delivered heating and cooling across multiple days in the winter, summer, and shoulder seasons, respectively. The figures are generated from the minimal test suite case with R-7 wall insulation in Denver. The delivered heat profile shapes from OCHRE and EnergyPlus match very closely, but the magnitude differs. The largest errors occur during the shoulder season, when the indoor temperature floats from the heating setpoint to the cooling setpoint. OCHRE and EnergyPlus use different approaches for modeling thermal mass—in particular as it relates to radiation heat transfer—which can lead to large changes in HVAC cooling delivered during the shoulder season; however, these differences do not contribute significantly to the annual energy consumption.

Table 5.2 Validation of HVAC heating delivered for multiple locations and scenarios in the test suite.

Location	Name	OCHRE Annual (kWh)	EnergyPlus Annual (kWh)	Difference Annual (kWh)	Hourly RMSE (kW)
Denver	Baseline Minimal Building	425.3	343.7	81.65 (23.8%)	0.02 (34.9%)
	Infiltration - 1 ACH	1027.6	920.4	107.25 (11.7%)	0.03 (23.9%)
	Infiltration - 7 ACH	4359.2	4468.9	-109.62 (-2.5%)	0.11 (20.6%)
	Infiltration - 50 ACH	31275.5	30435.1	840.46 (2.8%)	0.79 (21.9%)
	Wall Insulation - Uninsulated	14874.0	14755.2	118.80 (0.8%)	0.29 (15.4%)
	Wall Insulation - R-7	6926.9	6843.8	83.15 (1.2%)	0.10 (11.8%)
	Wall Insulation - R-11	5963.3	5911.9	51.34 (0.9%)	0.09 (11.4%)
	Wall Insulation - R-19	4133.9	4149.4	-15.46 (-0.4%)	0.05 (9.8%)
Phoenix	Baseline Minimal Building	37.1	5.1	32.00 (632.2%)	0.01 (294.6%)
	Infiltration - 1 ACH	54.6	85.4	-30.82 (-36.1%)	0.01 (45.8%)
	Infiltration - 7 ACH	716.7	734.2	-17.52 (-2.4%)	0.04 (22.4%)
	Infiltration - 50 ACH	5829.0	5764.4	64.63 (1.1%)	0.26 (21.1%)
	Wall Insulation - Uninsulated	2963.7	2521.1	442.63 (17.6%)	0.16 (23.1%)
	Wall Insulation - R-7	1206.2	1023.3	182.87 (17.9%)	0.07 (22.1%)
	Wall Insulation - R-11	1014.5	862.2	152.31 (17.7%)	0.06 (22.2%)
	Wall Insulation - R-19	662.1	569.7	92.47 (16.2%)	0.04 (20.7%)

Table 5.3 Validation of HVAC cooling delivered for multiple locations and scenarios in the test suite.

Location	Name	OCHRE Annual (kWh)	EnergyPlus Annual (kWh)	Difference Annual (kWh)	Hourly RMSE (kW)
Denver	Baseline Minimal Building	119.6	186.0	-66.37 (-35.7%)	0.02 (47.3%)
	Infiltration - 1 ACH	97.5	152.5	-55.01 (-36.1%)	0.02 (49.4%)
	Infiltration - 7 ACH	54.7	98.7	-43.92 (-44.5%)	0.03 (58.0%)
	Infiltration - 50 ACH	418.4	398.4	20.06 (5.0%)	0.13 (51.3%)
	Wall Insulation - Uninsulated	1711.1	1923.7	-212.58 (-11.1%)	0.19 (29.5%)
	Wall Insulation - R-7	670.2	803.3	-133.06 (-16.6%)	0.07 (25.1%)
	Wall Insulation - R-11	572.4	697.7	-125.28 (-18.0%)	0.06 (24.6%)
	Wall Insulation - R-19	402.4	505.8	-103.39 (-20.4%)	0.04 (25.1%)
Phoenix	Baseline Minimal Building	508.7	650.0	-141.29 (-21.7%)	0.02 (36.3%)
	Infiltration - 1 ACH	511.1	751.2	-240.04 (-32.0%)	0.04 (47.1%)
	Infiltration - 7 ACH	1349.0	1581.5	-232.42 (-14.7%)	0.07 (27.1%)
	Infiltration - 50 ACH	7649.6	7810.1	-160.47 (-2.1%)	0.36 (25.5%)
	Wall Insulation - Uninsulated	9693.5	10613.5	-919.93 (-8.7%)	0.35 (22.8%)
	Wall Insulation - R-7	4610.2	5009.2	-399.05 (-8.0%)	0.12 (17.5%)
	Wall Insulation - R-11	4010.4	4376.2	-365.87 (-8.4%)	0.10 (17.1%)
	Wall Insulation - R-19	2870.3	3161.1	-290.73 (-9.2%)	0.06 (15.0%)

We also note that there are significant differences in the attic temperature, with EnergyPlus simulating much higher temperatures in the summer season. This difference does not affect the HVAC delivered in this case because the ceiling is superinsulated. However, in other test cases and in real systems, this may cause OCHRE to underestimate the HVAC delivered heat requirements due to less conduction through the ceiling. Ongoing validation efforts are addressing this issue in attics as well as in foundations and garages.

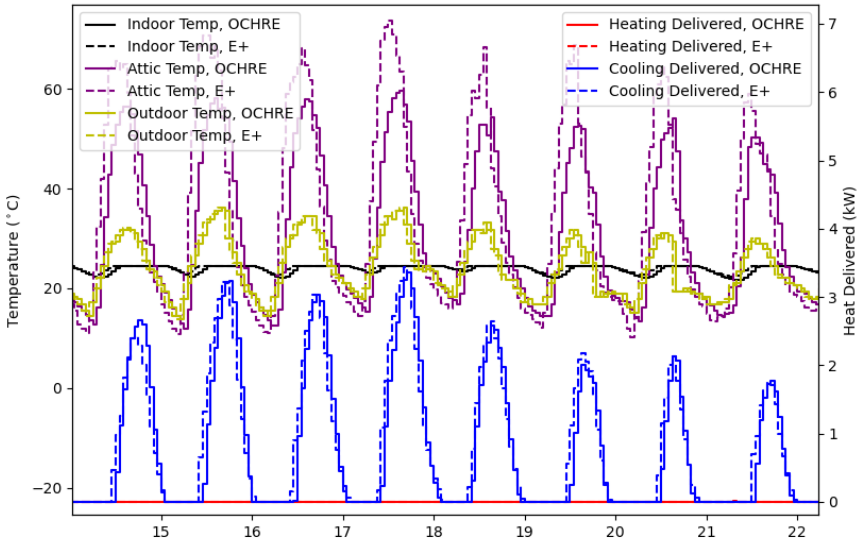

Figure 5.6 Minimal building validation results in the summer in Denver, comparing hourly HVAC delivered heat from OCHRE (solid) and EnergyPlus (dashed).

5.4 Control Model Validation

The control model developed in Section 4.1 was derived from the OCHRE models of individual devices. All device models are nearly identical except for the HVAC and envelope model. Here, we show the validate the model by showing the impact of the model reduction and linearization on the envelope model. The validation simulations use the same parameters as the case study in Section 7.2.

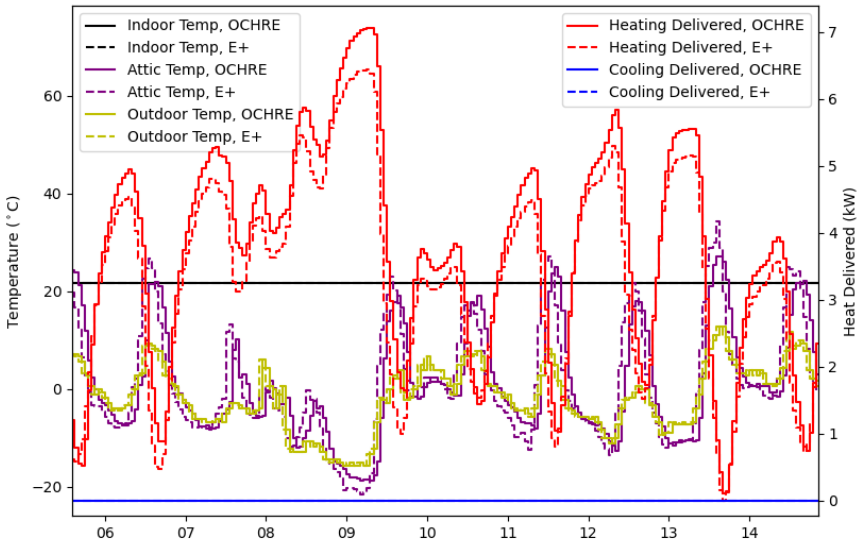

Figure 5.7 Minimal building validation results in the winter in Denver, comparing hourly HVAC delivered heat from OCHRE (solid) and EnergyPlus (dashed).

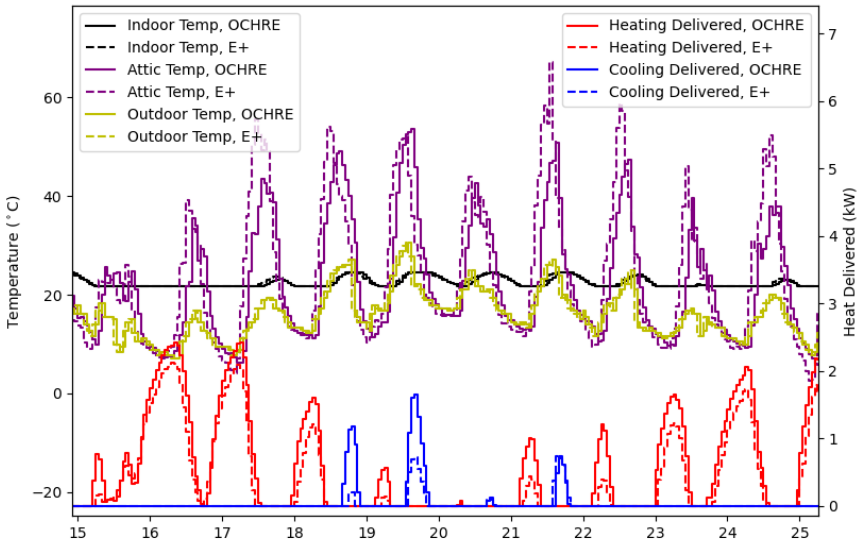

Figure 5.8 Minimal building validation results in the shoulder season in Denver, comparing hourly HVAC delivered heat from OCHRE (solid) and EnergyPlus (dashed).

The impacts of the model reduction and linearization of radiation and infiltration are shown in figures Figure 5.9 and Figure 5.10. Figure 5.9 shows the difference in the modeled indoor air temperature between the full OCHRE model and the linearized model described in Section 4.1.2. In both models, the air conditioner turns on around midday and cycles according to the deadband control with a constant set point. At night, the air conditioner turns off, and the temperature floats below the set point. During a 10- to 15-hour window each night, the maximum temperature deviation between the simulations is less than 1°C.

Figure 5.10 compares the air-conditioning energy consumption during the peak period under different modeling conditions to assess the impacts of linearization and model reduction. Three models—OCHRE, a full-order linear model, and the reduced-order linear model—were run with a constant HVAC set point and the heuristic precooling control. The linear models overestimate the HVAC consumption compared to the OCHRE model, and they underestimate the energy savings due to precooling controls. The reduced linear model underestimates the difference by 14%, indicating that the MPC might undervalue precooling controls in this use case.

5.5 Chapter Summary

This chapter provides validation results for the OCHRE model and the linear model for MPC. EnergyPlus is used to validate OCHRE's thermal models for HVAC and water heating equipment, EVI-pro is used to validate the EV model. The envelope linearization and model reduction are compared against OCHRE to ensure that the impact on temperature and HVAC consumption were small.

These results address Research Question 2 concerning the comparison between integrated residential energy models, such as OCHRE, and existing state-of-the-art models. We show that OCHRE performs similarly to EnergyPlus when comparing time-series data and aggregated metrics. For the control model validation, the linearization and model reduction lead to modeling errors, but the impact on HVAC consumption is within expected limits and is unlikely to significantly affect model-based control performance.

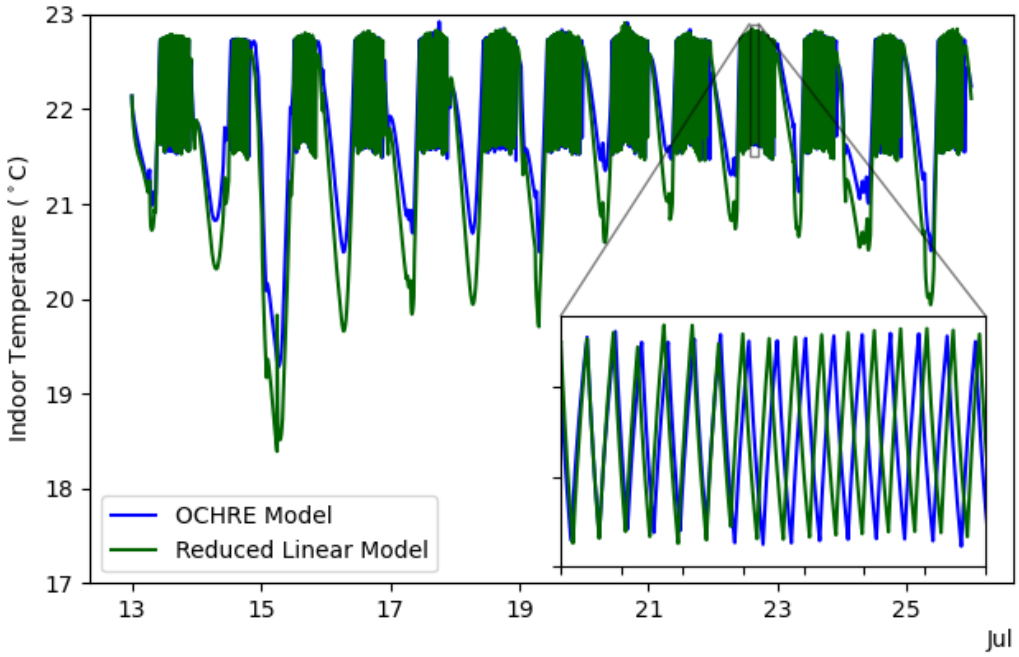

Figure 5.9 Indoor temperature using the full and linearized models

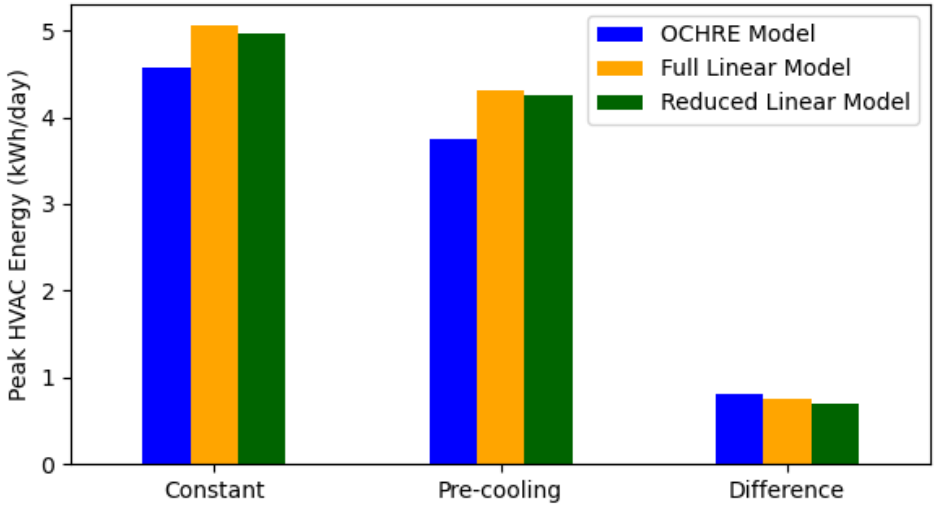

Figure 5.10 HVAC energy consumption during peak hours using various models and controls.

CHAPTER 6

COMMUNITY CO-SIMULATION MODELING

This chapter presents a co-simulation framework for integrating residential energy models, controllers, and a distribution system simulator. Section 6.1 describes the co-simulation framework, including the communication methods between models and controllers. Section 6.2 shows the benefits of using high-resolution models for simulating a demand response event using a community-level co-simulation; although we highlight multiple features of the model, we focus on the impact of time resolution on demand response magnitude and on power and voltage fluctuations. Section 6.3 shows results when coupling OCHRE with foresee [32], an existing HEMS controller.

6.1 Co-simulation Framework Description

In this section, we outline the methods for integrating OCHRE in an agent-based co-simulation framework. The framework contains three types of agents: controllers, house models, and a community grid model. A schematic of this framework is shown in Figure 6.1. The house models receive control signals from the controller and local voltage data from the grid model, solve for the net power of each house, and then send that power to the grid model. The framework is designed to be modular so that multiple control and modeling tools can be used interchangeably.

6.1.1 House Models

The model components described in Section 3.1 are combined in an object-oriented framework for simpler integration in a co-simulation. Each piece of equipment is represented by an object, and each has the ability to accept a control signal, consume energy, and contribute to internal heat gains. This framework allows for modular house models that can easily be modified by adding or replacing equipment.

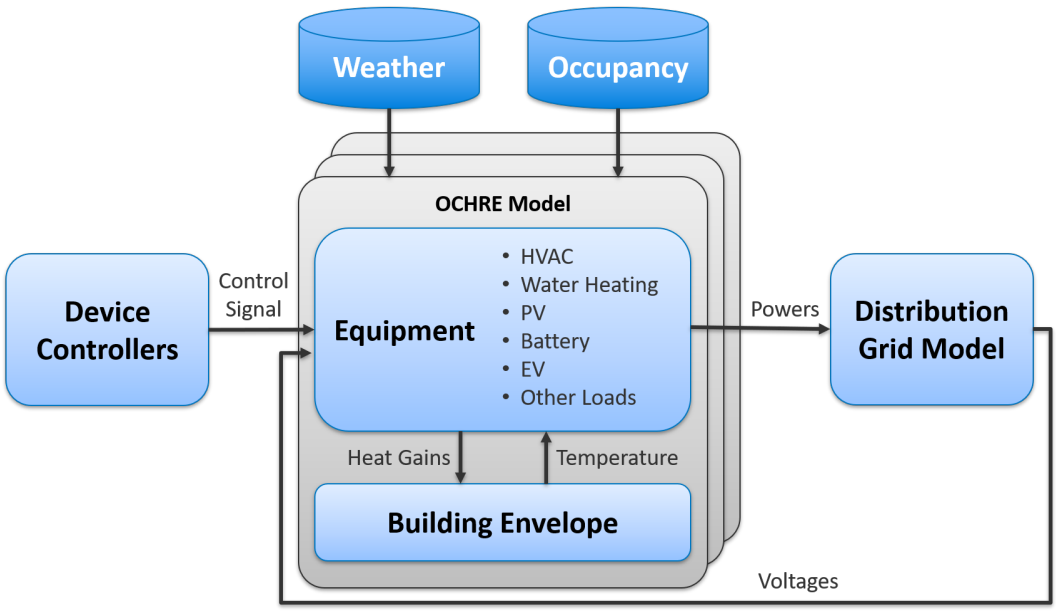

Figure 6.1 Schematic for the OCHRE model in a co-simulation framework.

Multiple house models are launched in parallel to simulate a residential community. In each house, the equipment powers are aggregated to determine the total house real and reactive power at each time step:

$$\begin{aligned} P_{net,d}(k) &= P_{load,d}(k) + P_{pv,d}(k) + P_{batt,d}(k) \\ Q_{net,d}(k) &= Q_{load,d}(k) \end{aligned} \tag{6.1}$$

where k is the time step and d is the house index. Note that the power for equipment that does not exist is set to 0. The real and reactive powers for each house are sent to the community grid model at each time step.

6.1.2 Distribution Grid Model

The distribution grid model considers each house as a load with time-varying real and reactive power. The grid model solves the power flow equation to calculate the voltages at each house. The co-simulation passes each house voltage back to the voltage-dependent load model at the next time step.

The distribution model may contain additional loads and other features external to the house models—for example, distributed generation resources, capacitor banks, and

commercial and industrial loads. These components are assumed to be uncontrollable in the co-simulation framework.

6.1.3 House Controllers

Controllers integrated in the co-simulation framework have access to a wide variety of information that could feasibly be measured from sensors in the home or on the distribution network. This includes house state information—for example, air temperature, water temperature, battery SOC, and energy consumption for each equipment. The controller can also receive grid state information—for example, the house voltage—and external parameters, such as utility rates and weather.

Control signals to the house model are modular and device-specific, i.e., each piece of equipment receives a different signal. This framework allows for the control of different sets of equipment at different times and for the use of multiple device-level controllers in the same building. Controllers can send the same signal to all houses or send a unique signal to each house.

6.2 New Construction Case Study

In this section, we run OCHRE and the co-simulation framework to demonstrate the features and benefits of OCHRE. We show the differences in simulation results when using 1-minute and 15-minute time resolutions and when sending control signals to multiple controllable device models. Results show that the time resolution can have a significant effect on measured load flexibility.

Each scenario uses the same 498-home, all-electric, zero energy-ready community based in Fort Collins, Colorado, during a 24-hour period on a hot summer day. A zero energy community of this size can present a challenge to grid operators because of the potential for substantial back-feeding. Scenarios show the community power during baseline conditions and during a demand response event with two types of control strategies: load shedding and load shifting.

6.2.1 Simulation Inputs

The house and grid models require a wide variety of inputs, including weather data, building properties, equipment properties, and distribution system inputs. We leverage a wide range of other models and tools to generate these inputs. Because of the variability and the large number of inputs, we do not provide values for each one; however, below are brief summaries of each input category:

- Weather data: Weather data are actual meteorological year data taken from Fort Collins, Colorado, in 2018 at hourly resolution.

- Building properties: The community model was developed based on plans from a high-efficiency home builder in Fort Collins for an actual community planned in the area. Based on the builder specifications, the buildings were modeled as being eligible for the U.S. Department of Energy's Zero Energy Ready program [157]. The National Renewable Energy Laboratory's (NREL's) BEopt^{TM}[168] tool was used to generate the building models. The community comprises 201 small single-family homes, 79 large single-family homes, 30 duplexes, and 48 townhomes with 2–6 units each. Homes are modeled in various orientations to more accurately model load diversity.

- Equipment properties: All 498 homes have an ASHP and an electric resistance water heater. Equipment capacity depends on the building type, with the HVAC sized according to ACCA Manual J [167]. All homes have a PV system with capacities ranging from 3–19 kW. The total community PV capacity is 3.4 MW. Fifty homes have an EV (25 battery EV and 25 plug-in hybrid EV), and the same 50 homes have a 3 kW, 6 kWh battery.

- Distribution system properties: The distribution grid model was developed in collaboration with the City of Fort Collins Utilities. It includes an existing medium-voltage feeder as well as a new secondary network for the proposed

all-electric community. The secondary network combines typical practices of distribution design in the area with necessary upgrades for an all-electric community. AMI data at 15-minute resolution are used to simulate existing buildings on the medium-voltage feeder to set up realistic grid conditions for the community system under study. The new community adds approximately 2 MW of peak load to the existing 6 MW feeder.

For most equipment controls in this section, we employ an open-loop, schedule-based control strategy that sends the same signal to all houses. However, batteries are operated such that they charge only from solar and discharge to load when the total load is larger than the PV generation. The BESS power is defined by control logic:

$$\begin{aligned} P_{chg}(k) &= \min(-P_{pv}(k), \overline{P_{batt}}, \frac{\kappa_{batt}}{t_s \eta_{chg}}(\overline{SOC} - SOC(k)) \\ P_{dis}(k) &= \min(\max(P_{load}(k) + P_{pv}(k), 0), \overline{P_{batt}}, \frac{\kappa_{batt}\eta_{dis}}{t_s}(SOC(k) - \underline{SOC}) \end{aligned} \tag{6.2}$$

where P_{load} and P_{pv} are described in sections 3.1.6 and 3.1.7, $\overline{P_{batt}}$ is the battery power capacity, and $\underline{SOC}$ and $\overline{SOC}$ are the SOC battery limits. When both P_{chg} and P_{dis} are non-zero, their values are reduced until one equals zero. This self-consumption control logic was chosen to reduce battery discharge power when there is some PV generation.

6.2.2 Simulation Engine

We use the Hierarchical Engine for Large-scale Infrastructure Co-Simulation (HELICS) platform [88] to run the scenarios. Separate agents are used for each of the 498 house models and for the grid model. The OCHRE models are coded in Python using standard libraries. We use the Python package OpenDSSDirect.py to connect the co-simulation framework to an OpenDSS distribution grid model [89, 169].

The scenarios were run using NREL's high-performance computing system [170]. The 498 homes ran in parallel on 5 nodes. The 24-hour simulations with 1-minute time resolution took 239 seconds total, with an individual home taking 1.83 seconds on a single

node. The simulations with 15-minute resolution took 126 seconds total.

6.2.3 Baseline Results

The results of the baseline scenarios show the community power output without any control signals under varying time resolutions. The aggregated community power by end use for the 1-minute and 15-minute baseline simulations are shown in figures Figure 6.2 and Figure 6.3, respectively. Most end uses show a similar profile in these two scenarios, although the HVAC cooling has much more variability in the 1-minute scenario. The community power does not have as much variability as the individual units because of diversity in the house models.

Figure 6.4 shows the total community power and minimum and maximum voltages for the 1- and 15-minute time resolution simulations. The 1-minute simulation results have noticeably more variability than the 15-minute results, including a much larger peak power (1605 kW compared to 807 kW) and minimum voltage (0.975 p.u. compared to 0.987 p.u.) near 6 PM. The percentage of voltage violations (accounting for duration and quantity of violations) greater than 1.05 p.u. increased by 59% in the 15-minute resolution simulation.

The increased variability in the 1-minute simulation is primarily caused by the HVAC and water heater models because these models include realistic equipment cycling, but the models in the 15-minute simulations do not. This cycling directly leads to variability in distribution power and voltages; therefore, it is very likely that distribution studies that do not include high-resolution load models with equipment cycling will underestimate voltage variations. This finding is important for utilities and regulators to consider when evaluating distribution simulation studies.

6.2.4 Load-Shedding and Load-Shifting Control

The load-shedding controller is called to perform a demand response event in which loads should be reduced from 5 PM to 9 PM. The controller modifies all of the house models in the following ways during the demand response event:

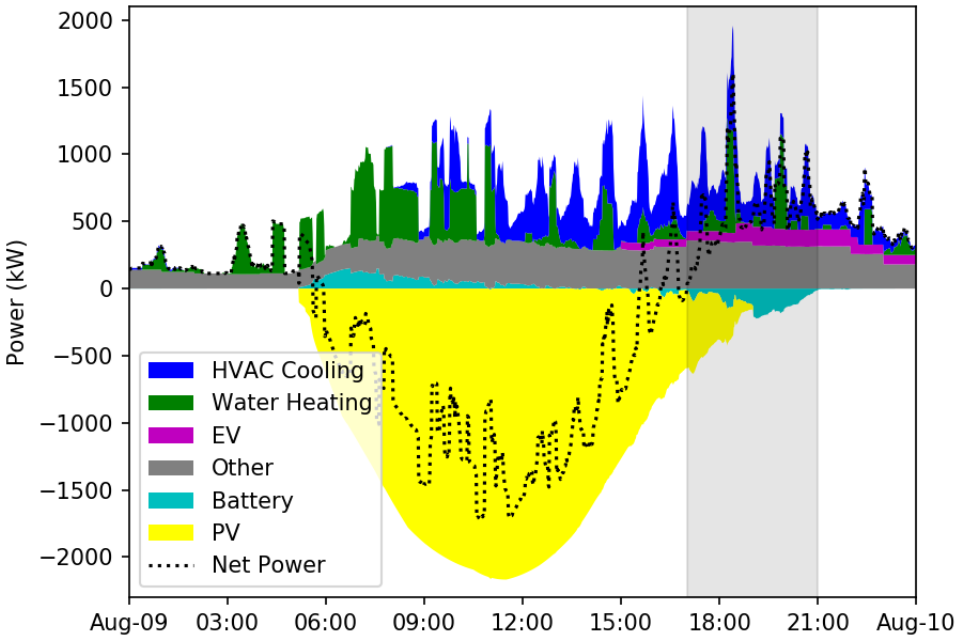

Figure 6.2 Total community power by end use for the baseline scenario at 1-minute time resolution.

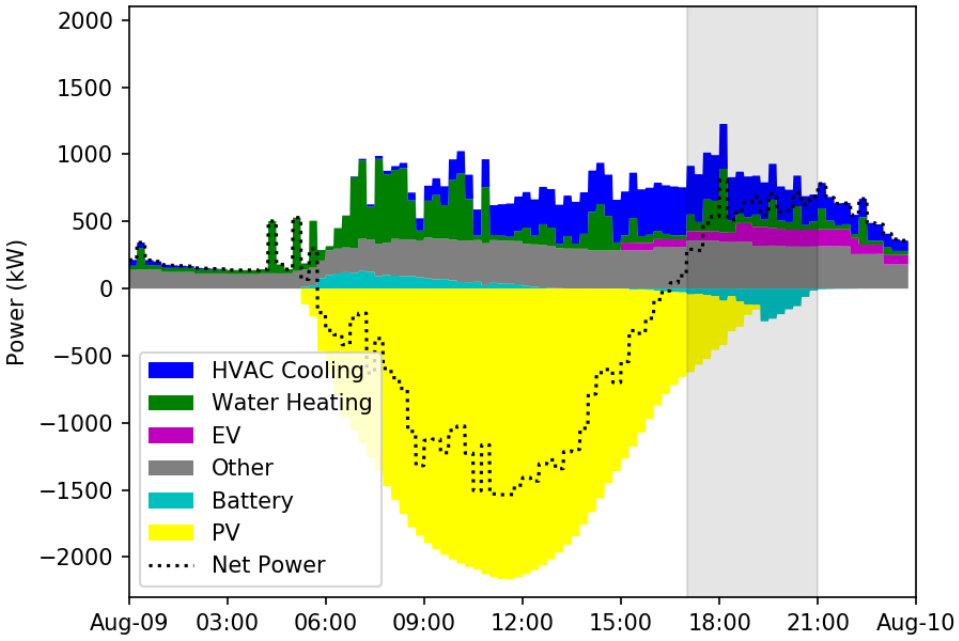

Figure 6.3 Total community power by end use for the baseline scenario at 15-minute time resolution.

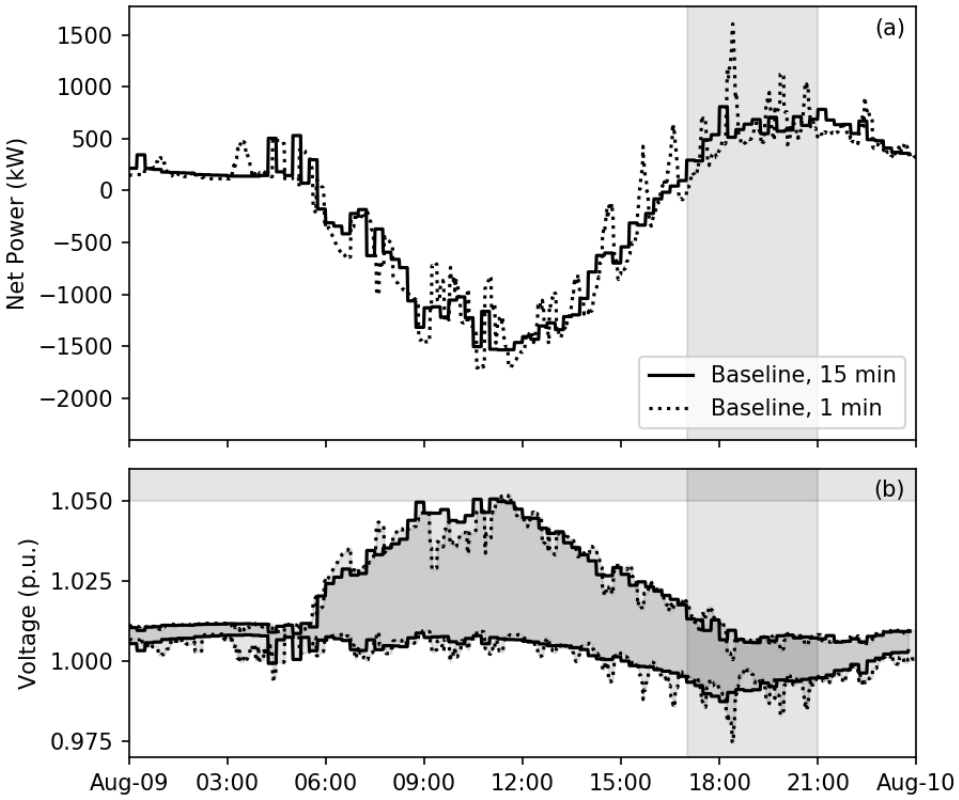

Figure 6.4 Community power and voltages for baseline scenarios at 1- and 15-minute time resolution. Subplots show community total power (a) and maximum and minimum voltage (b).

- Cooling set point T_c increases from 72°F to 75°F
- Water heater set point decreases from 125°F to 120°F
- Battery power set to fully discharge at a constant rate by 9 PM
- EV charging delayed until 9 PM, if necessary

The load-shifting controller assumes the same demand response event, uses the same load-shedding controls, and modifies all of the house models from 2 PM to 5 PM, before the event, in the following ways:

- Cooling set point T_c decreases from 72°F to 69°F
- Water heater set point increases from 125°F to 130°F
- Battery power set to fully charge at a constant rate by 5 PM

Because there are similar results from the two controllers, we show detailed results only for the load-shifting controller in Figure 6.5. The controller reduces loads during the critical peak period, but it also causes large spikes in community power at 2 PM and 9 PM, due to the control logic that synchronizes equipment cycles in many homes. The effects of synchronized cycles can also be seen in the smaller spikes after 2 PM and after 9 PM. These spikes can cause voltage violations and overloaded equipment. OCHRE can be used to evaluate the ability for more advanced control strategies—for example, DER aggregation or market-based dispatch—to solve these issues.

The community power for all six scenarios is shown in Figure 6.6. All of the controlled scenarios show lower total community power during the critical peak period, and the load-shifting control has slightly lower community power than the load-shedding control. Both controllers have a power spike at 9 PM, and the load-shifting control has a spike at 2 PM. The magnitude of the spike is smaller when using the load-shifting controller, showing that the controller successfully moved some of the load ahead of the peak period.

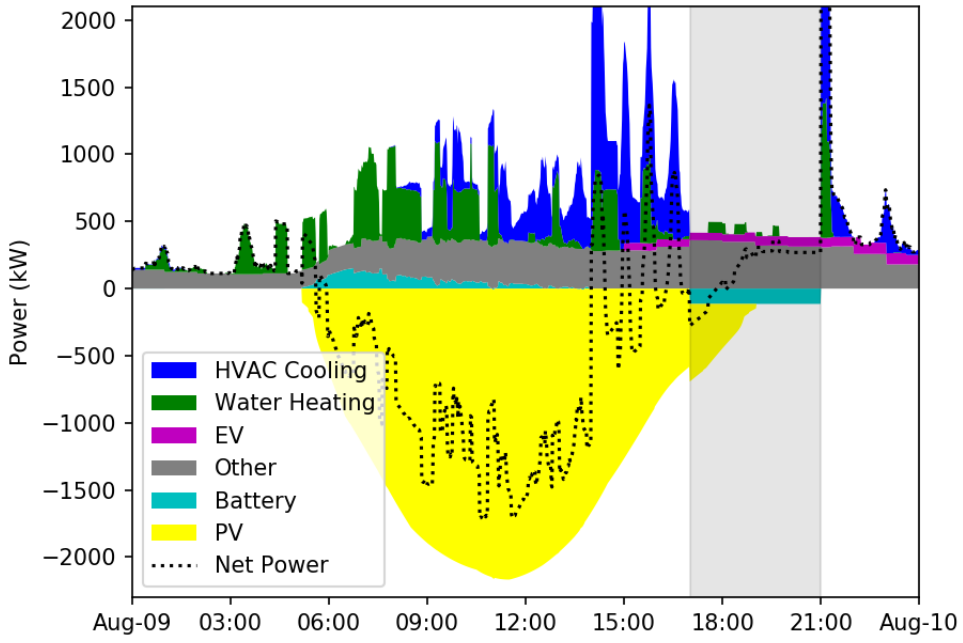

Figure 6.5 Total community power by end use for the load-shifting scenario at 1-minute time resolution.

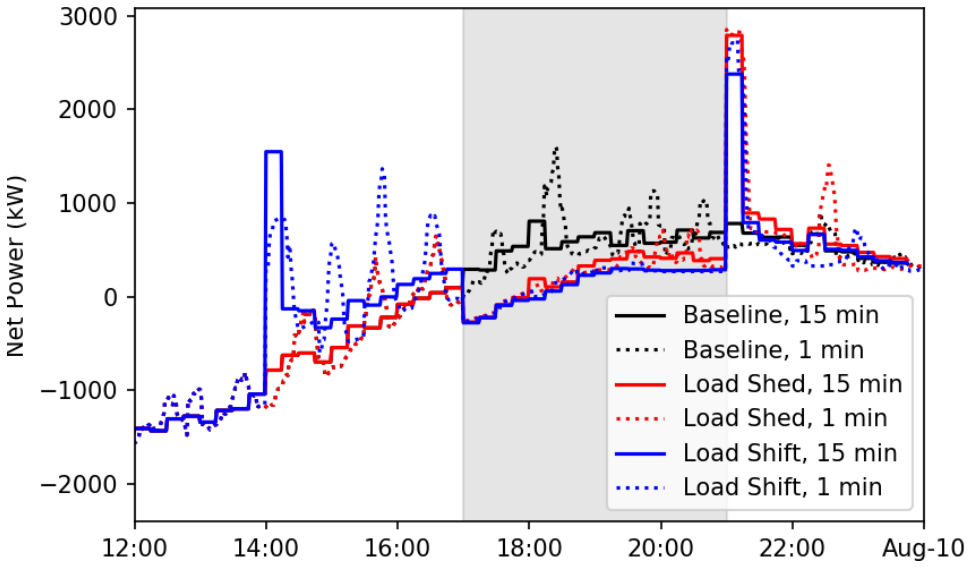

Figure 6.6 Total community power for all scenarios.

All 1-minute scenarios have more power variability and larger power spikes than their corresponding 15-minute scenario, which led to a larger peak demand reduction during the critical peak period. After averaging power in all scenarios to 15-minute resolution, the load-shedding controller reduced peak demand by 755 kW (60%) in the 1-minute simulation but by only 324 kW (40%) in the 15-minute simulation. Similarly, the load-shifting controller reduced peak demand by 930 kW (73%) in the 1-minute simulation but by only 506 kW (63%) in the 15-minute simulation. These results show that low-resolution load models may underestimate the benefits of load-reduction strategies in distribution systems.

It is also interesting to note the difference in peak demand reduction by end use. For the load-shifting controller in the 1-minute scenario, the average power reduction during the critical peak period was 298 kW for HVAC, 104 kW for water heating, 45 kW for EV, and 11 kW for batteries. However, this result may not be generalizeable because it is highly dependent on timing, weather conditions, building properties, and equipment adoption rates.

6.3 Case Study with foresee

This section presents results using OCHRE with foresee, an existing HEMS controller. We show simulation results for an existing community with additional DERs including PV, batteries, and EVs. We compare scenarios with multiple control strategies to show their impacts on peak load reduction with a focus on EV peak demand.

foresee is a HEMS capable of coordinating various behind-the-meter resources in residential homes including PV, batteries, HVAC equipment, and water heaters in response to a time-varying tariff or utility signal. foresee is formulated as a multi-objective MPC problem and determines the optimal schedule for all resources simultaneously. The details regarding the formulation of foresee can be found in [32] and [104].

6.3.1 Simulation Inputs

We simulate a community with high EV penetration under multiple control strategies to reduce peak demand from EVs. Simulations were run for one week at a 1-minute time resolution. The HEMS operated at a 15-minute time resolution.

The simulated community consists of 50 residential homes, each with a different level of insulation and a different set of equipment. The house models were generated using ResStock^{TM}[171], which contains probability distributions of residential building characteristics across the entire U.S. We use the distributions for an area near Washington D.C. to come up with a series of typical building models to represent the community. Each day of the simulation had an average daily temperature between 25 and 30 °C.

We assume the 50-home community includes 13 PHEV with Level 1 chargers and 12 BEV with Level 2 chargers. PHEV size ranges from 20 to 50 miles, and BEV size ranges from 100 to 250 miles. For the control scenarios with foresee, the Level 1 chargers were turned off when $P_{ev} < \frac{P_{max}}{2}$ and on when $P_{ev} \geq \frac{P_{max}}{2}$. The Level 2 chargers followed the control signal exactly.

PV and battery sizes were designed to simulate a community with high levels of DERs and minimal community-level grid export. The community includes a total of 162 kW of PV, split among 30 of the 50 homes. Batteries are included in 20 homes; 10 homes have a 3kW/6kWh battery and 10 homes have a 6kW/12kWh battery.

6.3.2 Baseline Results

A baseline scenario was run to show the community power with no controls. Figure 6.7 shows the total community power by end use for three simulation days, two weekdays followed by one weekend day. Air conditioning accounts for most of the load, and PV generation significantly reduces daytime load, but not enough to cause net export of the community.

Figure 6.8 shows the total community power with a basic delayed EV charge control. The EV charging was delayed by up to 5 hours to reduce load during the peak period from 2 P.M. to 7 P.M. The EV power shifted from the afternoon to the evening to reduce the peak load. The on-peak maximum demand (averaged across all days of the simulation) reduced from 178 kW to 156 kW. However, the average daily EV peak demand increased from 43 kW to 45 kW (see Figure 6.10), indicating that this control scheme may lead to a spike in demand in the evening.

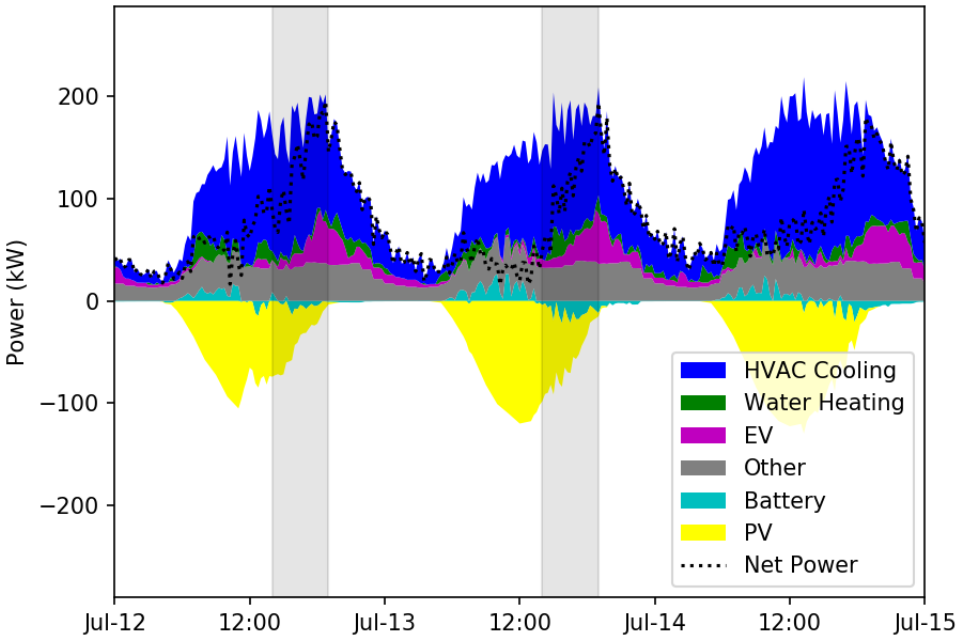

Figure 6.7 Total community power by end use for the baseline scenario. ©2021 IEEE

6.3.3 HEMS Control

Next, we run a scenario with the same community, using foresee as the control system. The HEMS uses a time-of-use (TOU) rate from the local area with a peak period from 2 P.M. to 7 P.M on weekdays and a peak-to-off-peak price ratio of 4.875 [172]. Regarding the user-preferences in foresee, cost-saving had highest preference, followed by EV discomfort, air temperature discomfort, hot water discomfort, and battery degradation.

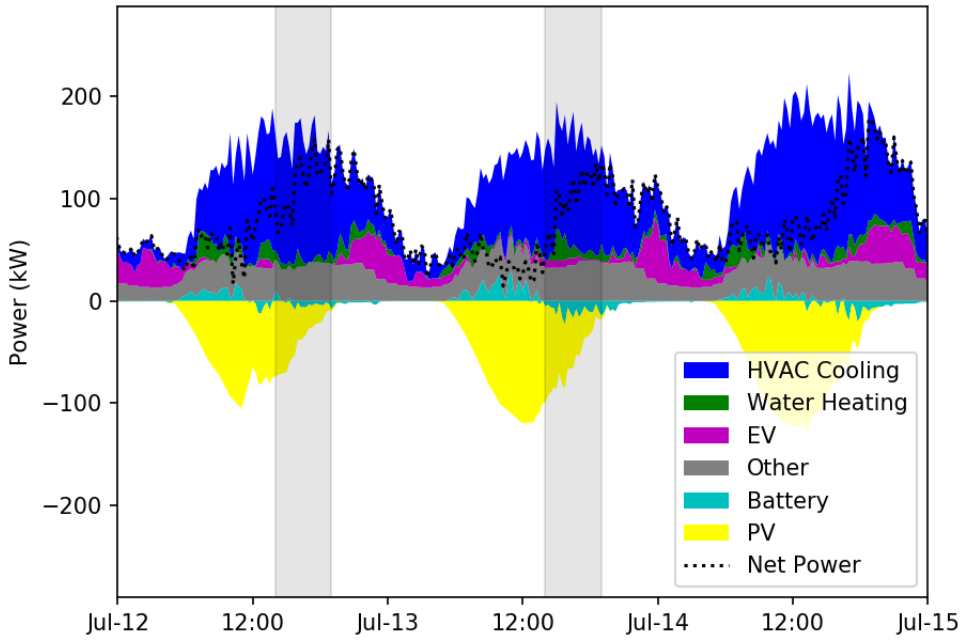

Figure 6.8 Total community power for the EV delay scenario. ©2021 IEEE

Figure 6.9 shows the results of this scenario for the same three days. The HVAC and battery profiles change considerably, and the EV profile shifts to later in the evening. The EV tends to charge when the HVAC and other load powers are low to reduce any demand spikes. The peak demand increases due to HVAC load before the peak period, but the on-peak maximum demand decreases considerably, from 178 kW in the baseline case to 120 kW in the HEMS case.

A comparison of the EV profiles from all scenarios is shown in Figure 6.10. The baseline scenario has a considerable EV usage during the peak period, and all control scenarios are able to shift that consumption to later in the day. The HEMS scenarios (TOU and Demand) shift the consumption later than the basic delay control, and are able to reduce the daily average on-peak maximum demand from 12 kW (in the basic control case) to 1.2 kW.

The HEMS scenarios also reduce the average daily peak demand due to EVs (at 15-minute resolution) from 45 kW to 34 kW, a 23% reduction. This reduction is critical when considering an increase in residential EV adoption. As EV charging becomes a

significant portion of residential energy consumption, smoother EV charging profiles will reduce peak demand and allow for more efficient grid operations.

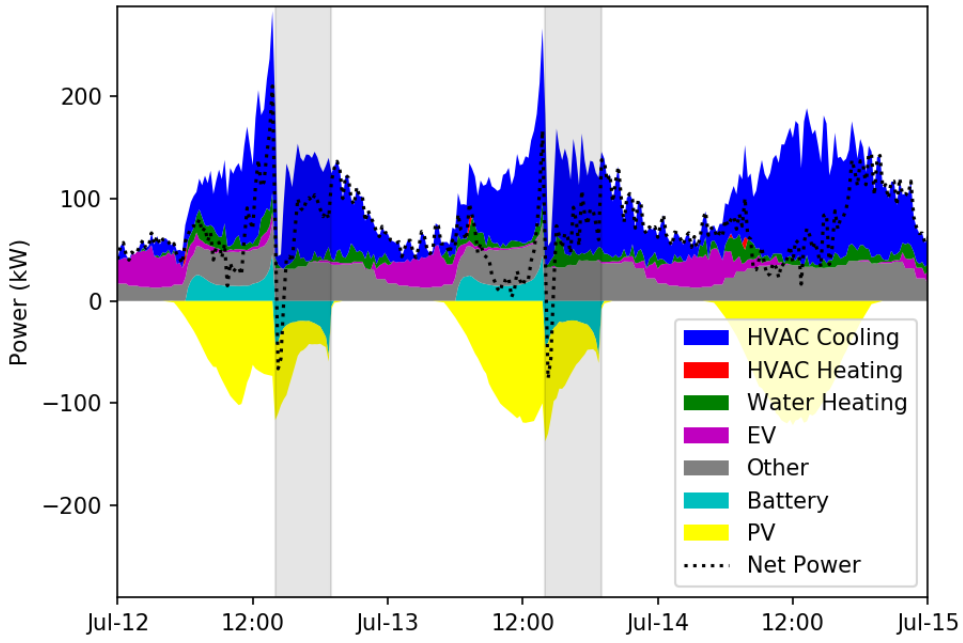

Figure 6.9 Total community power for the HEMS control scenario with foresee controls and a TOU rate. ©2021 IEEE

6.3.4 Demand Charge Control

We run a fourth scenario with foresee controls using an additional demand charge term similar to Equation (4.15). We use the same TOU rate and a demand charge of $10 per kW. As shown in Figure 6.10, the EV profile is very similar to the profile from the HEMS scenario without a demand charge.

The demand charge does not have a significant effect on the EV controls because EV consumption does not often coincide with the peak demand. Residential peak demand tends to occur in the afternoon in the summer when air conditioning loads are high, and EV charging tends to occur later in the evening. It is likely that this control would have a larger effect on EV charging when EV loads contribute more to the peak demand, for example during times and locations with less HVAC demand.

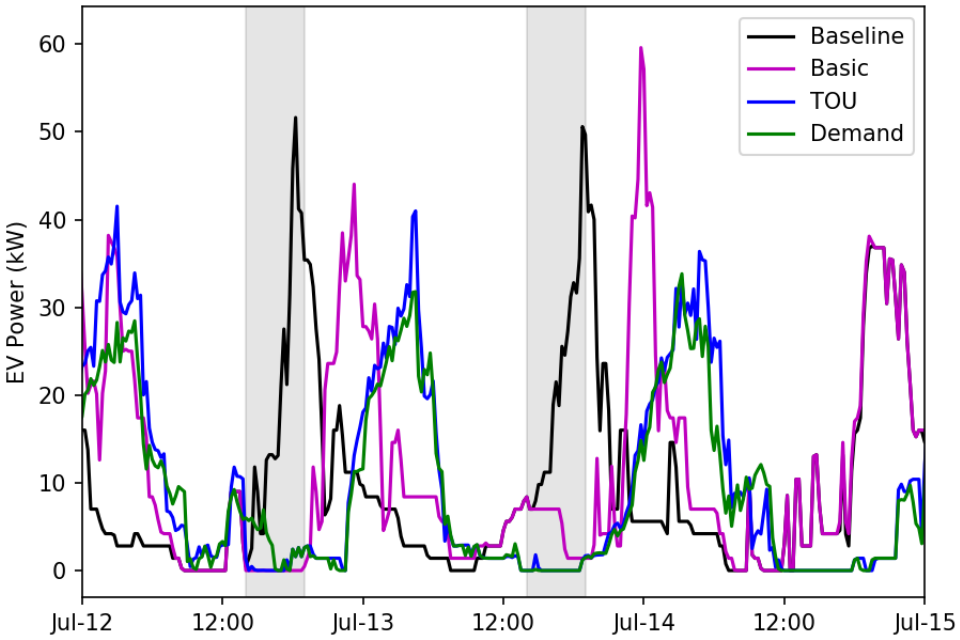

Figure 6.10 Total EV power in the community for all scenarios. ©2021 IEEE

6.4 Chapter Summary

In this chapter, we describe a co-simulation framework that incorporates multiple OCHRE models with controllers and a distribution system simulator. We show two case studies that simulate a new, all-electric community and an existing community with high DER penetration. The case studies show OCHRE's ability to handle various control signals. The first case study highlights the importance of high-resolution load modeling when evaluating peak demand strategies. The second shows the benefits of device-level outputs to analyze the impacts of a control strategy on different types of DERs.

This chapter addresses Research Question 3 by describing a co-simulation framework that captures the impacts of flexible load control strategies on grid services, including distribution system peak demand reduction and voltage regulation. The framework enables OCHRE to integrate with external controllers and a distribution system simulator and combines the results to show the effects of control strategies on energy usage, grid services, and occupant well-being.

CHAPTER 7

ASSESSMENT OF STOCHASTIC CONTROL METHODS FOR HOME ENERGY MANAGEMENT SYSTEMS

This chapter applies the stochastic control framework described in Chapter 4 to two case studies. Both case studies evaluate the control performance of heuristic, deterministic, and stochastic control strategies. The first case study evaluates battery controls for a tariff with a demand charge in conditions with very high ambient temperatures. The second case study evaluates a full HEMS in a typical building in Denver, CO. In both cases, the SMPC strategy is shown to perform best under conditions with uncertainty.

7.1 Battery Control with Demand Charge

This case study assesses the control performance for customer-sited, behind-the-meter batteries that incorporates uncertainty in customer load and ambient temperature. We use residential customer AMI data to show the benefits of the controller and the importance of understanding risk and uncertainty in this application. The key contributions of this case study include the integration of:

- a thermo-electric battery model
- a stochastic model predictive controller to minimize customer energy costs and battery degradation
- a demand charge in the SMPC optimization

7.1.1 Simulation Inputs

The battery model from Section 3.1.8 is used for this case study, including the battery internal temperature model. The same model was used for the system and the MPC, i.e., no model uncertainty was considered. The battery was the only controllable load

considered, and all other residential loads were grouped into the uncontrollable load profile P_{unc}.

The objective function used in this case study includes a subset of the terms in Equation (4.20): J_{tou}, J_{peak}, $J_{batt,P}$, $J_{batt,T}$, and J_{batt}. The first two terms capture costs associated with a time-based rate and a demand charge, respectively. The second two terms capture lifetime degradation costs associated with high power and high temperature. The final term captures the future benefit for maintaining charge in the battery at the end of the horizon.

We test the battery model and controller and assess the control performance in multiple scenarios. Two reference scenarios test an MPC controller with a perfect forecast and with a forecast with high uncertainty. SMPC scenarios test the control performance by varying the level of risk and forecast uncertainty. All scenarios are run for a single residential customer with high PV generation over a 1-month period. The simulations are run at 30-minute time intervals, and the horizon is 24 hours, or 48 time steps.

All scenarios use parameter values described in Table 7.1 unless otherwise noted. The load profile was taken from an open-source dataset of residential customers with rooftop PV near Sydney, Australia [173]. We used data over a month for a single customer with high energy consumption, a high PV capacity of 4.5 kW, and no controllable loads. The temperature profile was taken from the Sydney airport for the corresponding month and year [174]. Figure 7.1 shows the load and temperature profiles as well as their mean and variance across the month. Note that the battery is assumed to be installed outside and subjected to the ambient temperature and no direct solar radiation.

The TOU rate and demand charge are taken from [175]. The TOU rate has a peak to off-peak ratio of about 5-to-1, which is larger than most TOU rates [176]. The demand charge uses 30-minute average demand and, in our formulation, is not restricted to the on-peak period. Battery electrical parameters were taken or derived from [177–180]. We assume the battery is AC-coupled, and do not consider inverter power limits. Thermal

parameters were estimated from [79, 179, 180]. Other values were estimated using the previous sources to achieve reasonable values for a typical residential battery.

Table 7.1 Model and Control Parameters Used for Scenarios

Parameter	Value
P_{unc} and $\sigma^2_{P_{unc}}(k)$	varies, see Figure 7.1
T_a and $\sigma^2_{T_a}(k)$	varies, see Figure 7.1
η_{chg}	95 %
η_{chg}	95 %
$\eta_{batt,th}$	98 %
C_{batt}	90 kJ/K
$R_{batt,a}$	60 K/kW
Σ_v	$\begin{bmatrix} 0.05\text{ kW} & 0 \\ 0 & 1°\text{C} \end{bmatrix}$
t_s	30 minutes
n_h	48
λ_{tou}	Off-peak: 0.012376 \$/kWh Shoulder: 0.026377 \$/kWh On-peak: 0.123296 \$/kWh
λ_{peak}	8.5674 \$/kW
λ_P	0.001
λ_T	0.002
$\beta_{P_{unc}}$	2.33 (99^{th} percentile)
$\beta_{T_{batt}}$	2.33 (99^{th} percentile)
$T_{batt,high}$	30 °C
$\overline{T_{batt}}$	40 °C
$\underline{s_{batt}}$	0 kWh
$\overline{s_{batt}}$	10 kWh

The controller performance was assessed using the cost function from Equation (4.20). To determine the actual cost to the customer across the entire month, we replace n_h with the total number of time steps throughout the simulation, use the actual total power $P_{house}(k)$ instead of $\hat{P}_{house}(k)$, and set $\sigma_{P_{unc}} = 0$.

7.1.2 MPC Reference Scenarios

Reference scenarios are run using the MPC framework proposed in Section 4.2.2. The same objective is used for the MPC framework with all variance parameters (σ_{T_a}, $\sigma_{P_{unc}}$,

and $\sigma_{T_{batt}}$) set to zero. The Perfect Forecast scenario uses the exact load and temperature as the forecasts for the MPC optimization. The MPC Baseline uses the same forecast as the SMPC Baseline scenario.

Table 7.2 shows the results of all the scenarios. The TOU and demand costs are taken from the first two terms in the objective, and other costs include costs due to degradation. As expected, the MPC with a perfect forecast performs very well, significantly lowering the total cost. The baseline MPC run performs poorly, especially considering the demand charge cost, since there are significant deviations between the baseline forecast and the actual power.

7.1.3 Baseline Scenario

The SMPC Baseline scenario uses the mean and variance of the load and temperature profiles calculated on an hourly basis as shown in Figure 7.1. Note that the $\hat{z} \pm 2\sigma_z$ interval contains the majority of the data, although a few days of the month have very high powers and high temperatures. The two days with the largest load correspond to the two days with the highest temperatures.

The controller successfully reduces the total cost to the customer across the month from \$19.94 (from the MPC Baseline scenario) to \$15.01 as shown in Table 7.2. This improvement primarily comes from a reduction in peak demand that is enabled by the controller's load forecast. The energy cost increased slightly, likely due to the focus of the SMPC control on the demand charge; for example, if there is a risk of approaching the peak power, the controller will reduce the chance of exceeding it by discharging more or charging less, even if that leads to increased energy costs.

Figure 7.2 shows the results of the baseline scenario for the peak load day of the month. The battery charged during night-time hours when electricity prices are low and uncertainty in load is low. It waits to discharge the battery until about 16:00 during the on-peak period, which is about when the load power increases and becomes more variable. It successfully lowered the peak demand before 20:00. However, the controller did not

expect the load power to remain high after 20:00, and it almost fully discharged during the on-peak period. Right after 20:00, the battery stopped discharging and the net load increased dramatically, which led to a large increase in the peak power, and the largest peak of the month.

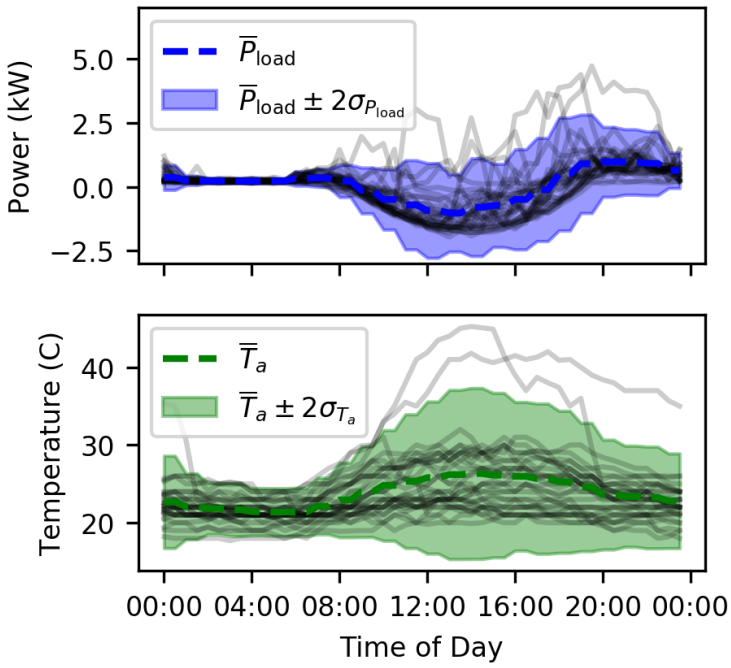

Figure 7.1 Battery case study daily profiles for (a) Customer Load P_{unc} and (b) Ambient Temperature T_a for each day of simulation. Shaded region shows $\hat{z} \pm 2\sigma_z$. ©2020 IEEE

The baseline controller had no information about the high demand or high temperature of this day; it was only provided the expected value and variance shown in Figure 7.1. Therefore, it could not have predicted the high load power, nor the high ambient temperature late in the day.

The simulation ran in 45 seconds, or 31 ms per time step, on a Dell PC with a 1.9 GHz Intel Core i7 processor and 16 GB of RAM. The simulation is run in Python with a publicly available convex optimization solver [181].

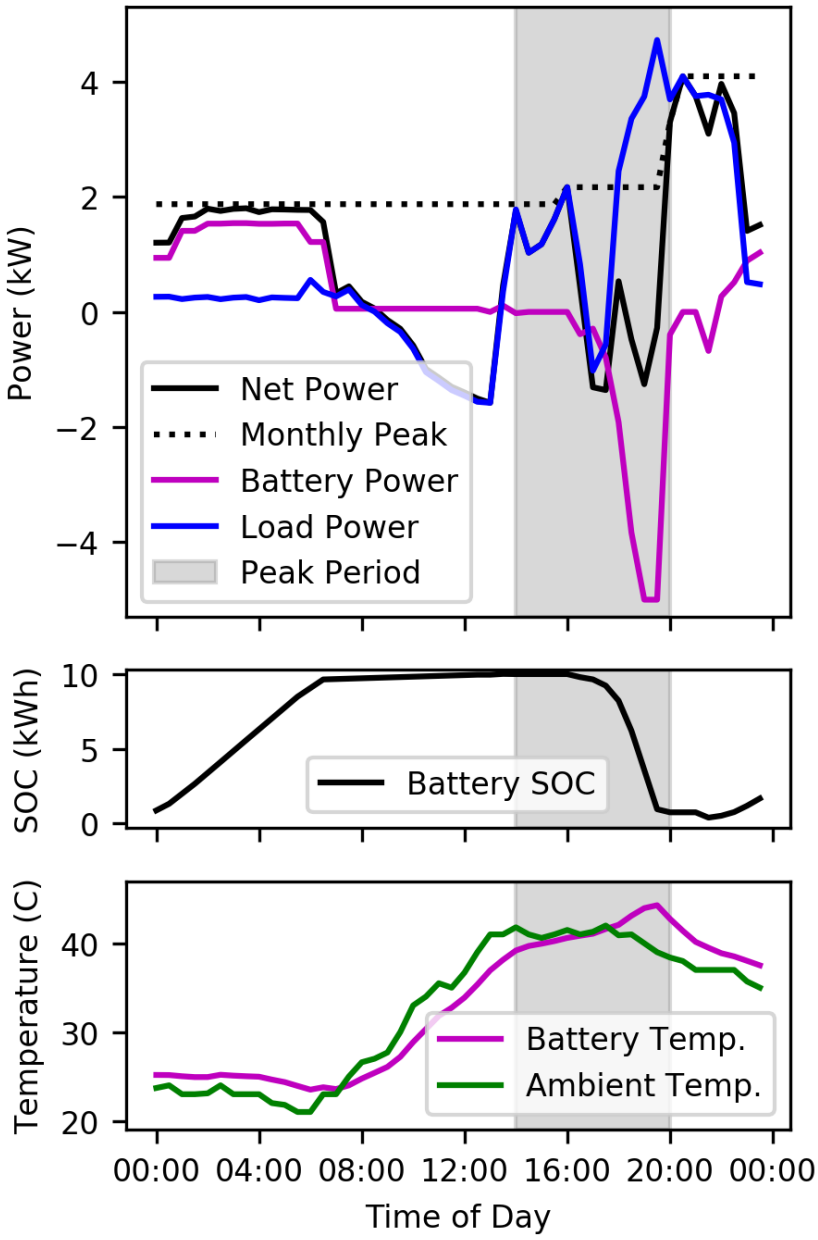

Figure 7.2 Results for SMPC Baseline Scenario on the Peak Load Day. ©2020 IEEE

7.1.4 Impacts of Varying Risk

One method to improve the performance of the baseline controller is to increase the risk tolerance for high peak demand and high battery temperatures by decreasing the back-off magnitudes $\beta_{P_{unc}}$ and $\beta_{T_{batt}}$. Decreasing $\beta_{P_{unc}}$ will decrease the value of the demand charge term in the objective for time steps when there is a risk of exceeding the previous peak demand, leading to more charging or less discharging when the load is estimated to be high or is more uncertain. Decreasing $\beta_{T_{batt}}$ will reduce the cost of Equation (4.17), which will increase the battery charge and discharge power when the battery temperature is close to $\overline{T_{batt}}$. Both of these changes will make the controller behave more aggressively during times when the load power and the ambient temperature is high.

We run the controller with High Risk conditions $\beta_{P_{unc}} = 1.28$ and $\beta_{T_{batt}} = 1.28$, corresponding to the 90^{th} percentile of a Gaussian distribution. The performance results are shown in Table 7.2 and are slightly improved over the SMPC baseline scenario. The more aggressive control was able to reduce the energy cost without increasing the demand charge cost. The peak time and day was the same for this scenario and for the baseline scenario.

We note that lower risk tolerance and more aggressive control behavior will not improve performance in all instances. The nature of the data used in these scenarios, and in particular the load profile on the peak day, cause the higher risk scenarios to lower the total costs.

7.1.5 Impacts of Varying Uncertainty

A preferable method to improve the controller performance, when possible, is to provide a more accurate prediction of load and temperature forecasts to the controller. Using the monthly load data and a publicly available model estimation tool, we develop an auto-regressive exogenous (ARX) model of the load power to reduce the uncertainty of the load forecast [163]. While more complex methods can create more accurate forecasts, we

chose a first order ARX model for simplicity. The load power is estimated as:

$$\begin{aligned} P_{unc}(k) &= \hat{P}_{unc}(k) + P_{AR}(k) \\ P_{AR}(k) &= 0.7977 P_{AR}(k-1) + \epsilon_{AR}(k) \end{aligned} \tag{7.1}$$

where $P_{AR}(k)$ is the difference between the actual load power and the mean load power. The mean load power $\hat{P}_{unc}(k)$ is the same as in the original formulation, but the variance of $P_{unc}(k)$ is now defined by $\epsilon_{AR}(k) \sim \mathcal{N}(0, \sigma^2_{P_{AR}(k)})$. We note that $\sigma_{P_{AR}(k)} < \sigma_{P_{unc}(k)}$ for all hours of the day.

The ARX Model scenario reduces total cost relative the the previous SMPC scenarios. Table 7.2 shows the energy cost increases while the demand cost decreases. The improved demand forecast allows the controller to predict high consumption in the future, which greatly reduces the peak demand and the demand cost. It is likely that the conservative back-off parameter $\beta_{T_{batt}}$ causes the controller to reduce discharge power during the hot afternoons, which then increases the energy cost since that is when the on-peak period occurs.

The final scenario tests the ARX model with a higher risk tolerance by reducing the β parameters. The combination of these effects lowers the total cost to \$9.56 for the month. The addition of higher risk and more aggressive controls leads to lower energy costs and higher demand costs.

Figure 7.3 shows the results of the scenario with the ARX model and a higher risk tolerance for the peak load day of the month. Compared to the SMPC baseline scenario, the battery discharges more slowly during the on-peak period to conserve battery charge. It is able to more closely follow the peak power and limit the peak power increase during the peak period. It is also able to keep the battery temperature lower than the baseline SMPC controller did. The peak power still achieves its maximum value around 22:00, but at a lower value than in previous scenarios.

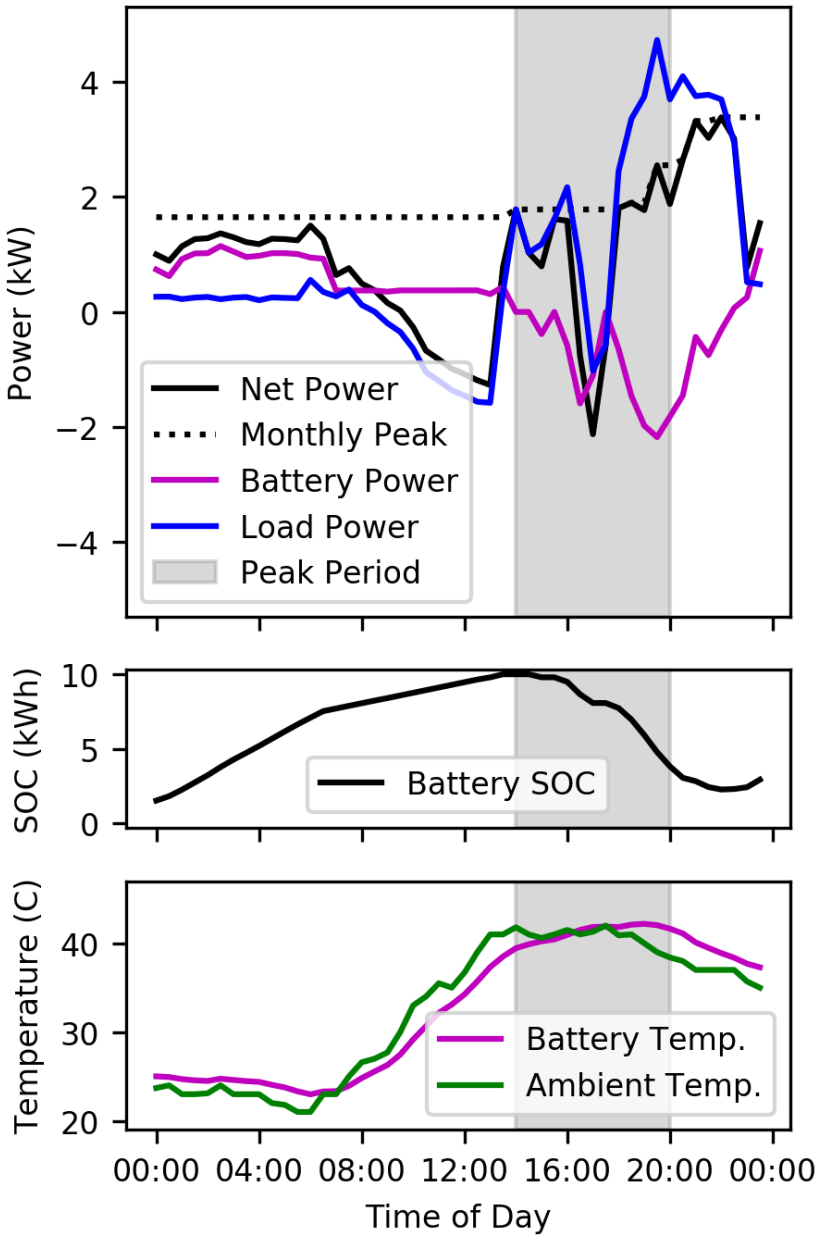

Figure 7.3 Results for SMPC Scenario with ARX Model and High Risk Tolerance on the Peak Load Day. ©2020 IEEE

Table 7.2 Performance Results for All Scenarios

Scenario	Energy cost	Demand Cost	Other Costs	Total Cost
No Battery	-$2.01	$40.47	$0	$38.47
Perfect Forecast	-$26.62	$14.74	$10.81	-$1.07
MPC Baseline	-$33.20	$41.64	$11.50	$19.94
SMPC Baseline	-$31.17	$35.07	$11.10	$15.01
SMPC, High Risk	-$32.89	$35.07	$11.23	$13.41
SMPC, ARX Model	-$23.62	$25.96	$10.49	$12.83
ARX + High Risk	-$30.65	$29.52	$10.69	$9.56

7.1.6 Case Study Summary

In this case study, we use a thermo-electric battery model and a stochastic MPC controller that optimizes battery cycling over a TOU and demand charge rate structure. The controller accounts for uncertainty in the load forecast and ambient temperature forecast, maintains low battery temperatures, and maintains low charge and discharge rates to minimize the effects of degradation. Simulation results show that all SMPC scenarios perform better than the MPC when there is uncertainty in the forecast. We show that reducing forecast uncertainty improves the performance of the SMPC controller. Increasing risk tolerance to force a more aggressive control strategy also improves performance, although that result may not be generalizable to other scenarios.

7.2 HEMS Control for a Typical Building

This case study evaluates multiple control strategies for a HEMS for a typical building. The HEMS controls four controllable loads: an air conditioner, a water heater, an EV, and a battery. Simulations are run with different control strategies and different forecasting methods to determine the effect of uncertainty on the control performance. The results show that the SMPC has the best performance when using uncertain forecasts.

7.2.1 Simulation Inputs

All simulations were performed using measured weather data from Denver, CO. Weather data were collected in real time in July 2021 using an online application programming interface (API) [182]. The same weather API was used to get weather forecast data. The weather data and forecast were collected every 1 hour, and the forecast had a duration of 48 hours and a time resolution of 1 hour.

Weather data used in the simulation include ambient temperature, pressure, relative humidity, cloud cover, and wind speed. Cloud cover data were converted to irradiance values using a clear-sky scaling method [183]. Irradiance data was combined with the area and absorptivity of each exterior house surface to determine the solar heat gains.

A single-occupant schedule was used for all simulations. The schedule was generated using the ResStock^{TM}stochastic occupancy generator for a typical single-family home with a single occupant in Denver, CO [152]. The schedule has 1-minute resolution profiles for occupancy, power usage for uncontrollable loads, and hot water draws for appliances and fixtures. The EV schedule was generated from OCHRE using parking event data from EVI-Pro [68]. Note that because the EV schedule came from a different data source, the occupancy and EV schedules do not directly match.

The OCHRE model was run with the occupant schedule for a full year with typical meteorological year weather data. The annual profile was used to create forecasts for water draws, EV parking status, uncontrollable loads, and internal heat gains as described in Section 4.3.2. All forecasts use a time resolution of 30 minutes.

All simulations were run with the same house model, equipment characteristics, weather data, and occupancy schedules. Scenarios without MPC were run for 14 days in July, and scenarios with MPC were run for 13 days. Key simulation parameters are shown in Table 7.3. The electricity price λ_{tou} was taken from Xcel Energy Colorado's summer time-of-use rate [184], which includes an off-peak rate of \$0.10/kWh, a shoulder period from 1–3 PM at \$0.19/kWh, and a peak period from 3–7 PM at \$0.27/kWh.

Table 7.3 Key simulation parameter values

Model Parameter	Value	Control Parameter	Value
ΔT_{op}	10°C	n_h	48
$T_{op,rad}$	20°C	λ_{tou}	\$0.10–0.27/kWh
η_{hvac}	3.8	λ_{hvac}	\$0.125/°C-hr
$(\theta_1 - \theta_{wm})_{op}$	33.1°C	λ_{wh}	\$0.01/°C-L
η_{wh}	4.5	λ_{ev}	\$1/kWh
P_{drive}	0.65 kW	$\lambda_{ev,low}$	\$2/kWh
E_{ev}	32.5 kWh	λ_{peak}	$\$10^{-5}$/kW
E_{batt}	12 kWh	$\overline{T_m}$	22.7°C
		$\underline{\theta_1}$	46.1°C
		ϵ_{x_i} (all)	20%

The values of the cost coefficients associated with occupant comfort were estimated using assumptions for a typical person's willingness to pay for the desired comfort metric. The air temperature comfort cost λ_{hvac} was based on an occupant willing to pay \$1 for a 2°C increase in air temperature for 4 hours. The water heater cost assumed a \$5 cost for a 65 L shower at 10°C colder than the typical setpoint. The EV cost was set at \$1/kWh to achieve 100% SOC, and at a higher cost of \$3/kWh ($\lambda_{ev} + \lambda_{ev,low}$) to achieve 50% SOC.

The MPC formulation includes all models from Section 4.1.6 except for the battery thermal model. It includes all objective terms in $\mathcal{P}_1$ except for the battery degradation terms and the demand charge cost term.

7.2.2 Deterministic MPC

We next compare the control performance between the baseline heuristic controls and the DMPC with an exact forecast. Although this DMPC case does not include forecast or measurement uncertainty, there is still some model uncertainty due to the model linearization and the difference in time resolution between OCHRE and the control model.

Figure 7.4 shows the state of each controllable equipment and the total house power for these two cases for a subset of the simulation time. Both controllers adjust the HVAC set

point before the peak period, but the air temperature is very similar for the rest of the day. The baseline heuristic control maintains a constant hot water set point, whereas the DMPC keeps the set point very low except when large water draws are expected during the peak period. The DMPC EV controller delays charging until after the peak period and slowly reaches full SOC right before the EV leaves. It also charges the battery more slowly than the scheduled heuristic controller.

Note that the heat pump water heater temperature stays very close to the set point temperature in the DMPC control because the deadband size reduces as the set point approaches the minimum comfort temperature. Although this helps achieve low energy costs and low water discomfort, it leads to a lot of equipment cycling, which can degrade the equipment.

Imperfect forecasts reduce the DMPC performance, particularly for the water heater controls. Figure 7.5 shows the difference in water heater results from the DMPC cases with an exact forecast and the ARIMAX forecast. The ARIMAX case tends to have a lower set point temperature because the forecast expects more frequent but smaller water draws. The forecast error leads to more discomfort due to low water temperatures, but it also slightly reduces the water heater energy cost. Both controls cycle the water heater frequently when no draws are expected.

The DMPC forecasts also impact the EV controls as shown in Figure 7.6. The baseline controller always charges the EV as fast a possible, and the DMPC with an exact forecast always charges the EV as slow as possible while achieving full charge before the EV leaves. The DMPC with the ARIMAX forecast often charges in between these two cases, delaying charging during the peak period but charging more quickly after that. We note that the energy cost due to EV charging was identical for all MPC cases. The low SOC cost $\lambda_{ev,low}$ did not significantly impact the results, as the EV SOC was rarely as low as the $s_{ev,low}$ threshold.

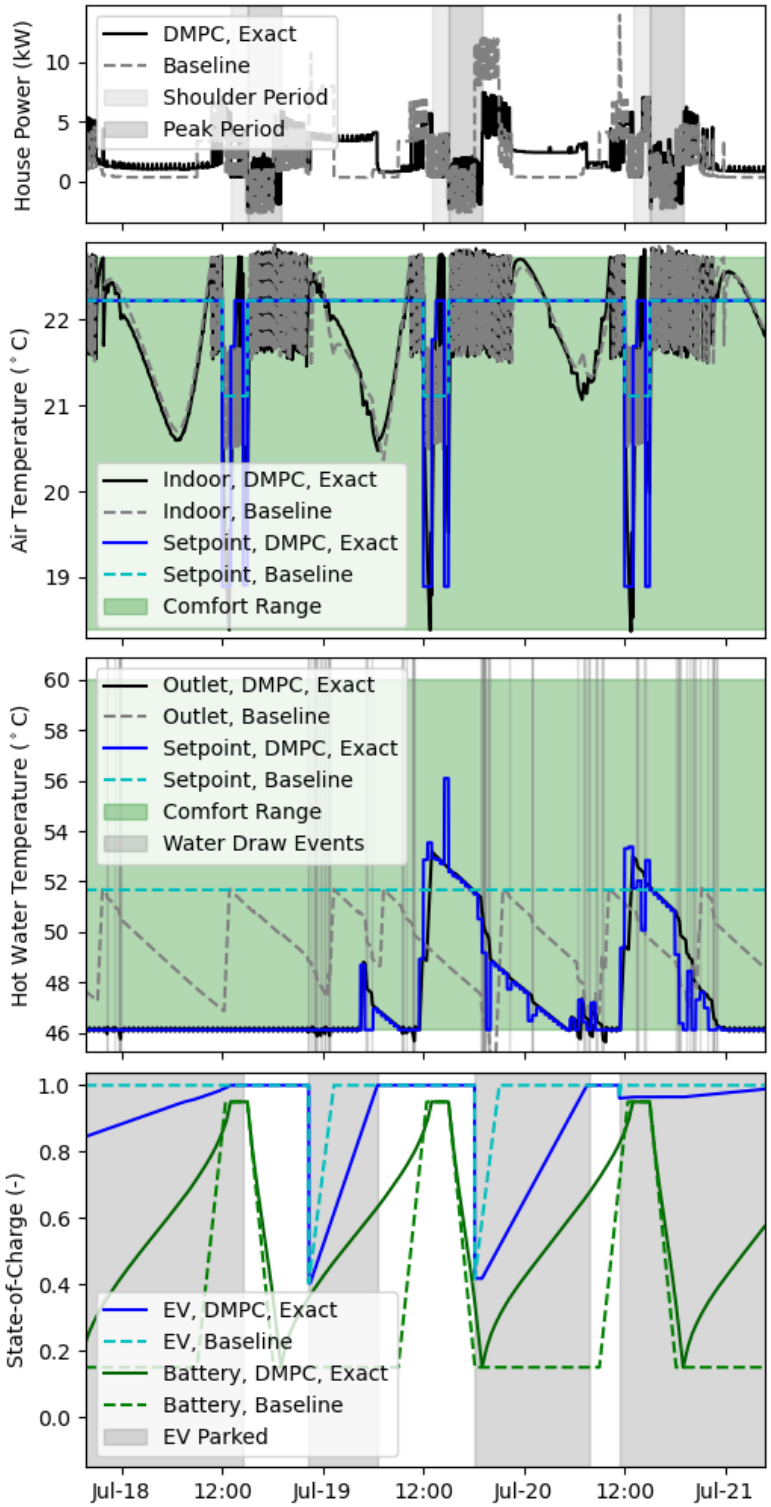

Figure 7.4 HEMS results for DMPC cases with exact forecasts and heuristic controls

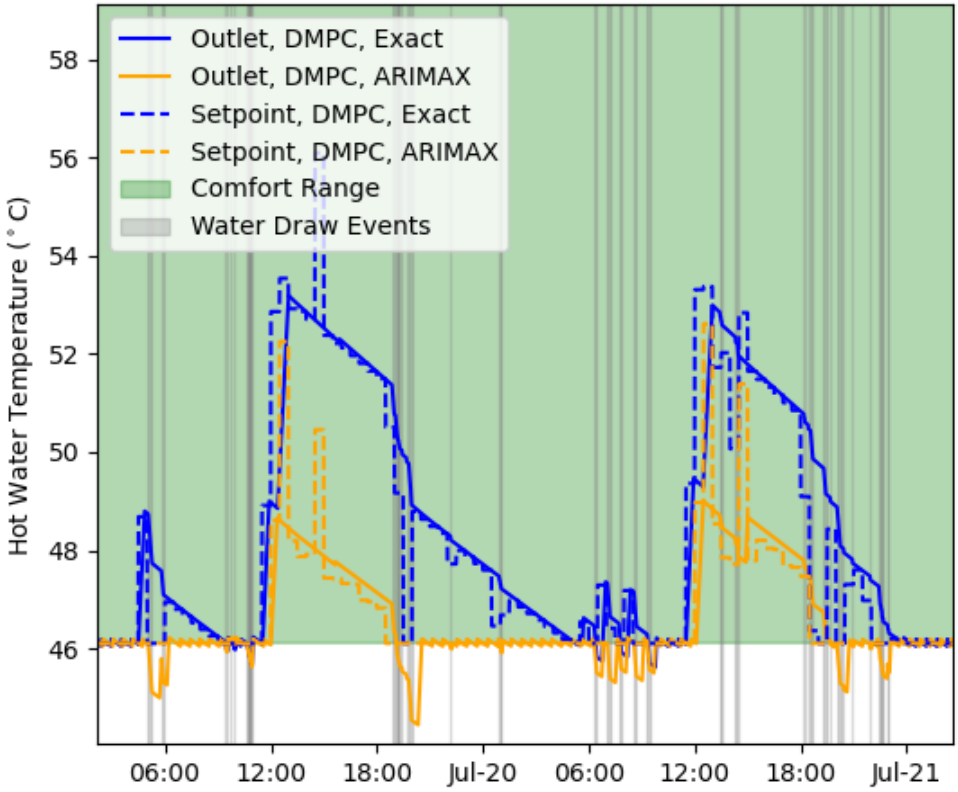

Figure 7.5 Water heater results for DMPC cases with exact and ARIMAX forecasts

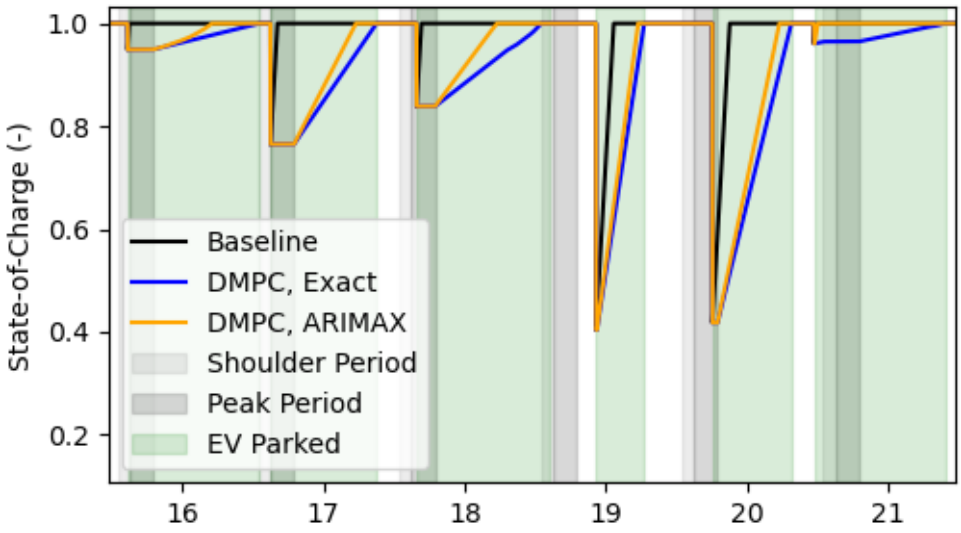

Figure 7.6 EV results for heuristic controls and DMPC cases with exact and ARIMAX forecasts

7.2.3 Stochastic MPC

Compared to the DMPC cases with imperfect forecasts, the SMPC is able to improve water comfort as well as reduce water heater cycling. Figure 7.7 shows the water temperature for the DMPC and SMPC cases with the ARIMAX forecast. The SMPC case maintains a higher set point most of the time, leading to less water discomfort, less water heater cycling, and slightly higher energy costs. The SMPC water heater set point depends on the distribution of water draw volume for the next MPC time step. The set point temperature increases when either the mean value increases or when the variance increases. The set point also increases significantly before the peak demand periods.

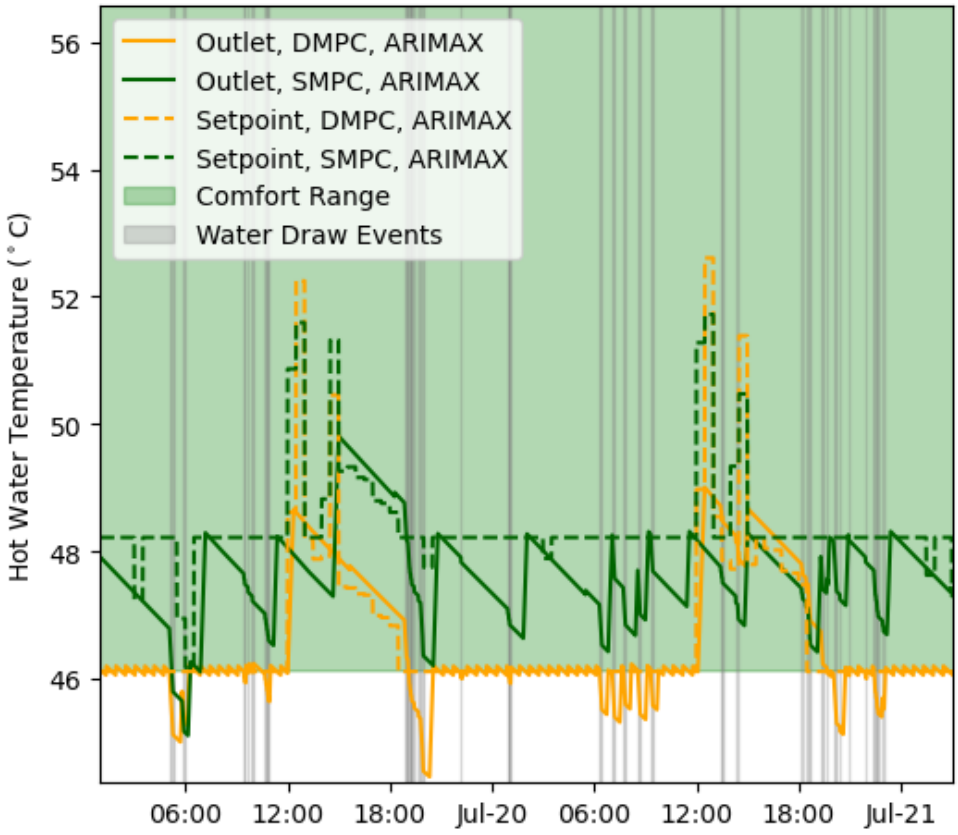

Figure 7.7 Water heater results for DMPC and SMPC cases with ARIMAX forecasts

The SMPC led to small differences in the HVAC controls as shown in Figure 7.8. Although both the DMPC and SMPC controls precool the space before the peak period,

the SMPC case reduces the cooling set point by approximately 0.1°C for the rest of the day. This has little impact on the nighttime air temperature, but it does reduce the temperature while the air conditioner is on. This leads to a small increase in energy costs and a very small decrease in air comfort as quantified by the cost J_{hvac}.

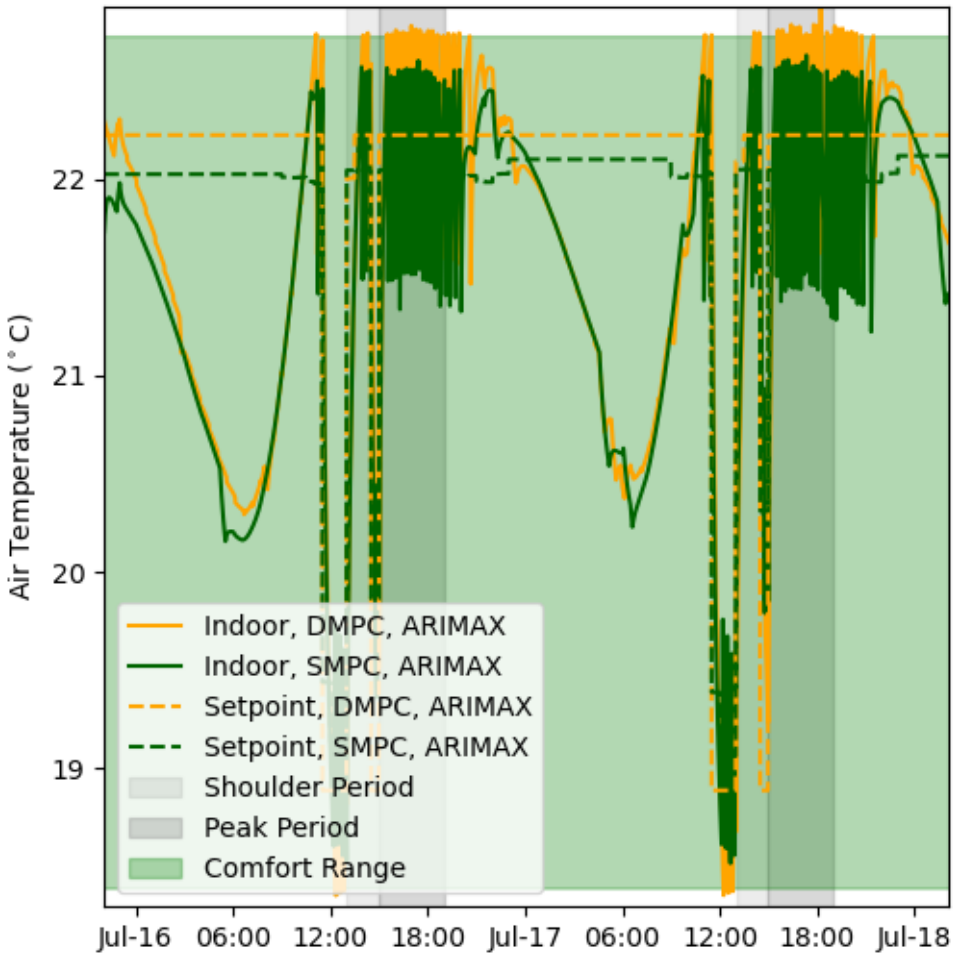

Figure 7.8 HVAC simulation results for the DMPC and SMPC cases with ARIMAX forecasts.

We note that there is no change in the DMPC and SMPC controls for the EV and battery. In theory, the SMPC EV controls should be more conservative and might charge the EV sooner to ensure a low EV inconvenience cost J_{ev}; however, this behavior was not shown in the simulation results.

Table 7.4 Control performance results for each simulation

Control Type	Forecast Type	J_{tou} ($/mo)	J_{wh} ($/mo)	WH Cycles (1/day)
Heuristic	N/A	119.4	1.1	2.0
DMPC	Exact	94.6	2.4	27.9
DMPC	30-day	94.2	9.2	24.5
DMPC	ARIMAX	94.2	7.6	22.3
SMPC	30-day	96.9	1.4	4.0
SMPC	ARIMAX	97.0	1.0	4.2

7.2.4 Control Performance

The control performance for all the simulations is shown in Table 7.4. The energy cost J_{tou} and water heater comfort cost J_{wh} were the only costs from the MPC objective that significantly contributed to the overall cost. All other costs were exactly zero except for J_{hvac}, which was as large as \$0.04/mo for some scenarios due to small temperature deviations that exceeded the comfort range. Costs were calculated using the power and states from the system model in OCHRE. The costs were aggregated over the full simulation time of 13 days and then scaled to show monthly costs. We also report the average number of water heating (WH) heat pump cycles per day from OCHRE. We note that the electric resistance element was not turned on in any of the cases.

As expected, the DMPC with the exact forecast performs best when considering only the objective function costs and not the water heater cycles. All MPC cases outperform the heuristic case, primarily because of the delayed EV charging after the peak period. The 30-day horizon forecasts perform very similarly to the ARIMAX forecasts and had very similar control strategies.

The SMPC cases outperform all other cases excluding the case with an exact forecast. Compared to the heuristic control, they significantly reduce the energy cost and slightly increase the number of water heater cycles. Compared to the DMPC cases, they have slightly higher energy costs, much lower water discomfort costs, and much less water

heating cycling.

The SMPC control had the largest impact on the device with the highest uncertainty in the control variable: the water heater. Due to difficulty in forecasting water draws, the water heater model inputs and outputs had significant uncertainty, which caused a large difference between the DMPC and SMPC set points. The improvements in the SMPC performance highlights the importance of stochastic controls, especially in systems with high levels of uncertainty.

There is an interesting parallel between the differences in set points between the DMPC and SMPC cases and the deadband of the heuristic control. The SMPC back-off magnitudes act as a deadband that buffers the control variable from exceeding its constraints. In this sense, the SMPC algorithm combines the best features of the heuristic control and the DMPC control. In addition, the SMPC improves upon the heuristic control by varying the size of the "deadband" based on the uncertainty in the control variable. We also note that the back-off magnitudes are easily adjustable by updating the risk tolerance of exceeding a constraint ϵ_{x_i}.

7.2.5 Pareto Optimality Analysis

The cost coefficients that quantify the cost of occupant discomfort or inconvenience are difficult to define in practice. Costs would vary considerably for different occupants, and self-reported data may not reflect occupants' actual preferences. For this reason, we conduct a Pareto optimality analysis to assess the impact of these cost coefficients on the control strategy. We focus on the hot water comfort cost coefficient because that cost term contributed to the total control cost more than all other comfort costs, combined.

We vary the hot water cost coefficient λ_{wh} above and below the nominal value of \$0.01/°C-L. We run 7 simulations with cost coefficient values from $\$3 \times 10^{-5}$/°C-L to \$0.03/°C-L with logarithmic increments of approximately 3x. For each case, we solve the SMPC and DMPC optimization problems for a single time step and record the energy cost and the hot water discomfort amount for the horizon time. We note that this methodology

is equivalent to weighted goal programming by setting the target costs to zero and varying the weights of the two objective functions.

Figure 7.9 shows the Pareto front resulting from this analysis. Both the SMPC and DMPC curves show that energy costs do not change significantly (less than \$0.20/day), while the hot water discomfort costs increase dramatically when the hot water cost coefficient is small. There are multiple points on the left side of the figure, indicating that there is a wide range of values for the cost coefficient that have a very small impact on the control strategy. We note that the SMPC costs are much larger than the DMPC costs because the SMPC uses conservative estimates for the water draws that lead to an overestimation of costs.

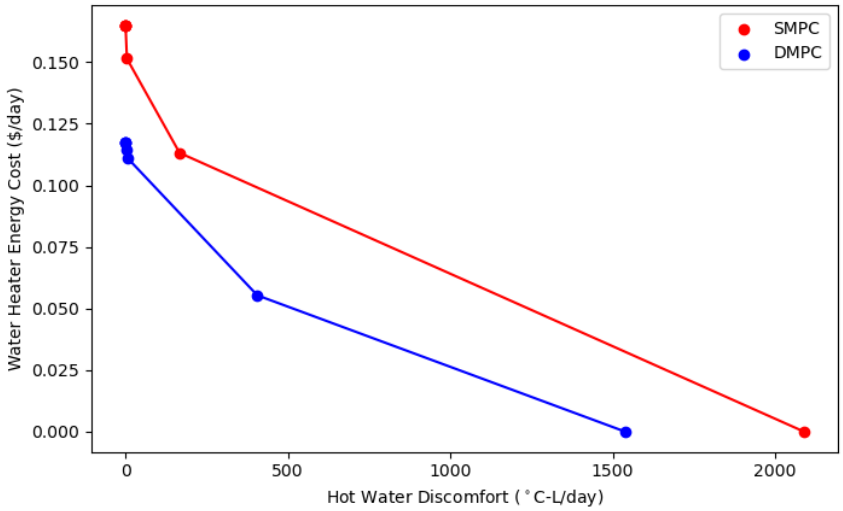

Figure 7.9 Pareto front for water heater energy and discomfort costs for SMPC and DMPC optimizations.

We find that there is a simple breakeven cost coefficient at which the control strategy changes and hot water discomfort increases. This cost corresponds to the peak electricity cost of the TOU rate, which in this case is \$0.27/kWh. The heat capacity of water can be written as 0.00116 kWh/°C-L. Using the heat capacity and the water heater COP of 4.5, the ideal breakeven cost would be about $\$7 \times 10^{-5}$/°C-L. This cost roughly corresponds to being willing to pay \$0.05 to have a standard 65-L shower that is 10°C hotter. We believe

that occupants are willing to pay more than this threshold in most cases.

7.2.6 Case Study Summary

This case study uses the full stochastic control framework from Chapter 4 to evaluate multiple control strategies for a HEMS in a typical residential building under uncertain conditions. We find that the SMPC algorithm performs best when using common forecasts methods that incorporate uncertainty. While the results of this case study may not be generalizeable to scenarios with other building properties, weather data, or occupant schedules, we find that SMPC is able to incorporate the features of both MPC and heuristic controls and is likely to provide benefits for systems with high levels of uncertainty. We also use Pareto optimality analysis to show that the control strategy is not dependent on the cost coefficient for water heating for reasonable parameter values.

7.3 Chapter Summary

This chapter presents two case studies that apply the stochastic control framework from Chapter 4 to residential control applications with uncertain conditions. Both case studies show that stochastic control methods improve control performance under conditions with uncertainty. The first case study shows the benefits of stochastic battery controls when optimizing for a demand charge and battery degradation. The second case study shows the full functionality of the control framework for a HEMS in a typical building, and finds that stochastic controls combine the best features of heuristic and deterministic control strategies.

CHAPTER 8
CONCLUSIONS AND FUTURE WORK

This dissertation presents the development of novel modeling and control methods for residential applications. It provides a background on load flexibility and a literature review of residential energy modeling and control research and best practices. It combines the research and results of the author's contributions in many publications to present a novel residential energy model and a SMPC framework for controlling residential devices through a HEMS. Modeling results for individual buildings and a community highlight the key features of the model, and comparisons with other modeling techniques validate the methods used. Case studies using the stochastic control framework highlight the importance of incorporating modeling uncertainty in residential control applications and show that stochastic methods outperform heuristic and deterministic methods under uncertain conditions.

8.1 Key Findings

This section highlights the key findings of the dissertation and answers the five research questions posed in Chapter 1. Key findings are categorized using the research questions, which roughly correspond to the previous chapters of the dissertation.

8.1.1 Integrated Residential Energy Modeling

This section summarizes the key findings of Chapter 3 and answers the research question:

1. How can integrated residential energy models accurately capture the impacts of load flexibility on house power usage and occupant comfort?

We present the OCHRE model, a high-resolution, controllable, integrated residential energy model. OCHRE models multiple controllable devices as DERs and can quantify load flexibility for a residential building. The device models track power as well as state

variables including temperature and state of charge. OCHRE includes a multi-node, multi-zone building envelope model for accurate HVAC modeling, as well as a voltage-dependency model for accurate modeling within distribution systems. These detailed methods are essential components of an integrated residential energy model and allow OCHRE to evaluate system performance in terms of energy consumption, costs, and occupant comfort.

The proposed model captures the impacts of load flexibility on power usage and occupant comfort. Simulation results show the impacts of various control strategies on residential buildings using the OCHRE model. Time series analysis shows that common control strategies, for example preconditioning and daily battery schedules, can shift DER load profiles. This impacts the energy costs of the building and multiple occupant comfort metrics, including air comfort, hot water comfort, and convenience associated with a fully charged EV.

8.1.2 Model Validation

This section summarizes the key findings of Chapter 5 and answers the research question:

2. How do integrated residential energy models compare against existing state-of-the-art models?

Validation results show that OCHRE closely matches state-of-the-art models when comparing time-series data and annual energy metrics. We compare the HVAC and water heating models against EnergyPlus, and the EV model against EVI-pro. Different modeling techniques lead to differences in energy consumption, particularly due to thermal mass estimates, HVAC efficiency methods, and solar radiation through windows. The models include similar output metrics for device power and occupant comfort. Ongoing validation efforts will continue to improve these results.

Linearizing the OCHRE model for use in computationally efficient model-based control methods creates small modeling errors. The model described in Chapter 4 uses

linearization and model reduction techniques on the OCHRE envelope model, which allow the linear model to be used efficiently in model-based controls. We show that these changes lead to small errors in temperature and HVAC consumption that are unlikely to significantly impact control performance.

8.1.3 Distributed Control Strategies

This section summarizes the key findings of Chapter 6 and answers the research question:

3. How can integrated residential energy models capture the impacts of distributed control strategies on grid services?

Community-scale co-simulation platforms are able to evaluate the grid impacts of distributed control strategies. We develop a co-simulation framework that incorporates multiple OCHRE building models, building-level controllers, and a distribution system simulator. Two case studies show that flexible building loads are capable of shifting system demand to reduce peak demand and to achieve a smoother community load profile. The distribution system model also enabled the evaluation of local grid services including distribution voltage regulation.

Many features of integrated residential energy models were critical in testing distributed control strategies. Models needed to be modular, integrated, and computationally efficient to work well in a co-simulation environment. Using physics-based models that can measure occupant comfort allowed for additional metrics for evaluation. Using diversified, occupant-based, and high-fidelity models allowed the co-simulation to run at a high time resolution and led to finer resolution results to evaluate grid impacts.

8.1.4 Uncertainty in HEMS Controls

This section summarizes the key findings of Chapter 4 and answers the research question:

4. How can uncertainty from weather and occupancy behavior be incorporated in model-based controls for residential energy systems?

Multiple forecasting methods quantify the uncertainty in weather and occupancy behavior for use in model-based controls. These inputs are critical in residential energy controls, and we show that their forecasts can have a significant amount of uncertainty. By developing forecasts for these inputs, we can test control strategies with inputs that closely match the information that would be available in real systems. Common forecasting methods, including ARX, ARIMAX, and moving horizon methods, were used to show that incorporating uncertainty in controls is feasible with inputs that are typically available.

Stochastic model predictive control is able to incorporate uncertain forecasts into the control objective. The proposed control framework uses SMPC to optimize a control objective while accounting for uncertainty in the model inputs and states. Forecasts with uncertainty provide the input distributions, and a Kalman Filter is used to propagate the uncertainty throughout the control horizon. The framework uses chance constraints to ensure that metrics associated with occupant comfort are met with high probability.

The control framework incorporates other sources of uncertainty as well. While forecast uncertainty from weather and occupant behavior is often the most important source, uncertainty can also arise from the control model and from sensor measurements. SMPC requires a linear control model to maintain computational efficiency and solvability, but linearization creates modeling errors. Sensors can be noisy or biased or have low resolution, leading to errors in state estimation. All of these sources can be incorporated in the control framework.

8.1.5 HEMS Control Performance

This section summarizes the key findings of Chapter 7 and answers the research question:

5. Do model-based controls perform better than rule-based controls for residential energy systems with DERs when weather and occupancy forecasts are uncertain?

Stochastic model predictive control performs better than deterministic or heuristic methods in multiple case studies. The SMPC lead to more conservative control signals that reduce the risk of incurring high costs from the impacts of uncertain variables. We show that overall control preformance improves for a wide range of control applications, including mitigating demand charge costs and occupant discomfort due to low hot water temperatures.

Stochastic controls combine useful features of common deterministic and heuristic control strategies. SMPC is an extension of deterministic MPC, which is the most common control method for HEMS. Stochastic formulations include back-off magnitudes that mimic deadbands that are often used in heuristic controls. These deadbands can vary over time based on the uncertainty in the system variables and the risk tolerance of the user.

The forecast accuracy and the distribution of uncertain inputs can have a large impact on the stochastic control performance. The highest costs are often incurred at times when inputs—for example, peak demand or water draws—are at their maximum value. The stochastic control is more likely to perform well if the forecast can accurately predict these events. Because events like these are often infrequent and hard to predict, we do not conclude that SMPC is the optimal strategy in all circumstances.

User-specified parameters can impact the performance of SMPC. Each objective with an uncertain variable includes a parameter that quantifies the risk tolerance of the user. Adjusting the parameter value leads to more conservative or aggressive controls and impacts the control performance. Objective costs associated with occupant comfort also include a coefficient that quantifies the cost of discomfort, which must be defined by the user.

8.2 Future Work

Future work in both the modeling and control methods developed in this dissertation can help make this work relevant to a broader range of applications.

The OCHRE model can be a useful tool for residential energy modeling of communities, single buildings, or individual devices. Additional validation work will enhance the validity of the model, especially for use in a wider range of climates. Incorporating smart appliances including refrigerators, clothes washers, and dryers, will enable more load diversity and controllability. We plan to make the OCHRE model open source to make the model more transparent and encourage more development and use from the research community.

The stochastic control framework for HEMS has many potential extensions. More sophisticated forecasting and estimation methods, including those that use non-Gaussian probability distributions, can more accurately quantify uncertainty and might improve control performance. Time-varying or parameter-varying models can reduce model uncertainty, and incorporating nonlinear models in the MPC framework with an Extended Kalman Filter might also improve performance. Asynchronous control methods that respond to real-time signals would be able to respond faster in real systems.

The control framework can also be used with additional objectives or in different applications. Control objectives can include more complex rate structures and additional costs associated with device degradation and cycling. Comfort cost objectives could use quadratic or other convex functions to more accurately represent occupant preferences. The control framework can also be used for related energy management problems for commercial buildings or for an aggregation of many DERs. We recommend evaluating the control framework under a more diverse set of scenarios and in laboratory testing before conducting field demonstration pilots.

REFERENCES

[1] Energy and environmental goals drive change. Technical report, CAISO, 2016. URL www.caiso.com.

[2] California ISO - Today's Outlook, 2021. URL https://www.caiso.com/TodaysOutlook/Pages/index.html.

[3] Andrew D Mills, Dev Millstein, Ryan Wiser, Joachim Seel, Juan Pablo Carvallo, Seongeun Jeong, and Will Gorman. Impact of Wind, Solar, and Other Factors on Wholesale Power Prices An Historical Analysis-2008 through 2017. Technical report, Lawrence Berkeley National Laboratory, 2019.

[4] Total Energy Monthly Data - U.S. Energy Information Administration (EIA), 2020. URL https://www.eia.gov/totalenergy/data/annual/index.php.

[5] EIA's residential energy survey now includes estimates for more than 20 new end uses - Today in Energy - U.S. Energy Information Administration (EIA), 2021. URL https://www.eia.gov/todayinenergy/detail.php?id=36412.

[6] Jürgen Weiss, J Michael Hagerty, and María Castañer. The Coming Electrification of the North American Economy Why We Need a Robust Transmission Grid. Technical report, The Brattle Group, 2019. URL www.wiresgroup.com.

[7] Trieu Mai, Paige Jadun, Jeffrey S Logan, Colin A McMillan, Matteo Muratori, Daniel C Steinberg, Laura J Vimmerstedt, Benjamin Haley, Ryan Jones, and Brent Nelson. Electrification Futures Study: Scenarios of Electric Technology Adoption and Power Consumption for the United States. Technical report, National Renewable Energy Laboratory, 2018. URL https://www.nrel.gov/docs/fy18osti/71500.pdf.

[8] Adam Cooper and Kellen Schefter. Electric Vehicle Sales Forecast and the Charging Infrastructure Required Through 2030, 2018. URL https://www.edisonfoundation.net/iei/publications/Documents/IEI_EEIEVForecastReport_Nov2018.pdf.

[9] U.S. National Electrification Assessment, 2021. URL https://www.epri.com/research/products/3002013582.

[10] Michael Coddington, Rebecca O'Neil, and Emma Stewart. Distributed Energy Resources (DER): Presentation for Distribution Systems and Planning Training for Midwest Public Utility Commissions. Technical report, U.S. DOE GLMC, 2018. URL https://www.naruc.org/rate-design/.

[11] U.S. Solar Market Insight — SEIA, 2020. URL https://www.seia.org/us-solar-market-insight.

[12] Energy Commission Adopts Standards Requiring Solar Systems for New Homes, First in Nation, 2021. URL https://www.energy.ca.gov/news/2018-05/energy-commission-adopts-standards-requiring-solar-systems-new-homes-first.

[13] GTM Research and ESA. U.S. Energy Storage Monitor. Technical report, 2016. URL https://www.woodmac.com/research/products/power-and-renewables/us-energy-storage-monitor/.

[14] U.S. Energy Storage Monitor — Wood Mackenzie, 2020. URL https://www.woodmac.com/research/products/power-and-renewables/us-energy-storage-monitor/.

[15] BNEF EVO Report 2020 — BloombergNEF — Bloomberg Finance LP, 2020. URL https://about.bnef.com/electric-vehicle-outlook/.

[16] United States distributed energy resources outlook: DER installations and forecasts 2016-2025E Report — Wood Mackenzie, 2020. URL https://www.woodmac.com/reports/power-markets-united-states-distributed-energy-resources-outlook-der-installations-and-forecasts-2016-2025e-416181.

[17] Residential and public EV charging outlet forecast 2019-2030: H1 2020 Report — Wood Mackenzie, 2020. URL https://www.woodmac.com/reports/power-markets-residential-and-public-ev-charging-outlet-forecast-2019-2030-h1-2020-405724.

[18] Energy Management in the Connected Home: Competitive Landscape, Forecasts and Case Studies Report — Wood Mackenzie, 2020. URL https://www.woodmac.com/reports/power-markets-energy-management-in-the-connected-home-competitive-landscape-forecasts-and-case-studies-58129606.

[19] Vishakha D. Vaidya and Pinki Vishwakarma. A Comparative Analysis on Smart Home System to Control, Monitor and Secure Home, based on technologies like GSM, IOT, Bluetooth and PIC Microcontroller with ZigBee Modulation. *2018 International Conference on Smart City and Emerging Technology, ICSCET 2018*, nov 2018. doi: 10.1109/ICSCET.2018.8537381.

[20] Ryan Hledik, Ahmad Faruqui, Tony Lee, and John Higham. The National Potential for Load Flexibility. Technical report, The Brattle Group, 2019.

[21] Grid-Interactive Efficient Buildings — Department of Energy, 2020. URL https://www.energy.gov/eere/buildings/grid-interactive-efficient-buildings.

[22] Andrew Satchwell, Mary Ann Piette, Aditya Khandekar, Jessica Granderson, Natalie Mims Frick, Ryan Hledik, Ahmad Faruqui, Long Lam, Stephanie Ross, Jesse Cohen, Kitty Wang, Daniela Urigwe, Dan Delurey, Monica Neukomm, and David Nemtzow. A National Roadmap for Grid-Interactive Efficient Buildings. Technical report, 2021.

[23] Matteo Muratori. Impact of uncoordinated plug-in electric vehicle charging on residential power demand. *Nature Energy*, 3(3):193–201, mar 2018. ISSN 20587546. doi: 10.1038/s41560-017-0074-z.

[24] Michael Blonsky, Adarsh Nagarajan, Shibani Ghosh, Killian McKenna, Santosh Veda, and Benjamin Kroposki. Potential Impacts of Transportation and Building Electrification on the Grid: A Review of Electrification Projections and Their Effects on Grid Infrastructure, Operation, and Planning. *Current Sustainable/Renewable Energy Reports*, 6(4):169–176, dec 2019. ISSN 2196-3010. doi: 10.1007/s40518-019-00140-5.

[25] Table CE3.1 Annual household site end-use consumption in the U.S. Technical report, U.S. EIA, 2020.

[26] Xiwang Li and Jin Wen. Review of building energy modeling for control and operation. *Renewable and Sustainable Energy Reviews*, 37:517–537, sep 2014. ISSN 13640321. doi: 10.1016/j.rser.2014.05.056.

[27] Wesley J. Cole, Kody M. Powell, Elaine T. Hale, and Thomas F. Edgar. Reduced-order residential home modeling for model predictive control. *Energy and Buildings*, 74:69–77, may 2014. ISSN 03787788. doi: 10.1016/j.enbuild.2014.01.033.

[28] Amin Mirakhorli and Bing Dong. Occupancy behavior based model predictive control for building indoor climate—A critical review, oct 2016. ISSN 03787788.

[29] Killian McKenna and Andrew Keane. Residential Load Modeling of Price-Based Demand Response for Network Impact Studies. *IEEE Transactions on Smart Grid*, 7 (5):2285–2294, sep 2016. ISSN 19493053. doi: 10.1109/TSG.2015.2437451.

[30] Juan Miguel Gonzalez López, Edris Pouresmaeil, Claudio A. Cañizares, Kankar Bhattacharya, Abolfazl Mosaddegh, and Bharatkumar V. Solanki. Smart Residential Load Simulator for Energy Management in Smart Grids. *IEEE Transactions on Industrial Electronics*, 66(2):1443–1452, feb 2019. ISSN 02780046. doi: 10.1109/TIE.2018.2818666.

[31] Eoghan McKenna and Murray Thomson. High-resolution stochastic integrated thermal-electrical domestic demand model. *Applied Energy*, 165:445–461, mar 2016. ISSN 03062619. doi: 10.1016/j.apenergy.2015.12.089.

[32] Xin Jin, Kyri Baker, Dane Christensen, and Steven Isley. Foresee: A user-centric home energy management system for energy efficiency and demand response. *Applied Energy*, 205:1583–1595, nov 2017. ISSN 03062619. doi: 10.1016/j.apenergy.2017.08.166.

[33] Isha Sharma, Jin Dong, Andreas A. Malikopoulos, Michael Street, Jim Ostrowski, Teja Kuruganti, and Roderick Jackson. A modeling framework for optimal energy management of a residential building. *Energy and Buildings*, 130:55–63, oct 2016. ISSN 03787788. doi: 10.1016/j.enbuild.2016.08.009.

[34] Gregor P Henze, Gregory S Pavlak, Anthony R Florita, Robert H Dodier, and Adam I Hirsch. An energy signal tool for decision support in building energy systems. *Applied Energy*, 138:51–70, 2015. ISSN 03062619. doi: 10.1016/j.apenergy.2014.10.029.

[35] Shengwei Wang and Xinhua Xu. Simplified building model for transient thermal performance estimation using GA-based parameter identification. *International Journal of Thermal Sciences*, 45(4):419–432, apr 2006. ISSN 12900729. doi: 10.1016/j.ijthermalsci.2005.06.009.

[36] Scott Horowitz, Jeff Maguire, Paulo Cesar Tabares-Velasco, Jon Winkler, and Craig Christensen. EnergyPlus and SEEM Modeling Enhancements via Software-to-Software Comparison Using NREL's BEopt Test Suite. Technical report, NREL, 2016. URL https://www.nrel.gov/docs/fy16osti/65858.pdf.

[37] Amirreza Fateh, Davide Borelli, Alessandro Spoladore, and Francesco Devia. A state-space analysis of a single zone building considering solar radiation, internal radiation, and PCM effects. *Applied Sciences (Switzerland)*, 9(5):832, feb 2019. ISSN 20763417. doi: 10.3390/app9050832.

[38] M.H. Sherman and D.T. Grimsrud. Infiltration-Pressurization Correlation: Simplified Physical Modeling. *ASHRAE Transactions*, 86(2):778–807, 1980.

[39] Donghun Kim and James E Braun. Reduced-Order Building Modeling for Application to Model-Based Predictive Control. *Proceedings of SimBuild*, 5(1): 554–561, 2012. URL http://ibpsa-usa.org/index.php/ibpusa/article/view/475.

[40] EnergyPlus — EnergyPlus, 2020. URL https://energyplus.net/.

[41] Engineering Reference — EnergyPlus 8.9, 2021. URL https://bigladdersoftware.com/epx/docs/8-9/engineering-reference/index.html.

[42] Tianshu Wei, Yanzhi Wang, and Qi Zhu. Deep Reinforcement Learning for Building HVAC Control. In *Proceedings - Design Automation Conference*, volume Part 12828, pages 1–6, New York, NY, USA, jun 2017. Institute of Electrical and Electronics Engineers Inc. ISBN 9781450349277. doi: 10.1145/3061639.3062224.

[43] Kristopher A. Pruitt, Sven Leyffer, Alexandra M. Newman, and Robert J. Braun. A mixed-integer nonlinear program for the optimal design and dispatch of distributed generation systems. *Optimization and Engineering*, 15(1):167–197, aug 2014. ISSN 15732924. doi: 10.1007/s11081-013-9226-6.

[44] EnergyPlus Validation Reports. URL https://simulationresearch.lbl.gov/dirpubs/valid_ep.html.

[45] Paulo Cesar Tabares-Velasco, Craig Christensen, and Marcus Bianchi. Verification and validation of EnergyPlus phase change material model for opaque wall assemblies. *Building and Environment*, 54:186–196, 2012. ISSN 03601323. doi: 10.1016/j.buildenv.2012.02.019.

[46] Brock Glasgo, Chris Hendrickson, and Inês Lima Azevedo. Assessing the value of information in residential building simulation: Comparing simulated and actual building loads at the circuit level. *Applied Energy*, 203:348–363, 2017. ISSN 03062619. doi: 10.1016/j.apenergy.2017.05.164.

[47] M. J. Jiménez, H. Madsen, and K. K. Andersen. Identification of the main thermal characteristics of building components using MATLAB. *Building and Environment*, 43(2):170–180, 2008. ISSN 03601323. doi: 10.1016/j.buildenv.2006.10.030.

[48] D. A. Coley and J. M. Penman. Second order system identification in the thermal response of real buildings. Paper II: Recursive formulation for on-line building energy management and control. *Building and Environment*, 27(3):269–277, 1992. ISSN 03601323. doi: 10.1016/0360-1323(92)90028-N.

[49] Peder Bacher and Henrik Madsen. Identifying suitable models for the heat dynamics of buildings. *Energy and Buildings*, 43(7):1511–1522, 2011. ISSN 03787788. doi: 10.1016/j.enbuild.2011.02.005.

[50] Rohit Chintala, Jon Winkler, and Xin Jin. Automated fault detection of residential air-conditioning systems using thermostat drive cycles. *Energy and Buildings*, 236: 110691, apr 2021. ISSN 0378-7788. doi: 10.1016/J.ENBUILD.2020.110691.

[51] Peter Radecki and Brandon Hencey. Online thermal estimation, control, and self-excitation of buildings. In *Proceedings of the IEEE Conference on Decision and Control*, pages 4802–4807. Institute of Electrical and Electronics Engineers Inc., 2013. ISBN 9781467357173. doi: 10.1109/CDC.2013.6760642.

[52] Shengwei Wang and Xinhua Xu. Parameter estimation of internal thermal mass of building dynamic models using genetic algorithm. *Energy Conversion and Management*, 47(13-14):1927–1941, aug 2006. ISSN 01968904. doi: 10.1016/j.enconman.2005.09.011.

[53] D. Cutler, J. Winkler, N. Kruis, C. Christensen, M. Brendemuehl, and M. Brandemuehl. Improved Modeling of Residential Air Conditioners and Heat Pumps for Energy Calculations. Technical report, NREL, Golden, CO, jan 2013. URL http://www.osti.gov/servlets/purl/1219902/.

[54] Satoru Ihara and Fred C. Schweppe. Physically based modeling of cold load pickup. *IEEE Transactions on Power Apparatus and Systems*, PAS-100(9):4142–4150, 1981. ISSN 00189510. doi: 10.1109/TPAS.1981.316965.

[55] He Hao, Borhan M. Sanandaji, Kameshwar Poolla, and Tyrone L. Vincent. Aggregate flexibility of thermostatically controlled loads. *IEEE Transactions on Power Systems*, 30(1):189–198, jan 2015. ISSN 08858950. doi: 10.1109/TPWRS.2014.2328865.

[56] Yudong Ma, Jadranko Matusko, and Francesco Borrelli. Stochastic model predictive control for building HVAC systems: Complexity and conservatism. *IEEE Transactions on Control Systems Technology*, 23(1):101–116, jan 2015. ISSN 10636536. doi: 10.1109/TCST.2014.2313736.

[57] Mehdi Maasoumy, Meysam Razmara, Mahdi Shahbakhti, and Alberto Sangiovanni Vincentelli. Selecting building predictive control based on model uncertainty. In *Proceedings of the American Control Conference*, pages 404–411. Institute of Electrical and Electronics Engineers Inc., 2014. ISBN 9781479932726. doi: 10.1109/ACC.2014.6858875.

[58] Xiaojing Zhang, Georg Schildbach, David Sturzenegger, and Manfred Morari. Scenario-based MPC for energy-efficient building climate control under weather and occupancy uncertainty. In *2013 European Control Conference, ECC 2013*, pages 1029–1034. IEEE Computer Society, 2013. ISBN 9783033039629. doi: 10.23919/ecc.2013.6669664.

[59] Xin Jin, Kyri Baker, Steven Isley, and Dane Christensen. User-preference-driven model predictive control of residential building loads and battery storage for demand response. In *Proceedings of the American Control Conference*, pages 4147–4152. Institute of Electrical and Electronics Engineers Inc., jun 2017. ISBN 9781509059928. doi: 10.23919/ACC.2017.7963592.

[60] Wooyoung Jung and Farrokh Jazizadeh. Human-in-the-loop HVAC operations: A quantitative review on occupancy, comfort, and energy-efficiency dimensions. *Applied Energy*, 239:1471–1508, apr 2019. ISSN 03062619. doi: 10.1016/j.apenergy.2019.01.070.

[61] Md Tofael Ahmed, Pedro Faria, Omid Abrishambaf, and Zita Vale. Electric Water Heater Modelling for Direct Load Control Demand Response. In *Proceedings - IEEE 16th International Conference on Industrial Informatics, INDIN 2018*, pages 490–495. Institute of Electrical and Electronics Engineers Inc., sep 2018. ISBN 9781538648292. doi: 10.1109/INDIN.2018.8472102.

[62] Jay Burch and Paul Erickson. Using ratings data to derive simulation-model inputs for storage-tank water heaters. *Solar 2004 Conference and 29th National Passive Solar Conference*, (July):394–398, 2004.

[63] Robert Cruickshank, Gregor Henze, Rajagopalan Balaji, Bri Mathias Hodge, and Anthony Florita. Quantifying the opportunity limits of automatic residential electric load shaping. *Energies*, 12(17):3204, aug 2019. ISSN 19961073. doi: 10.3390/en12173204.

[64] Jeffrey Brad Maguire. A Parametric Analysis of Residential Water Heaters, Master's Thesis, University of Colorado, 2012. URL https://scholar.colorado.edu/downloads/j6731418j.

[65] Mike Logsdon. HPWHsim: Under the Hood of a Heat Pump Water Heater Performance and Energy Simulator. Technical report, ACEEE Hot Water Forum, 2017.

[66] Ian Richardson, Murray Thomson, David Infield, and Alice Delahunty. Domestic lighting: A high-resolution energy demand model. *Energy and Buildings*, 41(7): 781–789, jul 2009. ISSN 03787788. doi: 10.1016/j.enbuild.2009.02.010.

[67] U.S. DOE. Building America Analysis Spreadsheets, 2011. URL https://www.energy.gov/eere/buildings/building-america-analysis-spreadsheets.

[68] Alternative Fuels Data Center: Electric Vehicle Infrastructure Projection Tool (EVI-Pro) Lite Assumptions and Methodology, 2020. URL https://afdc.energy.gov/evi-pro-lite/load-profile/assumptions.

[69] Nicholas Good, Lingxi Zhang, Alejandro Navarro-Espinosa, and Pierluigi Mancarella. High resolution modelling of multi-energy domestic demand profiles. *Applied Energy*, 137:193–210, jan 2015. ISSN 03062619. doi: 10.1016/j.apenergy.2014.10.028.

[70] Ian Richardson, Murray Thomson, David Infield, and Conor Clifford. Domestic electricity use: A high-resolution energy demand model. *Energy and Buildings*, 42 (10):1878–1887, oct 2010. ISSN 03787788. doi: 10.1016/j.enbuild.2010.05.023.

[71] Maomao Hu and Fu Xiao. Quantifying uncertainty in the aggregate energy flexibility of high-rise residential building clusters considering stochastic occupancy and occupant behavior. *Energy*, 194:116838, mar 2020. ISSN 03605442. doi: 10.1016/j.energy.2019.116838.

[72] PV Performance Modeling Collaborative, 2020. URL https://pvpmc.sandia.gov/modeling-steps/.

[73] M. Yousefi, N. Kianpoor, A. Hajizadeh, and M. Soltani. Smart Energy Management System for Residential Homes Regarding Uncertainties of Photovoltaic Array and Plug-in Electric Vehicle. In *IEEE International Symposium on Industrial Electronics*, volume 2019-June, pages 2201–2206. Institute of Electrical and Electronics Engineers Inc., jun 2019. ISBN 9781728136660. doi: 10.1109/ISIE.2019.8781471.

[74] PVWatts, 2020. URL https://pvwatts.nrel.gov/.

[75] Nate Blair, Nicholas Diorio, Janine Freeman, Paul Gilman, Steven Janzou, Ty Neises, Michael Wagner, Nate Blair, Nicholas Diorio, Janine Freeman, Paul Gilman, Steven Janzou, Ty Neises, and Michael Wagner. System Advisor Model (SAM) General Description (Version 2017.9.5). *National Renewable Energy Laboratory*, (May), 2018. URL https://www.nrel.gov/docs/fy18osti/70414.pdf.

[76] Emma Raszmann, Kyri Baker, Ying Shi, and Dane Christensen. Modeling stationary lithium-ion batteries for optimization and predictive control. In *2017 IEEE Power and Energy Conference at Illinois, PECI 2017*. Institute of Electrical and Electronics Engineers Inc., may 2017. ISBN 9781509055517. doi: 10.1109/PECI.2017.7935755.

[77] Partha Pratim Mishra, Aadil Latif, Michael Emmanuel, Ying Shi, Killian McKenna, Kandler Smith, and Adarsh Nagarajan. Analysis of degradation in residential battery energy storage systems for rate-based use-cases. *Applied Energy*, 264:114632, apr 2020. ISSN 03062619. doi: 10.1016/j.apenergy.2020.114632.

[78] Nicholas Diorio. An Overview of the Automated Dispatch Controller Algorithms in the System Advisor Model. Technical report, National Renewable Energy Laboratory, 2017. URL https://www.nrel.gov/docs/fy18osti/68614.pdf.

[79] L. H. Saw, Y. Ye, and A. A.O. Tay. Electro-thermal analysis and integration issues of lithium ion battery for electric vehicles. *Applied Energy*, 131:97–107, oct 2014. ISSN 03062619. doi: 10.1016/j.apenergy.2014.06.016.

[80] Xinfan Lin, Hector E Perez, Shankar Mohan, Jason B Siegel, Anna G Stefanopoulou, Yi Ding, and Matthew P Castanier. A lumped-parameter electro-thermal model for cylindrical batteries. *J. Power Sources*, 257:1–11, 2014. doi: 10.1016/j.jpowsour.2014.01.097.

[81] Hector Eduardo Perez, Xiaosong Hu, Satadru Dey, and Scott J. Moura. Optimal Charging of Li-Ion Batteries with Coupled Electro-Thermal-Aging Dynamics. *IEEE Transactions on Vehicular Technology*, 66(9):7761–7770, sep 2017. ISSN 00189545. doi: 10.1109/TVT.2017.2676044.

[82] Kandler Smith, Ying Shi, and Shriram Santhanagopalan. Degradation mechanisms and lifetime prediction for lithium-ion batteries - A control perspective. In *Proceedings of the American Control Conference*, volume 2015-July, pages 728–730. Institute of Electrical and Electronics Engineers Inc., jul 2015. ISBN 9781479986842. doi: 10.1109/ACC.2015.7170820.

[83] Theis Heidmann Pedersen and Steffen Petersen. Investigating the performance of scenario-based model predictive control of space heating in residential buildings. *Journal of Building Performance Simulation*, 11(4):485–498, jul 2018. ISSN 1940-1493. doi: 10.1080/19401493.2017.1397196.

[84] Jingran Ma, S. Joe Qin, and Timothy Salsbury. Model predictive control of building energy systems with balanced model reduction. In *Proceedings of the American Control Conference*, pages 3681–3686, 2012. ISBN 9781457710957. doi: 10.1109/acc.2012.6315516.

[85] Michael Wetter and Philip Haves. A Modular Building Controls Virtual Test Bed for the Integration of Heterogeneous Systems. *SimBuild 2008*, pages 69–76, 69. URL https://facades.lbl.gov/publications/modular-building-controls-virtual.

[86] Marina Sofos, Jared Langevin, Michael Deru, Erika Gupta, Kyle S Benne, David Blum, Ted Bohn, Robert Fares, Nick Fernandez, Glenn Fink, Steven Frank, Jennifer Gerbi, Jessica Granderson, Dale Hoffmeyer, Tianzhen Hong, Amy Jiron, Stephanie Johnson, Srinivas Katipamula, Teja Kuruganti, Jared Langevin, William C Livingood, Ralph Muehleisen, Monica Neukomm, Valerie Nubbe, Patrick Phelan, MaryAnn Piette, Janet Reyna, Amir Roth, Aven Satre-Meloy, Michael Specian, Draguna Vrabie, Michael Wetter, and Steve Widergren. Innovations in Sensors and Controls for Building Energy Management: Research and Development Opportunities Report for Emerging Technologies. Technical report, U.S. DOE EERE, 2020. URL http://www.osti.gov/servlets/purl/1601591/.

[87] GridLAB-D Simulation Software. URL https://www.gridlabd.org/.

[88] HELICS. URL https://helics.org/.

[89] OpenDSS, . URL https://www.epri.com/pages/sa/opendss.

[90] Jing Wang, Michael Blonsky, Fei Ding, Seth C. Drew, Harsha Padullaparti, Shibani Ghosh, Ismael Mendoza, Soumya Tiwari, Jorge E. Martinez, Jose J.D. Dahdah, Francisco A.M. Bazzani, Murali Baggu, Martha Symko-Davies, Chris Bilby, and Bryan Hannegan. Performance evaluation of distributed energy resource management via advanced hardware-in-the-loop simulation. In *2020 IEEE Power and Energy Society Innovative Smart Grid Technologies Conference, ISGT 2020*. Institute of Electrical and Electronics Engineers Inc., feb 2020. ISBN 9781728131030. doi: 10.1109/ISGT45199.2020.9087667.

[91] Bruce C. Moore. Principal Component Analysis in Linear Systems: Controllability, Observability, and Model Reduction. *IEEE Transactions on Automatic Control*, 26 (1):17–32, 1981. ISSN 15582523. doi: 10.1109/TAC.1981.1102568.

[92] Frauke Oldewurtel, Alessandra Parisio, Colin N. Jones, Dimitrios Gyalistras, Markus Gwerder, Vanessa Stauch, Beat Lehmann, and Manfred Morari. Use of model predictive control and weather forecasts for energy efficient building climate control. *Energy and Buildings*, 45:15–27, feb 2012. ISSN 03787788. doi: 10.1016/j.enbuild.2011.09.022.

[93] He Hao, Abhishek Somani, Jianming Lian, and Thomas E. Carroll. Generalized aggregation and coordination of residential loads in a smart community. In *2015 IEEE International Conference on Smart Grid Communications, SmartGridComm 2015*, pages 67–72. Institute of Electrical and Electronics Engineers Inc., mar 2016. ISBN 9781467382892. doi: 10.1109/SmartGridComm.2015.7436278.

[94] R. E. Kalman. A new approach to linear filtering and prediction problems. *Journal of Fluids Engineering, Transactions of the ASME*, 82(1):35–45, mar 1960. ISSN 1528901X. doi: 10.1115/1.3662552.

[95] H. Madsen and J. Holst. Estimation of continuous-time models for the heat dynamics of a building. *Energy and Buildings*, 22(1):67–79, 1995. ISSN 03787788. doi: 10.1016/0378-7788(94)00904-X.

[96] M. Maasoumy, M. Razmara, M. Shahbakhti, and A. Sangiovanni Vincentelli. Handling model uncertainty in model predictive control for energy efficient buildings. *Energy and Buildings*, 77:377–392, jul 2014. ISSN 03787788. doi: 10.1016/j.enbuild.2014.03.057.

[97] Mehdi Maasoumy, Barzin Moridian, Meysam Razmara, Mahdi Shahbakhti, and Alberto Sangiovanni-Vincentelli. Online simultaneous state estimation and parameter adaptation for building predictive control. In *ASME 2013 Dynamic Systems and Control Conference, DSCC 2013*, volume 2. American Society of Mechanical Engineers (ASME), mar 2013. ISBN 9780791856130. doi: 10.1115/DSCC2013-4064.

[98] Chengpu Yu, Michel Verhaegen, Shahar Kovalsky, and Ronen Basri. Identification of structured LTI MIMO state-space models. In *Proceedings of the IEEE Conference on Decision and Control*, pages 2737–2742, 2015. ISBN 9781479978861. doi: 10.1109/CDC.2015.7402630.

[99] Marc Beaudin and Hamidreza Zareipour. Home energy management systems: A review of modelling and complexity. *Renewable and Sustainable Energy Reviews*, 45: 318–335, may 2015. ISSN 13640321. doi: 10.1016/j.rser.2015.01.046.

[100] Tor Aksel N. Heirung, Joel A. Paulson, Jared O'Leary, and Ali Mesbah. Stochastic model predictive control — how does it work? *Computers and Chemical Engineering*, 114:158–170, jun 2018. ISSN 00981354. doi: 10.1016/j.compchemeng.2017.10.026.

[101] Mohammad Chehreghani Bozchalui, Syed Ahsan Hashmi, Hussin Hassen, Claudio A. Cañizares, and Kankar Bhattacharya. Optimal operation of residential energy hubs in smart grids. *IEEE Transactions on Smart Grid*, 3(4):1755–1766, 2012. ISSN 19493053. doi: 10.1109/TSG.2012.2212032.

[102] Carlos Henggeler Antunes, Vahid Rasouli, Maria Joao Alves, and Lvaro Gomes. A mixed-integer linear programming model for optimal management of residential electrical loads under dynamic tariffs. In *2018 International Conference on Smart Energy Systems and Technologies, SEST 2018 - Proceedings*. Institute of Electrical and Electronics Engineers Inc., oct 2018. ISBN 9781538653265. doi: 10.1109/SEST.2018.8495670.

[103] Amin Mirakhorli and Bing Dong. Occupant-behavior driven appliance scheduling for residential buildings. *Building Simulation*, 10(6):917–931, dec 2017. ISSN 19968744. doi: 10.1007/s12273-017-0402-z. URL https://doi.org/10.1007/s12273-017-0402-z.

[104] Prateek Munankarmi, Xin Jin, Fei Ding, and Changhong Zhao. Quantification of Load Flexibility in Residential Buildings Using Home Energy Management Systems. In *American Control Conference (ACC), 2020*, pages 1311–1316, jul 2020. doi: 10.23919/acc45564.2020.9147459.

[105] Kaitlyn Garifi, Kyri Baker, Behrouz Touri, and Dane Christensen. Stochastic Model Predictive Control for Demand Response in a Home Energy Management System. *IEEE Power and Energy Society General Meeting*, 2018-Augus, dec 2018. ISSN 19449933. doi: 10.1109/PESGM.2018.8586485.

[106] Omar Alrumayh and Kankar Bhattacharya. Flexibility of Residential Loads for Demand Response Provisions in Smart Grid. *IEEE Transactions on Smart Grid*, 10 (6):6284–6297, nov 2019. ISSN 19493061. doi: 10.1109/TSG.2019.2901191.

[107] Rahul Kadavil, Salvador Lurbé, Siddharth Suryanarayanan, Patricia A. Aloise-Young, Steven Isley, and Dane Christensen. An application of the Analytic Hierarchy Process for prioritizing user preferences in the design of a Home Energy Management System. *Sustainable Energy, Grids and Networks*, 16:196–206, dec 2018. ISSN 23524677. doi: 10.1016/j.segan.2018.07.009.

[108] Guillaume Mercere, Olivier Prot, and Jose A. Ramos. Identification of parameterized gray-box state-space systems: From a black-box linear time-invariant representation to a structured one. *IEEE Transactions on Automatic Control*, 59(11):2873–2885, nov 2014. ISSN 00189286. doi: 10.1109/TAC.2014.2351853.

[109] Emeline Georges, Bertrand Cornélusse, Damien Ernst, Vincent Lemort, and Sébastien Mathieu. Residential heat pump as flexible load for direct control service with parametrized duration and rebound effect. *Applied Energy*, 187:140–153, feb 2017. ISSN 03062619. doi: 10.1016/j.apenergy.2016.11.012.

[110] Clement Lork, Wen Tai Li, Yan Qin, Yuren Zhou, Chau Yuen, Wayes Tushar, and Tapan K. Saha. An uncertainty-aware deep reinforcement learning framework for residential air conditioning energy management. *Applied Energy*, 276:115426, oct 2020. ISSN 03062619. doi: 10.1016/j.apenergy.2020.115426.

[111] Omar Alrumayh and Kankar Bhattacharya. Model predictive control based home energy management system in smart grid. In *2015 IEEE Electrical Power and Energy Conference: Smarter Resilient Power Systems, EPEC 2015*, pages 152–157. Institute of Electrical and Electronics Engineers Inc., jan 2016. ISBN 9781479976645. doi: 10.1109/EPEC.2015.7379942.

[112] Emiliano Dall Anese, Swaroop S. Guggilam, Andrea Simonetto, Yu Christine Chen, and Sairaj V. Dhople. Optimal Regulation of Virtual Power Plants. *IEEE Transactions on Power Systems*, 33(2):1868–1881, mar 2018. ISSN 08858950. doi: 10.1109/TPWRS.2017.2741920.

[113] Hao Liang and Weihua Zhuang. Stochastic Modeling and Optimization in a Microgrid: A Survey. *Energies*, 7(4):2027–2050, mar 2014. ISSN 1996-1073. doi: 10.3390/en7042027.

[114] Julieta Giraldez, Andy Hoke, Peter Gotseff, Nick Wunder, Michael Blonsky, Michael Emmanuel, Aadil Latif, Earle Ifuku, Marc Asano, Thomas Aukai, and Reid Sasaki. Advanced Inverter Voltage Controls: Simulation and Field Pilot Findings. Technical report, National Renewable Energy Laboratory, oct 2018. URL http://dx.doi.org/10.2172/1481102.

[115] Wes Sunderman, Roger C. Dugan, and Jeff Smith. Open source modeling of advanced inverter functions for solar photovoltaic installations. In *Proceedings of the IEEE Power Engineering Society Transmission and Distribution Conference*. Institute of Electrical and Electronics Engineers Inc., jul 2014. ISBN 9781479936557. doi: 10.1109/tdc.2014.6863399.

[116] Alessandro Di Giorgio, Francesco Liberati, and Silvia Canale. Electric vehicles charging control in a smart grid: A model predictive control approach. *Control Engineering Practice*, 22:147–162, 2014.

[117] Ao Zhang, Bo Sun, Tian Liu, Xiaoqi Tan, Su Wang, and Danny H.K. K Tsang. Joint voltage and frequency regulation by EV charging scheduling in the distribution network. In *2018 IEEE Power Energy Society Innovative Smart Grid Technologies Conference (ISGT)*, pages 1–5. Institute of Electrical and Electronics Engineers Inc., feb 2018. ISBN 9781538624531. doi: 10.1109/ISGT.2018.8403363.

[118] H. Vincent Poor, Ye Shi, Hoang Duong Tuan, Andrey V. Savkin, and Trung Q. Duong. Model predictive control for smart grids with multiple electric-vehicle charging stations. *IEEE Transactions on Smart Grid*, 10(2):2127–2136, mar 2019. ISSN 19493053. doi: 10.1109/TSG.2017.2789333.

[119] Zahra Darabi and Mehdi Ferdowsi. Examining power grid's capacity to meet transportation electrification demand. In *2012 IEEE Power and Energy Society General Meeting*, pages 1–7, jul 2012. ISBN 9781467327275. doi: 10.1109/PESGM.2012.6345204.

[120] Dimitrios Thomas, Olivier Deblecker, and Christos S. Ioakimidis. Optimal operation of an energy management system for a grid-connected smart building considering photovoltaics' uncertainty and stochastic electric vehicles' driving schedule. *Applied Energy*, 210:1188–1206, jan 2018. ISSN 03062619. doi: 10.1016/j.apenergy.2017.07.035.

[121] Yan Zhang, Tao Zhang, Rui Wang, Yajie Liu, and Bo Guo. Optimal operation of a smart residential microgrid based on model predictive control by considering uncertainties and storage impacts. *Solar Energy*, 122:1052–1065, dec 2015. ISSN 0038092X. doi: 10.1016/j.solener.2015.10.027.

[122] Subho Paul and Narayana Prasad Padhy. Resilient Scheduling Portfolio of Residential Devices and Plug-In Electric Vehicle by Minimizing Conditional Value at Risk. *IEEE Transactions on Industrial Informatics*, 15(3):1566–1578, mar 2019. ISSN 15513203. doi: 10.1109/TII.2018.2847742.

[123] Kaitlyn Garifi, Kyri Baker, Dane Christensen, and Behrouz Touri. Stochastic Home Energy Management Systems with Varying Controllable Resources. *IEEE Power and Energy Society General Meeting*, 2019-Augus, aug 2019. ISSN 19449933. doi: 10.1109/PESGM40551.2019.8973708.

[124] Amin Mirakhorli and Bing Dong. Market and behavior driven predictive energy management for residential buildings. *Sustainable Cities and Society*, 38:723–735, apr 2018. ISSN 22106707. doi: 10.1016/j.scs.2018.01.030.

[125] Mehdi Rahmani-Andebili and Haiying Shen. Energy scheduling for a smart home applying stochastic model predictive control. In *2016 25th International Conference on Computer Communications and Networks, ICCCN 2016*. Institute of Electrical and Electronics Engineers Inc., sep 2016. ISBN 9781509022793. doi: 10.1109/ICCCN.2016.7568516.

[126] Zhi Wu, Xiao Ping Zhang, Joachim Brandt, Su Yang Zhou, and Jia Ning Li. Three Control Approaches for Optimized Energy Flow with Home Energy Management System. *IEEE Power and Energy Technology Systems Journal*, 2:21–31, 2015. ISSN 23327707. doi: 10.1109/JPETS.2015.2409202.

[127] Zhi Wu, Suyang Zhou, Jianing Li, and Xiao Ping Zhang. Real-time scheduling of residential appliances via conditional risk-at-value. *IEEE Transactions on Smart Grid*, 5(3):1282–1291, 2014. ISSN 19493053. doi: 10.1109/TSG.2014.2304961.

[128] Sorin C. Bengea, Anthony D. Kelman, Francesco Borrelli, Russell Taylor, and Satish Narayanan. Implementation of model predictive control for an HVAC system in a mid-size commercial building. *HVAC and R Research*, 20(1):121–135, jan 2014. ISSN 10789669. doi: 10.1080/10789669.2013.834781.

[129] Yudong Ma, Sergey Vichik, and Francesco Borrelli. Fast stochastic MPC with optimal risk allocation applied to building control systems. In *Proceedings of the IEEE Conference on Decision and Control*, pages 7559–7564, 2012. doi: 10.1109/CDC.2012.6426251.

[130] G. Bruni, S. Cordiner, V. Mulone, V. Sinisi, and F. Spagnolo. Energy management in a domestic microgrid by means of model predictive controllers. *Energy*, 108:119–131, mar 2015. ISSN 03605442. doi: 10.1016/j.energy.2015.08.004.

[131] Ali Hooshmand, Mohammad H. Poursaeidi, Javad Mohammadpour, Heidar A. Malki, and Karolos Grigoriads. Stochastic model predictive control method for microgrid management. In *Innovative Smart Grid Technologies (ISGT), 2012 IEEE PES*, pages 1–7. IEEE, 2012. ISBN 9781457721588. doi: 10.1109/ISGT.2012.6175660.

[132] Stefano Raimondi Cominesi, Marcello Farina, Luca Giulioni, Bruno Picasso, and Riccardo Scattolini. A Two-Layer Stochastic Model Predictive Control Scheme for Microgrids. *IEEE Transactions on Control Systems Technology*, 26(1):1–13, jan 2018. ISSN 10636536. doi: 10.1109/TCST.2017.2657606.

[133] Seho Park and Changsun Ahn. Stochastic model predictive controller for battery thermal management of electric vehicles. In *2019 IEEE Vehicle Power and Propulsion Conference, VPPC 2019 - Proceedings*. Institute of Electrical and Electronics Engineers Inc., oct 2019. ISBN 9781728112497. doi: 10.1109/VPPC46532.2019.8952340.

[134] Jidong Wang, Chenghao Li, Peng Li, Yanbo Che, Yue Zhou, and Yinqi Li. MPC-based interval number optimization for electric water heater scheduling in uncertain environments. *Frontiers in Energy*, 2019. ISSN 20951698. doi: 10.1007/s11708-019-0644-9. URL https://doi.org/10.1007/s11708-019-0644-9.

[135] Kate Doubleday, Vanessa Van Scyoc Hernandez, and Bri Mathias Hodge. Benchmark probabilistic solar forecasts: Characteristics and recommendations. *Solar Energy*, 206:52–67, aug 2020. ISSN 0038092X. doi: 10.1016/j.solener.2020.05.051.

[136] National Weather Service, 2020. URL https://www.weather.gov/.

[137] ECMWF — Advancing global NWP through international collaboration, 2020. URL https://www.ecmwf.int/.

[138] Eoghan McKenna, Michal Krawczynski, and Murray Thomson. Four-state domestic building occupancy model for energy demand simulations. *Energy and Buildings*, 96: 30–39, jun 2015. ISSN 03787788. doi: 10.1016/j.enbuild.2015.03.013.

[139] Timothy M. Hansen, Edwin K.P. Chong, Siddharth Suryanarayanan, Anthony A. Maciejewski, and Howard Jay Siegel. A partially observable markov decision process approach to residential home energy management. *IEEE Transactions on Smart Grid*, 9(2):1271–1281, 2018. ISSN 19493053. doi: 10.1109/TSG.2016.2582701.

[140] Luca Serafini, Emanuele Principi, Susanna Spinsante, and Stefano Squartini. Multi-Household Energy Management in a Smart Neighborhood in the Presence of Uncertainties and Electric Vehicles. *Electronics 2021, Vol. 10, Page 3186*, 10(24): 3186, dec 2021. ISSN 2079-9292. doi: 10.3390/ELECTRONICS10243186.

[141] Bing Dong and Khee Poh Lam. A real-time model predictive control for building heating and cooling systems based on the occupancy behavior pattern detection and local weather forecasting. *Building Simulation*, 7(1):89–106, feb 2014. ISSN 19963599. doi: 10.1007/s12273-013-0142-7.

[142] Abdul Afram and Farrokh Janabi-Sharifi. Theory and applications of HVAC control systems - A review of model predictive control (MPC), feb 2014. ISSN 03601323.

[143] Prateek Munankarmi, Jeff Maguire, Sivasathya Pradha Balamurugan, Michael Blonsky, David Roberts, and Xin Jin. Community-scale interaction of energy efficiency and demand flexibility in residential buildings. *Applied Energy*, 298:117149, sep 2021. ISSN 03062619. doi: 10.1016/j.apenergy.2021.117149.

[144] Yumiko Iwafune, Takashi Ikegami, Joao Gari Da Silva Fonseca, Takashi Oozeki, and Kazuhiko Ogimoto. Cooperative home energy management using batteries for a photovoltaic system considering the diversity of households. *Energy Conversion and Management*, 96:322–329, may 2015. ISSN 01968904. doi: 10.1016/j.enconman.2015.02.083.

[145] Amir Roth and Janet Reyna. Innovations in Building Energy Modeling: Research and Development Opportunities for Emerging Technologies. Technical report, US Department of Energy, Building Technologies Office, 2020. URL https://www.nrel.gov/docs/fy21osti/77835.pdf.

[146] Amir Roth. Grid-interactive Efficient Buildings Technical Report Series: Whole-Building Controls, Sensors, Modeling, and Analytics. Technical report, US Department of Energy, Building Technologies Office, 2019. URL https://www.nrel.gov/docs/fy20osti/75478.pdf.

[147] Xinhua Xu, Shengwei Wang, and Gongsheng Huang. Robust MPC for temperature control of air-conditioning systems concerning on constraints and multitype uncertainties. *Building Services Engineering Research and Technology*, 31(1):39–55, feb 2010. ISSN 01436244. doi: 10.1177/0143624409352420.

[148] Hongyu Wu, Annabelle Pratt, and Sudipta Chakraborty. Stochastic optimal scheduling of residential appliances with renewable energy sources. *IEEE Power and Energy Society General Meeting*, 2015-Septe, sep 2015. ISSN 19449933. doi: 10.1109/PESGM.2015.7286584.

[149] E Wilson, C Engebrecht Metzger, S Horowitz, and R Hendron. 2014 Building America House Simulation Protocols. Technical report, NREL, 2014. URL https://www.nrel.gov/docs/fy14osti/60988.pdf.

[150] Jay Burch and Craig Christensen. Towards development of an algorithm for mains water temperature. In *American Solar Energy Society, 2007*, pages 173–178, 2007. ISBN 9781604233087.

[151] Abdulkadir Bedir, Noel Crisostomo, Jennifer Allen, Eric Wood, and Clement Rames. California Plug-In Electric Vehicle Infrastructure Projections: 2017-2025. Technical report, California Energy Commission, 2018. URL https://www.nrel.gov/docs/fy18osti/70893.pdf.

[152] Jianli Chen, Rajendra Adhikari, Eric Wilson, Joseph Robertson, Anthony Fontanini, Ben Polly, and Opeoluwa Olawale. Stochastic simulation of residential building occupant-driven energy use in a bottom-up model of the U.S. housing stock. *Arxiv*, nov 2021. URL https://arxiv.org/abs/2111.01881v2.

[153] Anmar Arif, Zhaoyu Wang, Jianhui Wang, Barry Mather, Hugo Bashualdo, and Dongbo Zhao. Load modeling - A review, nov 2018. ISSN 19493053.

[154] Abdullah Bokhari, Ali Alkan, Rasim Dogan, Marc Diaz-Aguilo, Francisco De Leon, Dariusz Czarkowski, Zivan Zabar, Leo Birenbaum, Anthony Noel, and Resk Ebrahem Uosef. Experimental determination of the ZIP coefficients for modern residential, commercial, and industrial loads. *IEEE Transactions on Power Delivery*, 29(3): 1372–1381, 2014. ISSN 08858977. doi: 10.1109/TPWRD.2013.2285096.

[155] Les M. Hajagos. Laboratory measurements and models of modern loads and their effect on voltage stability studies. *IEEE Transactions on Power Systems*, 13(2): 584–592, 1998. ISSN 08858950. doi: 10.1109/59.667386.

[156] Ning Lu, Yulong Xie, Zhenyu Huang, Francis Puyleart, and Steve Yang. Load component database of household appliances and small office equipment. In *IEEE Power and Energy Society 2008 General Meeting: Conversion and Delivery of Electrical Energy in the 21st Century, PES*, 2008. ISBN 9781424419067. doi: 10.1109/PES.2008.4596224.

[157] U.S. Department of Energy. DOE Zero Energy Ready Home National Program Requirements (Rev. 07). Technical report, U.S. DOE, 2019. URL https://www.energy.gov/eere/buildings/downloads/doe-zero-energy-ready-home-national-program-requirements-rev-07.

[158] E. B. Curtis, D. Ingerman, and J. A. Morrow. Circular planar graphs and resistor networks. *Linear Algebra and Its Applications*, 283(1-3):115–150, nov 1998. ISSN 00243795. doi: 10.1016/S0024-3795(98)10087-3.

[159] Alan J. Laub, Michael T. Heath, Chris C. Paige, and Robert C. Ward. Computation of System Balancing Transformations and Other Applications of Simultaneous Diagonalization Algorithms. *IEEE Transactions on Automatic Control*, 32(2): 115–122, 1987. ISSN 15582523. doi: 10.1109/TAC.1987.1104549.

[160] S. Gugercin and A. C. Antoulas. A comparative study of 7 algorithms for model reduction. *Proceedings of the IEEE Conference on Decision and Control*, 3: 2367–2372, 2000. ISSN 01912216. doi: 10.1109/CDC.2000.914153.

[161] Amin Mirakhorli and Bing Dong. Model predictive control for building loads connected with a residential distribution grid. *Applied Energy*, 230:627–642, nov 2018. ISSN 03062619. doi: 10.1016/j.apenergy.2018.08.051.

[162] Kaitlyn Garifi, Kyri Baker, Dane Christensen, and Behrouz Touri. Control of Energy Storage in Home Energy Management Systems: Non-Simultaneous Charging and Discharging Guarantees. *Arxiv*, apr 2018. URL http://arxiv.org/abs/1805.00100.

[163] Skipper Seabold and Josef Perktold. Statsmodels: Econometric and Statistical Modeling with Python. In *Proc. of the 9th Python in Science Conf*, number Scipy, pages 92–96, 2010. URL http://statsmodels.sourceforge.net/.

[164] Paulo Cesar Tabares-Velasco, Jeff Maguire, Scott Horowitz, and Craig Christensen. Using the Beopt Automated Residential Simulation Test Suite to Enable Comparative Analysis Between Energy Simulation Engines. Technical report, NREL, 2014. URL https://www.nrel.gov/docs/fy14osti/62273.pdf.

[165] Jeff Maguire, Scott Horowitz, Nathan Moore, and Patrick Sullivan. Validation of Tendril TrueHome Using Software-to-Software Comparison. Technical report, NREL, 2017. URL https://www.nrel.gov/docs/fy18osti/70116.pdf.

[166] OpenStudio-HPXML documentation. URL https://openstudio-hpxml.readthedocs.io/en/latest/.

[167] Manual J: Residential Load Calculation. Technical report, ACCA, 2008.

[168] BEopt. URL https://beopt.nrel.gov/home.

[169] Dheepak Krishnamurthy. OpenDSSDirect.py 0.3.1 documentation. URL https://dss-extensions.org/OpenDSSDirect.py/.

[170] High Performance Computing — NREL. URL https://www.nrel.gov/hpc/.

[171] Eric Wilson, Craig Christensen, Scott Horowitz, Joseph Robertson, and Jeff Maguire. Energy Efficiency Potential in the U.S. Single-Family Housing Stock. Technical report, NREL, 2017. URL https://www.nrel.gov/docs/fy18osti/68670.pdf.

[172] Peak Savers — Pepco - An Exelon Company, 2020. URL https://www.pepco.com/Pages/peaksavers.aspx.

[173] Solar home electricity data - Ausgrid, 2020. URL https://www.ausgrid.com.au/Industry/Our-Research/Data-to-share/Solar-home-electricity-data.

[174] Howard J. Diamond, Thomas R. Karl, Michael A. Palecki, C. Bruce Baker, Jesse E. Bell, Ronald D. Leeper, David R. Easterling, Jay H. Lawrimore, Tilden P. Meyers, Michael R. Helfert, Grant Goodge, and Peter W. Thorne. U.S. Climate Reference Network after One Decade of Operations: Status and Assessment. *Bulletin of the American Meteorological Society*, 94(4):485–498, apr 2013. ISSN 0003-0007. doi: 10.1175/BAMS-D-12-00170.1.

[175] Sherin Ann Abraham, Killian McKenna, and Adarsh Nagarajan. Development and Clustering of Rate-Oriented Load Metrics for Customer Price-Plan Analysis. In *IEEE Power and Energy Society General Meeting*, volume 2019-Augus. IEEE Computer Society, aug 2019. ISBN 9781728119816. doi: 10.1109/PESGM40551.2019.8973711. URL https://www.nrel.gov/docs/fy19osti/72655.pdf.

[176] Ryan Hledik, Ahmad Faruqui, and Cody Warner. The National Landscape of Residential TOU Rates: A Preliminary Summary. Technical report, The Brattle Group, 2017. URL https://www.brattle.com/insights-events/publications/the-national-landscape-of-residential-tou-rates-a-preliminary-summary/.

[177] Public Report 6 Lithium Ion Battery Testing. Technical report, ITP Renewables, 2019. URL www.batterytestcentre.com.au.

[178] Jason Svarc. Tesla Powerwall 2 Vs LG chem RESU Vs Sonnen ECO Vs BYD — Clean Energy Reviews, 2019. URL https://www.cleanenergyreviews.info/blog/powerwall-vs-lg-chem-vs-sonnen-vs-byd.

[179] LG Chem. LG Home Battery, 2020. URL https://www.lgessbattery.com/us/home-battery/product-info.lg.

[180] Tesla Powerwall, 2020. URL https://www.tesla.com/sites/default/files/pdfs/powerwall/Powerwall2_AC_Datasheet_en_northamerica.pdf.

[181] Steven Diamond and Stephen Boyd. CVXPY: A Python-embedded modeling language for convex optimization. *Journal of Machine Learning Research*, 17:1–5, 2016. ISSN 15337928. URL http://www.cvxpy.org/.

[182] OpenWeatherMap One Call API, . URL https://openweathermap.org/api/one-call-api.

[183] PVlib Documentation. URL https://pvlib-python.readthedocs.io/en/stable/generated/pvlib.forecast.ForecastModel.cloud_cover_to_irradiance.html.

[184] Time of Use — Xcel Energy, 2022. URL https://co.my.xcelenergy.com/s/billing-payment/residential-rates/time-of-use-pricing.

APPENDIX

COPYRIGHT PERMISSIONS

The following email thread provides copyright permission from all co-authors that contributed to this dissertation. The citations of the published papers that require copyright permission are also included in the email.

Blonsky, Michael

From: Nagarajan, Adarsh
Sent: Tuesday, March 29, 2022 9:05 AM
To: Ghosh, Shibani; Balamurugan, Sivasathya Pradha; Kroposki, Benjamin; Munankarmi, Prateek; Jin, Xin; Blonsky, Michael; dylanscutler@gmail.com; santoshsveda@gmail.com
Cc: Tyrone Vincent; McKenna, Killian; Maguire, Jeff
Subject: Re: Permission to Reuse Copyrighted Materials

I grant permission to reuse.

Thanks,
Adarsh Nagarajan, PhD
Group Manager | Power System Design and Planning
Grid Planning and Analysis Center
National Renewable Energy Laboratory (NREL)
15013 Denver West Parkway | Golden, CO 80401
M: 281-902-7075
adarsh.nagarajan@nrel.gov

From: Ghosh, Shibani <Shibani.Ghosh@nrel.gov>
Sent: Wednesday, March 16, 2022 7:32 AM
To: Balamurugan, Sivasathya Pradha <SivasathyaPradha.Balamurugan@nrel.gov>; Kroposki, Benjamin <Benjamin.Kroposki@nrel.gov>; Munankarmi, Prateek <Prateek.Munankarmi@nrel.gov>; Jin, Xin <Xin.Jin@nrel.gov>; Blonsky, Michael <Michael.Blonsky@nrel.gov>; Nagarajan, Adarsh <Adarsh.Nagarajan@nrel.gov>; dylanscutler@gmail.com <dylanscutler@gmail.com>; Santosh Veda <private email>
Cc: Tyrone Vincent <tvincent@mines.edu>; McKenna, Killian <Killian.McKenna@nrel.gov>; Maguire, Jeff <Jeff.Maguire@nrel.gov>
Subject: Re: Permission to Reuse Copyrighted Materials

I grant permission to reuse.

Best Wishes,
Shibani

Get Outlook for iOS

From: Balamurugan, Sivasathya Pradha <SivasathyaPradha.Balamurugan@nrel.gov>
Sent: Tuesday, March 15, 2022 4:39:54 PM
To: Kroposki, Benjamin <Benjamin.Kroposki@nrel.gov>; Munankarmi, Prateek <Prateek.Munankarmi@nrel.gov>; Jin, Xin <Xin.Jin@nrel.gov>; Blonsky, Michael <Michael.Blonsky@nrel.gov>; Nagarajan, Adarsh <Adarsh.Nagarajan@nrel.gov>; Ghosh, Shibani <Shibani.Ghosh@nrel.gov>; dylanscutler@gmail.com <dylanscutler@gmail.com>; Santosh Veda <private email>
Cc: Tyrone Vincent <tvincent@mines.edu>; McKenna, Killian <Killian.McKenna@nrel.gov>; Maguire, Jeff <Jeff.Maguire@nrel.gov>
Subject: Re: Permission to Reuse Copyrighted Materials

I grant permission for reuse.

Best,

Sathya

From: "Kroposki, Benjamin" <Benjamin.Kroposki@nrel.gov>
Date: Tuesday, March 15, 2022 at 1:53 PM
To: "Munankarmi, Prateek" <Prateek.Munankarmi@nrel.gov>, "Jin, Xin" <Xin.Jin@nrel.gov>, "Blonsky, Michael" <Michael.Blonsky@nrel.gov>, "Balamurugan, Sivasathya Pradha" <SivasathyaPradha.Balamurugan@nrel.gov>, "Nagarajan, Adarsh" <Adarsh.Nagarajan@nrel.gov>, "Ghosh, Shibani" <Shibani.Ghosh@nrel.gov>, "dylanscutler@gmail.com" <dylanscutler@gmail.com>, Santosh Veda <private email>
Cc: Tyrone Vincent <tvincent@mines.edu>, "McKenna, Killian" <Killian.McKenna@nrel.gov>, "Maguire, Jeff" <Jeff.Maguire@nrel.gov>
Subject: Re: Permission to Reuse Copyrighted Materials

I grant permission for reuse.

Ben Kroposki

From: Santosh Veda <private email>
Sent: Tuesday, March 15, 2022 1:25 PM
To: Blonsky, Michael Michael.Blonsky@nrel.gov
Cc: Balamurugan, Sivasathya Pradha SivasathyaPradha.Balamurugan@nrel.gov; Jin, Xin Xin.Jin@nrel.gov; Nagarajan, Adarsh Adarsh.Nagarajan@nrel.gov; Ghosh, Shibani Shibani.Ghosh@nrel.gov; Kroposki, Benjamin Benjamin.Kroposki@nrel.gov; Munankarmi, Prateek Prateek.Munankarmi@nrel.gov; dylanscutler@gmail.com; Tyrone Vincent tvincent@mines.edu; McKenna, Killian Killian.McKenna@nrel.gov; Maguire, Jeff Jeff.Maguire@nrel.gov
Subject: Re: Permission to Reuse Copyrighted Materials

Hi Michael,
I grant permission for reuse of our shared work.
Santosh Veda

From: dylan cutler dylanscutler@gmail.com
Sent: Tuesday, March 15, 2022 12:33 PM
To: Blonsky, Michael Michael.Blonsky@nrel.gov
Cc: Balamurugan, Sivasathya Pradha SivasathyaPradha.Balamurugan@nrel.gov; Jin, Xin Xin.Jin@nrel.gov; Nagarajan, Adarsh Adarsh.Nagarajan@nrel.gov; Ghosh, Shibani Shibani.Ghosh@nrel.gov; Kroposki, Benjamin Benjamin.Kroposki@nrel.gov; Munankarmi, Prateek Prateek.Munankarmi@nrel.gov; Santosh Veda <private email>; Tyrone Vincent tvincent@mines.edu; McKenna, Killian Killian.McKenna@nrel.gov; Maguire, Jeff Jeff.Maguire@nrel.gov
Subject: Re: Permission to Reuse Copyrighted Materials

MIchael,

I grant permission for reuse of material identified below. Good luck with finishing up.

Dylan

From: "Munankarmi, Prateek" <Prateek.Munankarmi@nrel.gov>
Date: Tuesday, March 15, 2022 at 12:21 PM
To: "Jin, Xin" <Xin.Jin@nrel.gov>, "Blonsky, Michael" <Michael.Blonsky@nrel.gov>, "Balamurugan, Sivasathya Pradha" <SivasathyaPradha.Balamurugan@nrel.gov>, "Nagarajan, Adarsh" <Adarsh.Nagarajan@nrel.gov>, "Ghosh, Shibani" <Shibani.Ghosh@nrel.gov>, PE Ben Kroposki <Benjamin.Kroposki@nrel.gov>, "dylanscutler@gmail.com" <dylanscutler@gmail.com>, Santosh Veda <private email>
Cc: Tyrone Vincent <tvincent@mines.edu>, "McKenna, Killian" <Killian.McKenna@nrel.gov>, "Maguire, Jeff" <Jeff.Maguire@nrel.gov>
Subject: Re: Permission to Reuse Copyrighted Materials

I agree for permission for reuse.

Thanks,
Prateek Munankarmi

Get Outlook for iOS

From: Jin, Xin <Xin.Jin@nrel.gov>
Sent: Tuesday, March 15, 2022 12:19:54 PM
To: Blonsky, Michael <Michael.Blonsky@nrel.gov>; Balamurugan, Sivasathya Pradha <SivasathyaPradha.Balamurugan@nrel.gov>; Nagarajan, Adarsh <Adarsh.Nagarajan@nrel.gov>; Ghosh, Shibani <Shibani.Ghosh@nrel.gov>; Kroposki, Benjamin <Benjamin.Kroposki@nrel.gov>; Munankarmi, Prateek <Prateek.Munankarmi@nrel.gov>; dylanscutler@gmail.com <dylanscutler@gmail.com>; Santosh Veda <private email>
Cc: Tyrone Vincent <tvincent@mines.edu>; McKenna, Killian <Killian.McKenna@nrel.gov>; Maguire, Jeff <Jeff.Maguire@nrel.gov>
Subject: RE: Permission to Reuse Copyrighted Materials

I grant permission for reuse.

Thanks,

Xin

From: Blonsky, Michael <Michael.Blonsky@nrel.gov>
Sent: Tuesday, March 15, 2022 11:17 AM
To: Balamurugan, Sivasathya Pradha <SivasathyaPradha.Balamurugan@nrel.gov>; Jin, Xin <Xin.Jin@nrel.gov>; Nagarajan, Adarsh <Adarsh.Nagarajan@nrel.gov>; Ghosh, Shibani <Shibani.Ghosh@nrel.gov>; Kroposki, Benjamin <Benjamin.Kroposki@nrel.gov>; Munankarmi, Prateek <Prateek.Munankarmi@nrel.gov>; dylanscutler@gmail.com; Santosh Veda <private email>
Cc: Tyrone Vincent <tvincent@mines.edu>; McKenna, Killian <Killian.McKenna@nrel.gov>; Maguire, Jeff <Jeff.Maguire@nrel.gov>
Subject: Permission to Reuse Copyrighted Materials

Hello recent co-authors,

I am in the final stages of writing my PhD thesis, and I would like to include content that was co-authored by you. The Colorado School of Mines requires that I get your permission to use our shared work in my thesis. For more details on this, please see:
https://www.mines.edu/graduate-studies/thesis-writers-guide/

To grant permission for reuse in my thesis, **please reply all** to this email stating "I grant permission for reuse" or something of that nature. This email thread will be an appendix of the published thesis, so please be aware your reply will be public!

I am planning to include content from the following papers:

- Michael Blonsky, Jeff Maguire, Killian McKenna, Dylan Cutler, Sivasathya Pradha Balamurugan, and Xin Jin. OCHRE: The Object-oriented, Controllable, High-resolution Residential Energy Model for Dynamic Integration Studies. Applied Energy, May 2021. doi:10.1016/j.apenergy.2021.116732.
- Michael Blonsky, Adarsh Nagarajan, Shibani Ghosh, Killian McKenna, Santosh Veda, and Benjamin Kroposki. Potential Impacts of Transportation and Building Electrification on the Grid: A Review of Electrification Projections and Their Effects on Grid Infrastructure, Operation, and Planning. Current Sustainable/Renewable Energy Reports, Dec 2019. doi:10.1007/s40518-019-00140-5.
- Michael Blonsky, Killian McKenna, Tyrone Vincent, and Adarsh Nagarajan. Time-of-use and Demand Charge Battery Controller using Stochastic Model Predictive Control. IEEE SmartGridComm, Nov 2020. doi:10.1109/SmartGridComm47815.2020.9302943.
- Michael Blonsky, Prateek Munankarmi, and Sivasathya Pradha Balamurugan. Incorporating Residential Smart Electric Vehicle Charging in Home Energy Management Systems. IEEE Green Technologies Conference, Apr 2021. doi:10.1109/GREENTECH48523.2021.00039.
- Michael Blonsky, Killian McKenna, Jeff Maguire, and Tyrone Vincent. Home Energy Management under Realistic and Uncertain Conditions: A Comparison of Heuristic, Deterministic, and Stochastic Control Methods. Applied Energy (under review).

Thank you very much for your permission and your collaboration,
Michael

--
Michael Blonsky
Pronouns: he/him/his
Research Engineer | Grid Planning and Analysis Center

National Renewable Energy Laboratory (NREL)
15013 Denver West Parkway | Golden, CO 80401
303-275-3192 | M: 847-609-5990
Michael.Blonsky@nrel.gov | www.nrel.gov